

The Adaptive Response of Endothelial Cells to Shear Stress Alteration

by

Ji Zhang

Department of Biomedical Engineering
Duke University

Date: _____

Approved:

Morton H. Friedman, Supervisor

George A. Truskey

Nenad Bursac

Christopher D. Kontos

Jeffrey A. LaMack

Dissertation submitted in partial fulfillment of
the requirements for the degree of Doctor of Philosophy in the Department of
Biomedical Engineering in the Graduate School
of Duke University

2010

ABSTRACT

The Adaptive Response of Endothelial Cells to Shear Stress Alteration

by

Ji Zhang

Department of Biomedical Engineering
Duke University

Date: _____

Approved:

Morton H. Friedman, Supervisor

George A. Truskey

Nenad Bursac

Christopher D. Kontos

Jeffrey A. LaMack

An abstract of a dissertation submitted in partial
fulfillment of the requirements for the degree
of Doctor of Philosophy in the Department of
Biomedical Engineering in the Graduate School
of Duke University

2010

Copyright by
Ji Zhang
2010

Abstract

The adaptive response of vascular endothelial cells to shear stress alteration induced by global hemodynamic changes is an essential component of normal endothelial physiology *in vivo*; and an understanding of the transient regulation of endothelial phenotype during adaptation will advance our understanding of endothelial biology and yield new insights into the mechanism of atherogenesis. The objective of this study was to characterize the adaptive response of arterial endothelial cells to acute increases in shear stress magnitude and frequency in well-defined *in vitro* settings. Porcine endothelial cells were preconditioned by a basal level shear stress of ± 15 dynes/cm² at 1 Hz for 24 hours, and an acute increase in shear stress magnitude (30 ± 15 dynes/cm²) or frequency (2 Hz) was then applied. Endothelial permeability to bovine serum albumin was measured and gene expression profiling was performed using microarrays at multiple time points during a period of 6 hours after the shear stress alteration. The instantaneous endothelial permeability was found to increase rapidly in response to the acute increase in shear stress magnitude. Endothelial permeability nearly doubled after 40 minutes exposure to the elevated shear magnitude, and then decreased gradually. However, less dependency of endothelial permeability on shear stress frequency was observed. Endothelial permeability increased slowly from 120 minutes to 6 hours after exposure to the elevated shear frequency, but the increase was not statistically

significant and was relatively small (1.2 fold increase at 6 hours). The transcriptomics studies identified 86 genes that were sensitive to the elevated shear magnitude and 37 genes sensitive to the elevated frequency. A significant number of the identified genes are previously unknown as sensitive to shear stress. The acute increase in shear magnitude promoted the expression of a group of anti-inflammatory and anti-oxidative genes; while the acute increase in shear frequency upregulated a set of cell-cycle regulating genes and angiogenesis genes. The adaptive response of global gene expression profile to the elevated shear magnitude is found to be triphasic, consisting of an induction period, an early adaptive response (ca. 45 minutes) and a late remodeling response. However, no apparent temporal regulation pattern of global gene expression was found during the adaptation to the elevated shear frequency. The results from this dissertation suggest that endothelial cells exhibit a specific phenotype during the adaptive response to changes in shear stress; and the transient phenotype is different than that of fully-adapted endothelial cells and may alter arterial atherosusceptibility.

Contents

Abstract	iv
List of Tables	ix
List of Figures	x
Acknowledgements	xiii
1. Introduction	1
1.1 Objective, Hypothesis and Specific Aims	1
1.2 Dissertation Structure	4
2. Background and Related Studies	6
2.1 Background	6
2.1.1 Atherosclerosis.....	6
2.1.2 Shear Stress Affects Atherosusceptibility by regulating Endothelial Permeability and Gene Expression	10
2.1.3 Shear Stress Alteration and the Adaptive Responses of Endothelial Cells.....	15
2.2 Related in vivo Studies	16
2.3 Rationale for Research Design of the in vitro Studies	23
3. The Adaptive Dynamics of Endothelial Permeability	26
3.1 Experimental Design.....	26
3.2 Materials and Methods	28
3.2.1 Flow Circuit and Apparatus Design for Permeability Studies	28
3.2.1.1 Design of Flow Circuit	29
3.2.1.2 Design of the Two-chamber Permeability Apparatus	32

3.2.2 Optical-Fiber Based Fluorescence Detection System.....	35
3.2.3 Cell Culture	41
3.2.4 Permeability Experiments	42
3.2.5 Data Processing.....	44
3.3 Results	45
3.3.1 Endothelial Permeability in Response to Elevated Shear Stress Magnitude	45
3.3.2 Endothelial Permeability in Response to Elevated Shear Stress Frequency	47
4. The Adaptive Dynamics of Endothelial Transcriptional Regulation	50
4.1 Experimental Design.....	50
4.2 Materials and Methods	52
4.2.1 Design of Flow System and Laminar Flow Chamber	52
4.2.2 Cell Culture	58
4.2.3 Shear Stress Experiment	58
4.2.4 RNA Isolation and Microarray Protocol	59
4.2.5 Microarray Data Analysis	61
4.2.5.1 Preprocess	61
4.2.5.2 Identify differentially expressed genes and other basic analysis.....	62
4.2.5.3 Gene Ontology and network analysis.....	63
4.2.5.4 Gene Set Enrichment Analysis	63
4.2.6 Real-time quantitative-PCR	65
4.3 Results	66

4.3.1 Endothelial Gene Expression under Basal Level Shear Stress for 24 hours and 30 hours.....	66
4.3.2 Endothelial Gene Expression in Response to the Elevated Shear Stress Magnitude	69
4.3.2.1 Differentially Expressed Genes Identified at Each Time Point	69
4.3.2.2 Expression of an <i>a-priori</i> Selection of Atherosclerosis-related Shear-Sensitive Genes.....	90
4.3.2.3 Global Gene Expression Profiles during Adaptation	94
4.3.2.4 Gene Ontology and Gene Functional Analysis	101
4.3.3 Endothelial Gene Expression in Response to the Elevated Shear Stress Frequency	105
4.3.3.1 Differentially Expressed Genes Identified at Each Time Point	105
4.3.3.2 Expression of an <i>a-priori</i> Selection of Atherosclerosis-related Genes	118
4.3.3.3 Global Gene Expression Profiles during the Adaptation.....	120
4.3.3.4 Gene Ontology and Gene Functional Analysis	122
4.3.4 Gene Expression Validated by Real-time Quantitative PCR	125
5. Discussion	130
5.1 The response of endothelial permeability to altered shear stress.....	130
5.2 The response of endothelial gene expression to altered shear stress.....	134
5.3 Future Work	139
References	143
Biography.....	158

List of Tables

Table 1: Regulation of endothelial gene expression by shear stress.	14
Table 2: No. of s.d.e genes at 45 minutes, at 180 minutes, and for all three time points combined.	19
Table 3: Expression of the selected genes that are relevant to atherogenesis.	20
Table 4: Gene sets enriched in GESA. red: up-regulated, green: down-regulated	22
Table 5: The summary of collected samples for microarray experiments	61
Table 6: Primers for real-time quantitative-PCR	65
Table 7: The numbers of identified genes in the control study.	67
Table 8: The numbers of identified genes at different time points in the magnitude step-up experiment.	70
Table 9: List of genes identified at different time points in the magnitude step-up experiments.	71
Table 10: The expression of <i>a-priori</i> selected genes in response to the elevated shear stress.	93
Table 11: The numbers of identified genes at different time points in the frequency step-up experiment.	106
Table 12: List of genes identified at different time points in the frequency step-up experiments.	107
Table 13: The expression of <i>a-priori</i> selected genes in response to the elevated shear stress frequency.	119

List of Figures

Figure 1: Major stages in the development of atherosclerosis.....	8
Figure 2: Configurations of animal experiments.....	18
Figure 3: qPCR measurement of eNOS and KLF2 expression levels.....	20
Figure 4: Cellular functions and pathways identified to be altered in the adaptive response <i>in vivo</i>	21
Figure 5: Schematic of the experimental design of the <i>in vitro</i> studies.	25
Figure 6: Schematic of the flow circuit for permeability measurement.	30
Figure 7: Schematics of custom designed flow dampener (left) and separator (right) with 3D representations.	30
Figure 8: Photograph of the flow circuit for permeability studies assembled inside a cell culture incubator.	32
Figure 9: Schematic and 3D AutoCAD design of the permeability apparatus	34
Figure 10: Schematic of the light path of the fluorescence detection system.	36
Figure 11: Photograph of the fluorescence detector.....	38
Figure 12: Schematic of LED control and virtual lock-in amplifier.	39
Figure 13: Measurement of a series dilution of FITC-BSA solution..	41
Figure 14: A typical concentration measurement plot.....	45
Figure 15: Plot of endothelial permeability during the adaptive response to elevated shear stress magnitude.....	47
Figure 16: Plot of endothelial permeability during the adaptive response to elevated shear stress frequency.	49
Figure 17: Sampling schedule for gene expression studies.....	51

Figure 18: Schematic of flow circuit for transcriptional studies.....	54
Figure 19: Photograph of flow circuit for transcriptional studies.....	55
Figure 20: Schematic and 3D design of the laminar flow chamber.....	56
Figure 21: Venn diagram displaying the overlap of genes identified at 24 hours and 30 hours.	67
Figure 22: The scatter plot of gene expression profiles.....	68
Figure 23: Venn diagram displaying the overlap of genes identified in the magnitude step-up study and control study.....	70
Figure 24: The top ranked gene network generated by IPA from genes identified in the magnitude step-up experiment.....	75
Figure 25: Expression profiles of the selected genes in the magnitude step-up study.	86
Figure 26: Identified genes clustered to show the temporal gene regulation profiles.	89
Figure 27: Statistic summary of the transcriptional profiles at each time points.....	95
Figure 28: Matrix of scatter plots to compare the global expression profiles between different time points..	99
Figure 29: Clustering and principal component analysis of all genes.....	100
Figure 30: Principal component analysis.....	101
Figure 31: GeneGo identified pathways and cellular processes that are sensitive to the elevated shear stress magnitude.....	104
Figure 32: Venn diagram displaying the overlap of genes identified in the frequency step-up, magnitude step-up and control study.....	106
Figure 33: Gene network and clustering heat map generated from the identified genes in the frequency step-up study.....	110
Figure 34: Expression profiles of the selected genes in the frequency step-up study.....	117

Figure 35: Matrix of scatter plots (a) and hierarchical clustering (b) to compare the global expressional profiles between different time points in the shear stress frequency step-up experiments. (c) Statistic summary of the expression values at each time point.....	121
Figure 36: GeneGo identified pathways and cellular processes that are sensitive to the elevated shear stress frequency.....	124
Figure 37: Real-time PCR validates the microarray results of the magnitude step-up experiments.....	128
Figure 38: Real-time PCR validates the microarray results of the frequency step-up experiments.....	129
Figure 39: Plot of function δ in the mathematical model predicting endothelial permeability alteration in response to an acute increase in shear stress magnitude <i>in vivo</i>	133
Figure 40: Heat map of the expression values of the genes that were sensitive to both the preconditioning and elevated shear stress	138

Acknowledgements

I would like to thank my advisor and dissertation committee chair, Dr. Morton Friedman, for his guidance with my project and for years of support and advice. I would also like to thank my dissertation committee members Drs. George Truskey, Nenad Bursac, Jeffrey LaMack and Chris Kontos for their valuable insight and assistance with my research.

I would like to thank all my lab mates in the Duke Cardiovascular Simulation Laboratory for their help and advice throughout the years. In particular, I would like to acknowledge Drs. Heather Himburg, Jeff LaMack and Steve Wallace, who trained me numerous experimental techniques, from cell culturing to qPCR, and assisted me with the design of the flow circuits and flow chambers. I would also like to thank Ellen Dixon-Tulloch, Dr. Kelley Burrige, Amanda Basciano and Wei Huang for assistance with animal experiments.

Finally, I would like to extend my heart-felt appreciation to my wife Xin Tu and my parents Huizhen Wang and Shengyang Zhang, for their love and support throughout my time in graduate school.

1. Introduction

1.1 Objective, Hypothesis and Specific Aims

The response of vascular endothelial cells to changes in hemodynamic forces is an essential component of normal endothelial physiology, since local shear stress can be altered *in vivo* occasionally by the global hemodynamic changes that are caused by daily activities, such as exercise, sleep, smoking and stress. The duration of these changes ranges from minutes to hours. When adapting to the altered shear stress, endothelial cells may undergo a series of structural remodeling and morphological changes, and a transient alteration of endothelial phenotype may be induced. An understanding of the transient regulation of endothelial phenotype will not only improve our knowledge of normal endothelial physiology but also yield new insights into the mechanism of atherogenesis.

The objective of this research is to characterize the adaptive response of arterial endothelial cells to changes in hemodynamic shear stress in well-defined *in vitro* settings. We seek to dissect the adaptive dynamics at a fine temporal resolution. Of particular interest is to determine how the adaptive response affects endothelial permeability and inflammatory status, thus altering the arterial atherosusceptibility.

The central hypothesis is that endothelial cells exhibit a specific phenotype during the adaptive response to changes in local hemodynamic forces; furthermore, such a phenotype is different than that of fully-adapted endothelial cells and may alter

arterial atherosusceptibility. In this study, we hypothesize that in response to changing shear stress:

1. An acute increase in endothelial permeability will occur when endothelial cells begin cytoskeletal reorganization and junctional remodeling, and then the permeability will gradually decrease to baseline levels when the cells are adapted.
2. The endothelial transcriptome will be tightly regulated with different genes/pathways being turned on/off sequentially to orchestrate the adaptive response; inflammatory, oxidative and other stress response pathways will be transiently altered in this process, in ways that, *in vivo*, would affect arterial atherosusceptibility. Furthermore, the expression profiles during adaptation will bear little resemblance to those of fully-adapted endothelial cells.

Two specific aims were proposed in this study to test these hypotheses:

Specific Aim #1: Characterize the adaptive dynamics of endothelial permeability in response to hemodynamic changes in well defined *in vitro* settings. A

custom-designed laminar flow chamber system was used to generate precisely-controlled flow environments and shear alterations. Confluent endothelial monolayers were pre-conditioned at a basal level shear stress of 15 ± 15 dynes/cm² at 1 Hz until

they were fully-adapted, and then exposed to new shear stress profiles: 30 ± 15 dynes/cm² at 1 Hz or 15 ± 15 dynes/cm² at 2 Hz. The endothelial permeability was documented with fine temporal resolution before and after the shear stress alteration by measuring transendothelial flux of fluorescence-labeled bovine serum albumin (BSA). This study revealed the adaptive dynamics of endothelial permeability and tested the first hypothesis.

Specific Aim #2: Dissect the molecular mechanism of endothelial adaptation to hemodynamic changes by measuring global transcriptional profiles. To understand the underlying molecular events during adaptation, the transcriptional profiles of cells harvested from the flow chamber were measured using DNA microarrays and real-time quantitative PCR (qPCR). Similar to Aim 1, endothelial cells were exposed to the basal level shear stress and then an altered shear stress was applied. The endothelial cells were sampled and subjected to gene expression assays at multiple time points, covering the acute response phase and prolonged adaptation period. The focus was to investigate the effect of hemodynamic changes on the regulation of genes that are essential in atherogenesis, such as cellular structure, junction/adhesion, inflammatory response and oxidative stress related genes. This study provided a detailed temporal map of endothelial transcriptional activity during the adaptation process. Comprehensive bioinformatics methods and data mining tools, such as gene ontology/pathway analysis and gene set enrichment analysis, were used to compare the adaptive transcriptional

profiles with other shear-dependent endothelial gene expression data obtained in our laboratory and in the literature. The results were used to identify critical genes and pathways involved in the endothelial adaptive response, and tested the second hypothesis.

This study will increase our understanding of the cellular and molecular responses of vascular endothelial cells to normal diurnal shear stress variations, and provide insights into possible mechanisms by which these alterations affect the atherogenic process.

1.2 Dissertation Structure

This dissertation is organized into the following chapters:

- Chapter 2 summarizes the literature and background that are relevant to this dissertation. The related *in vivo* animal studies, carried out in our laboratory by the author and colleagues, are then discussed in detail. Finally, the rationale of the *in vitro* study is discussed.
- Chapter 3 presents the *in vitro* permeability study. The design and development of a small-perfusion-volume flow circuit, permeability apparatus and fluorescence detection system are introduced. The results reveal the adaptive dynamics of endothelial permeability in response to increased shear stress magnitude and frequency.

- Chapter 4 presents the *in vitro* transcriptomic studies. The design and development of a multichannel flow circuit and flow chambers are introduced. Microarray, real-time qPCR and bioinformatics methods used in this study are then described. The results provide a detailed temporal map of endothelial transcriptional activity during the adaptation process.
- In Chapter 5, we compare our *in vitro* findings to the previous *in vivo* results and other relevant studies in the literature. The significance of this study is discussed, and recommendations for future research are proposed.

2. Background and Related Studies

Atherosclerosis is a complex cardiovascular disease of great clinical importance. Its progression involves the transport of pro-atherogenic and anti-atherogenic molecules across the endothelium and the inflammatory response of the endothelial cells. Shear stress applied on the endothelial cells by flowing blood can regulate both processes. In this chapter, we first discuss the pathogenesis of atherosclerosis, the role of shear stress in atherogenesis and the importance of the endothelial adaptive response to altered shear. The related *in vivo* studies carried out in our laboratory are then introduced.

2.1 Background

2.1.1 Atherosclerosis

Atherosclerosis is a disease of large arteries characterized by the accumulation of lipids within the artery wall and intimal lesions. In atherosclerosis, localized plaques called atheromas, or fibrofatty plaques, protrude into and obstruct the vascular lumen, and thus reduce blood flow [1]. The atheromas also provide sites for thrombus formation, which can significantly occlude the blood supply to an organ. For example, if a blood clot blocks the right coronary artery, which supplies blood primarily to the right side of the heart, it can cause angina pectoris (chest pains) or myocardial infarction (heart attack).

Atherosclerosis is the most common cause of heart attacks and strokes, and accounts for 75 percent of deaths due to cardiovascular disease in the United States [2]

and 50% of all mortality in the United States, Europe and Japan [1]. This disease is discussed in the context of human physiology [1] pathology [3] and molecular biology [2]. Here, we give a brief background review on the pathogenesis of atherosclerosis.

Artery Structure

The wall of a human artery consists of three distinct layers (Figure 1a): they are, from innermost to outermost, the intima, media and adventitia. The intima consists of a single layer of endothelial cells, the endothelium, and underlying subendothelial connective tissue. Endothelial cells serve as the interface between the blood flow and the vessel wall. The intima is separated from the media by the internal elastic lamina, which is a layer of elastin fibers [1]. The media is made up of mainly smooth muscle cells, which control the diameter of the vessel lumen and thus influence blood pressure [2], and a combination of elastin and collagen connective tissue. The adventitia is composed of connective tissues. The intima and media are more important in the development of atherosclerosis.

Atherogenesis

Atherosclerosis is related to a number of factors. Immutable risk factors in an individual include age, sex and heredity. Other risk factors, especially diet, life style, and personal habits, can be controlled [3]. The four major mutable risk factors are hyperlipidemia (high blood cholesterol), hypertension (high blood pressure), cigarette

smoking and diabetes [3]. The various risk factors imply that the cause of atherosclerosis is complicated.

The clinical significance of the disease has stimulated enormous efforts to discover the cause. Although atherogenesis is not fully understood, the response-to-injury hypothesis is currently favored [3]. It was proposed by Ross as early as 1973 and has developed over the last 30 years [4, 5].

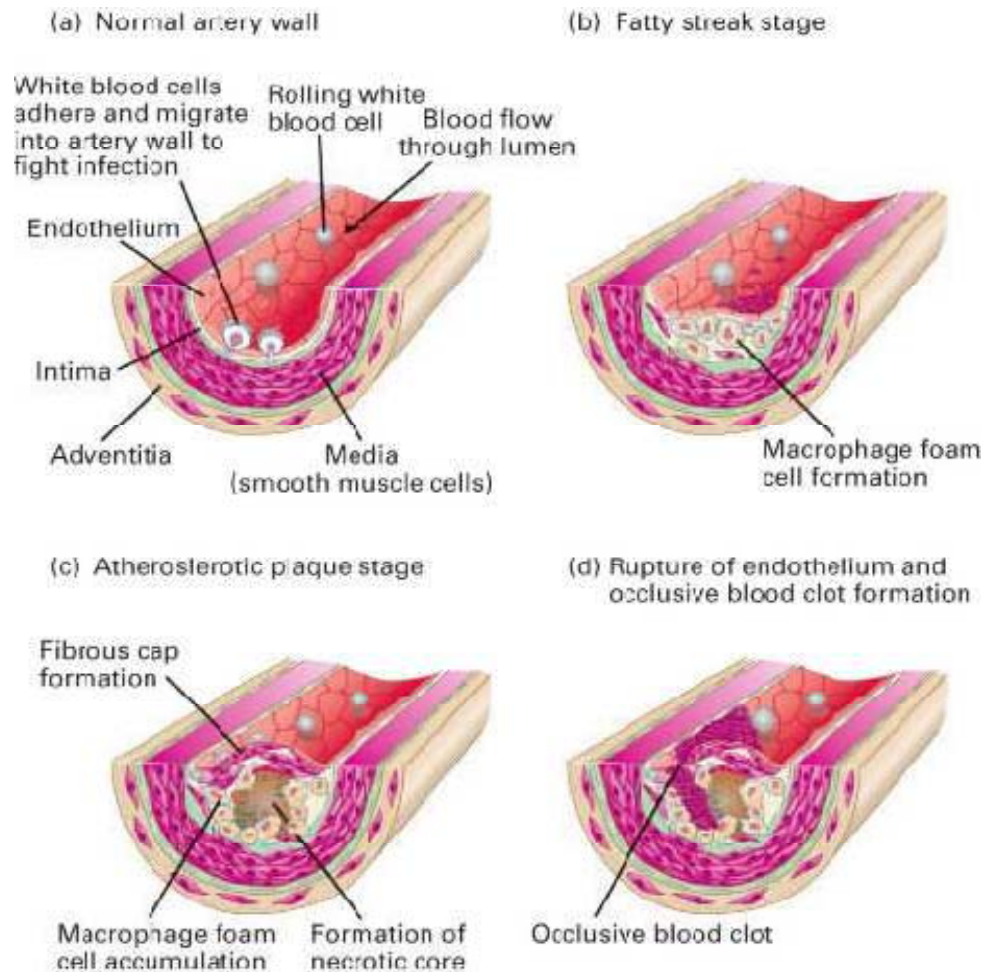


Figure 1: Major stages in the development of atherosclerosis. See text for details. (From [6] with permission)

Figure 1 illustrates the progression of atherosclerosis in the artery wall. Under normal circumstances, the plasma and blood cells flow over the endothelium, and endothelial cells serve as a barrier between blood and the arterial wall. According to the response-to-injury hypothesis, the first step in atherosclerosis is endothelial dysfunction [5]. It is believed that some type of chronic damage to endothelial cells leads to endothelial cell dysfunction which initiates atherosclerosis. Possible causes of this dysfunction under investigation include elevated plasma lipids, toxins from cigarette smoking, hypoxia and hemodynamic forces [3, 5]. Endothelial dysfunction results in increased endothelial permeability to macromolecules, enhanced leukocyte adhesion and alterations in endothelial gene expression [3]. As a result, blood-borne lipoproteins, mainly low-density-lipoprotein (LDL) with high cholesterol, are transported across endothelial cells into the intima and accumulate there. Blood monocytes and other leukocytes then adhere to endothelial cells and migrate into the intima in response to the injury, together with the adhesion of platelets to the injured endothelial cells [3]. In the intima, monocytes differentiate into macrophages. Macrophages engulf substantial amounts of cholesterol from lipoproteins deposited in the intima, in which case they become foam cells as shown in Figure 1b. This is the first unique step in atherosclerosis and the lesion is known as a fatty streak. Activated platelets, macrophages and vascular cells secrete proteins and growth factors that help recruit additional monocytes and other immune cells [2] from blood flow and smooth muscle cells from media into the

intima. Smooth muscle cells further proliferate and secrete extracellular matrix in the media. Some SMCs take up lipoprotein cholesterol and also become foam cells [2]. At this stage, a necrotic core of lipids is formed under a fibrous cap of smooth muscle cells and matrix (Figure 1c). As lipids further accumulate, both within cells and extracellularly, the lesion may grow large enough to intrude into the lumen and block the blood flow as shown in Figure 1d.

To summarize, atherosclerosis is a chronic inflammatory disease [5] that is a consequence of normal physiological inflammatory response to endothelial injury [2]. The response-to-injury theory includes most risk factors in the hypothesis, and is widely accepted.

2.1.2 Shear Stress Affects Atherosusceptibility by regulating Endothelial Permeability and Gene Expression

As discussed previously, it is generally believed that the initiation of atherosclerosis starts from endothelial cell dysfunction [5]. Endothelial dysfunction is a complex process, featuring increased permeability to macromolecules, enhanced leukocyte adhesion and expression of adhesion molecules, enhanced cell turnover, increased oxidant stress and reduced endothelial-dependent vasodilation. In this study, we will focus our research on two important aspects of endothelial dysfunction: alteration of the endothelial permeability and transcription activities, especially the expression of inflammatory and oxidative genes.

Increased endothelial permeability leads to the accumulation of LDL in the intima, which is a key step in atherosclerotic development. The inflammatory response of endothelial cells results in the recruitment of monocytes, which will migrate into the intima, differentiate into macrophages, then engulf oxidized LDL and finally form foam cells. The accumulation of foam cells in the subendothelial intima is the basis for the formation of atherosclerotic plaques. Therefore, endothelial permeability and inflammatory status greatly affect arterial atherosusceptibility.

Endothelial cells in the vasculature are constantly exposed to shear stress, the frictional force from blood flow. There is substantial evidence for a great effect of shear stress on endothelial phenotype and functions, such as production of nitric oxide, secretion of growth factors, inflammatory responses, production of reactive oxygen species (ROS), permeability and cytoskeleton remodeling [7-11].

Shear-dependent permeability to macromolecules has been examined both *in vitro* and *in vivo*. The application of shear stress to static cultured cells increased endothelial permeability to albumin [12] and dextran [13]. However, the increases are more likely caused by the transient response of endothelial cells to the onset of shear, since other *in vitro* studies suggested that decreased permeability is associated with higher shear stress under a relatively long term shear exposure [14, 15]. This was further demonstrated by Warboys et al. [16]. They discovered that acute exposure (1 hour) to shear stress increased porcine endothelial permeability to albumin but chronic exposure

(7 to 9 days) reduced the permeability *in vitro*. Conklin et al. showed that endothelial permeability to 20 nm gold particles was increased under lower shear stress using *ex vivo* cultured arteries [17]. Himburg et al. [18] demonstrated that endothelial permeability to albumin *in vivo* decreases with increasing time-average shear stress in porcine iliac arteries. Several other shear stress parameters, such as spatial gradients [19, 20], were also correlated with endothelial permeability *in vivo*. Although the exact mechanism is still under investigation, it has been suggested that shear stress affects macromolecular permeability through regulating endothelial junction proteins, such as occludin, ZO-1 [15, 17, 21] and claudin-5 [22]. Several signaling pathways, such as PAK [23], Rho, Rac [24] and PI3K-NO-cGMP [16] were also suggested to participate in the mediation of permeability [25] by shear stress.

Endothelial transcriptional activities are also tightly regulated by shear stress. Although the mechanism of endothelial mechanotransduction is not fully understood, a large number of signaling cascades have been found to be induced by shear stress, which include ion channels (K^+ and Ca^{+2}), Rho family GTPases, the activation of MAPK, PKC, Erk, FAK and JNK pathways and the activation of transcriptional factors AP1 and NF κ B [7-11, 24]. As a result, a significant number of downstream genes are regulated by shear stress, including eNOS [11, 26, 27], MCP1 [28, 29], KLF2 [27, 30], MnSOD [31], NADPH oxidase [28, 32], ET1 [33, 34] etc. The endothelial transcriptional regulations are sensitive to many parameters of shear stress profile, including shear stress magnitude

[35], frequency [36], temporal [37] and spatial [38] gradient and flow reversal [36].

Prolonged unidirectional shear stress is believed to be atheroprotective since it increases endothelial anti-inflammatory (e.g. upregulation of KLF2 [27, 30], downregulation of VCAM1 [39]) and anti-oxidative mechanisms (e.g. upregulation of MnSOD [31] and PRX1 [40], downregulation of NADPH [28, 32]). On the other hand, disturbed shear stress, e.g. oscillatory shear, promotes a pro-inflammatory endothelial phenotype by upregulating many inflammatory adhesion molecules, such as ICAM1 [29, 41, 42], VCAM1 [41, 42], P-selectin [29] and E-selectin [42]. Disturbed flow also upregulates the expression of BMP4 [43] and NADPH oxidase [28, 44], thus increasing endothelial oxidative stress. Overall, endothelial transcriptional regulation is highly sensitive to local shear stress profiles. Disturbed flow induces an atherosclerosis-prone phenotype of endothelial cells, while unidirectional shear stress provides an atheroprotective environment.

Table 1 is a collection of genes that are sensitive to shear stress. This list is for reference and by no means a complete list. Literature discussing the function of each gene and its expression regulation by shear stress was cited in the table.

Table 1: Regulation of endothelial gene expression by shear stress.

	Unidirectional high shear stress	Disturbed shear stress
Inflammatory and adhesion genes		
ICAM1	↓ [45] Inflammatory adhesion molecule [46-49].	↑ [29, 41, 42]
VCAM1	↓ [27, 45] Inflammatory adhesion molecule [46-49].	↑ [41, 42, 45]
CCL2	↓ [45, 50] biphasic [51] MCP1, inflammatory molecule [47-49].	↑ [45]
SELP	Adhesion molecule, P-selectin.	↑ [29]
SELE	↓ [45] Adhesion molecule, E-selectin [46-49].	↑ [42, 45]
JUN	LSS: ↓ [36] c-jun gene, activating protein-1, inflammatory [52, 53].	
KLF2	↑ [27, 54] Inflammatory regulation transcription factor [54-56].	
KLF4	↑ [57, 58] Inflammatory regulation transcription factor [57].	
BMP4	↓ [50, 59] Activates inflammatory [43, 60].	↑ [45]
NFKBIA	↓ [61] NFκB inhibitor, IκBα [47-49].	
IL8	↑ [62, 63] Inflammatory chemokine [47-49].	
Vasomotion		
NOS3	↑ [27] eNOS [11, 26].	
EDN1	↓ [50, 64] Endothelin-1 [26].	↑ [65]
Caveolin-1	↓ [27, 50, 59, 66] Caveolin-1 [11, 26].	
COX-1	↑ [67] Cyclooxygenase-1	
Oxidative state regulators and cytoprotective genes		
HMOX1	↑ [50] anti-oxidative, cytoprotective and anti-inflammatory gene [68, 69].	
GADD45β	↑ [70] or slightly ↓ [31] cytoprotective gene [31].	
SOD1	↑ [50] Cu/ZnSOD [68, 69].	
SOD2	↑ [27] cytoprotective, MnSOD [31].	↓ [45]

NAD(P)H	↑[71]	↑[28, 44]
	Oxidative state regulator.	
PRX1	↑[40]	
	peroxiredoxin-1[40]	

2.1.3 Shear Stress Alteration and the Adaptive Responses of Endothelial Cells

Endothelial permeability and transcriptional activities, two important factors in atherogenesis, are tightly regulated by the local shear stress. Endothelial cells *in vivo* are believed to adapt to the local hemodynamics, at least in the regions with unidirectional flow [10], to have a quiescent phenotype. However, the local shear stress profiles are not invariant over time and they are altered occasionally by changes in the global hemodynamic variables, such as heart rate and flow rate. These changes are caused by a number of normal physiologic events, such as exercise, smoking, sleep, stress, and digestion. The duration of these changes ranges from minutes to hours, and endothelial cells undergo structural remodeling and phenotypic transformation in order to adapt to the altered shear stress. During the adaptive response, endothelial permeability and gene expression will be affected dynamically, adding a new dimension to the endothelial response to shear stress. It is reasonable to expect that some previously established regulatory patterns *in vivo*, i.e. the dependences of endothelial permeability and transcription on shear profiles, may not be applicable to the dynamically-controlled adaptive response.

2.2 Related *in vivo* Studies

In an effort to understand the dynamics of the adaptation of endothelial permeability, shear stress levels in porcine iliac arteries were altered by opening and closing downstream arteriovenous femoral shunts; albumin uptake was found to be significantly increased only when the duration of alterations was greater than one minute [72]. An *ad hoc* mathematical model of adaptation developed by Friedman et al. [72] and Hazel et al. [73], was used to fit the albumin uptake data. The mathematical model predicted that endothelial permeability increases transiently in response to an acute increase in shear stress *in vivo*. Endothelial permeability peaks at around 7 minutes, and has a time constant of 90 minutes for the adaptive response. Although further studies are desirable to dissect the adaptive dynamics and validate the model by directly measuring the permeability alteration, this intriguing result suggested that increases in local shear stress can transiently increase endothelial permeability with a physiologically relevant time scale and thus provide an opportunity for macromolecules like LDL to penetrate the endothelium in greater quantity and accumulate in the intima. This result leads us to believe that the transient phenotypic alteration accompanying global hemodynamic change plays a role in endothelial pathophysiology and can be an important factor responsible for arterial atherosusceptibility.

To understand the adaptive response of endothelial transcriptome *in vivo*, we have conducted a series of studies using swine as an animal model. As illustrated in

Figure 2, stainless steel shunts (shown in brown) were installed as short-circuits to connect the femoral artery and femoral vein on both sides. Blood flow rates were monitored by volumetric ultrasonic flow meters and the pinch valves on the tubing were used to maintain the baseline femoral flow rates after shunting. To induce the adaptive response, the shear stress in one of the external iliac arteries (step-up side) was increased by opening the ipsilateral femoral shunt. The flow rate through the shunt was set to around three times the baseline level, which approximately doubled the flow rate in the external iliac artery [74]. The flow rate in the opposite side was maintained at the baseline level as a control. Previous studies [18, 75, 76] in our laboratory have characterized the baseline hemodynamic environment in the external iliac arteries and suggested a mean shear stress of around 15 dynes/cm². Thus, the shear stress in the step-up side external iliac was about 30 dynes/cm².

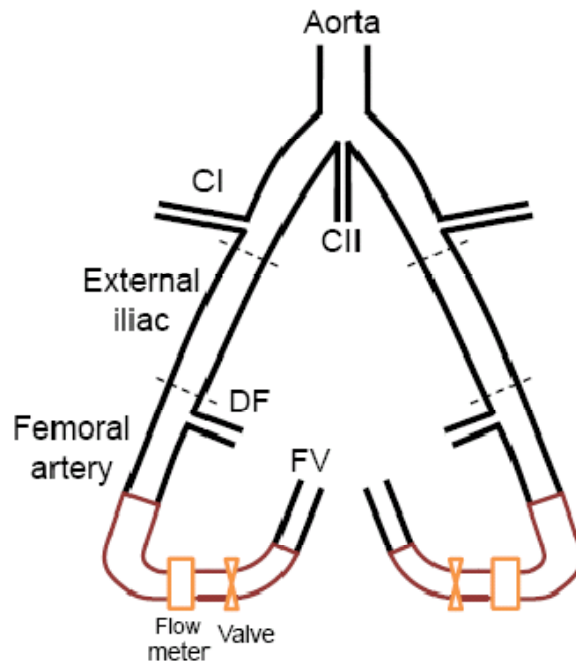


Figure 2: Configurations of animal experiments. CI: circumflex iliac artery, CII: common internal iliac artery, DF: deep femoral artery, FV: femoral vein.

Animals were sacrificed at 45 minutes (n=6), 90 minutes (n=3) and 180 minutes (n=6) after shear stress was increased. Both iliac arteries were immediately harvested, and endothelial RNA were extracted, amplified and hybridized to *Sus Scrofa* DNA microarrays (Operon). For each gene, the expression value on the step-up side was normalized by that on the corresponding control side. Table 2 summarizes the numbers of significantly differentially expressed (s.d.e) genes identified by GeneSpring (Agilent) using the t-test, for two p-values. Data at 90 minutes were not used separately due to the limited sample size.

Table 2: No. of s.d.e genes at 45 minutes, at 180 minutes, and for all three time points combined.

No. of s.d.e. genes	p<0.05		p<0.005	
	up	down	up	down
45' n=6	101	88	15	3
180' n=6	177	140	24	18
All time points n=15	170	120	16	8

Several interesting genes appeared in the lists, such as eNOS, fibronectin, integrins, junctional proteins, and members of the NF κ B family and inhibitors. The direction of regulation of these genes is given in Table 3. Quantitative PCR (qPCR) was carried out to confirm the expression values of eNOS and KLF2, as shown in Figure 3.

However, to generate candidate gene lists for discovery studies, the use of a false discovery rate is preferred [77, 78]. When the false discovery rate was controlled at 5%, no gene was identified by any of these tests. This suggests that the variation of the endothelial adaptive response among individual animals was significant. This large variability may come from the differences in basal transcriptional levels and basal hemodynamics among animals. Variability in the magnitude and duration of shear increases, which could not be exactly controlled in these animal experiments, can also be a source of noise.

Table 3: Expression of the selected genes that are relevant to atherogenesis.

	45 minutes	180 minutes
eNOS	-	↑
HMOX1	↑	-
KLF2	↑	↑
VE-cadherin	-	↑
zona occludens 2	↑	↑
Integrin α 3	↓	-
Integrin α 5	-	↑
Fibronectin 1	-	↑

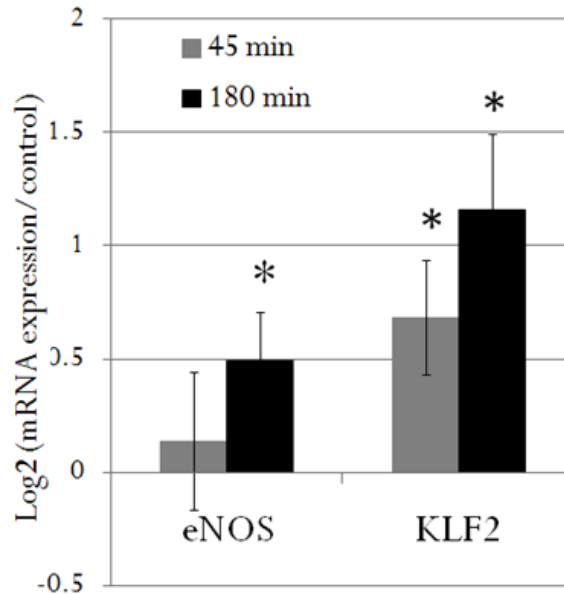


Figure 3: qPCR measurement of eNOS and KLF2 expression levels. N=6 for each bar. Expression values were normalized to the corresponding control. *: p<0.05; error bars: standard error of the means.

Since the strict tests with FDR control failed to identify any s.d.e gene at the sample size employed here, individual genes in Table 2 cannot be regarded as candidate

genes. However, these genes can be used for gene ontology (GO) and functional analysis, where the entire list of genes, instead of an individual gene, is used. Ingenuity Pathway Analysis (IPA) was used to perform the functional analysis. As indicated in Figure 4, the molecular and cellular functions involved at two time points seems to converge: every function identified at one time point is also significantly regulated at the other time point. Cell morphology and lipid metabolism functions are on the top five lists at both time points (although the specific genes are not exactly the same). Several canonical pathways were identified with a clear time-dependent pattern. Among the ten pathways, only three are significantly regulated at both time points. Four pathways, which are known to be shear-stress sensitive [9, 10], were identified as significantly regulated, i.e. integrin signaling, p38 MAPK at 45 minutes and PI3K/AKT, VEGF signaling at 180 minutes.

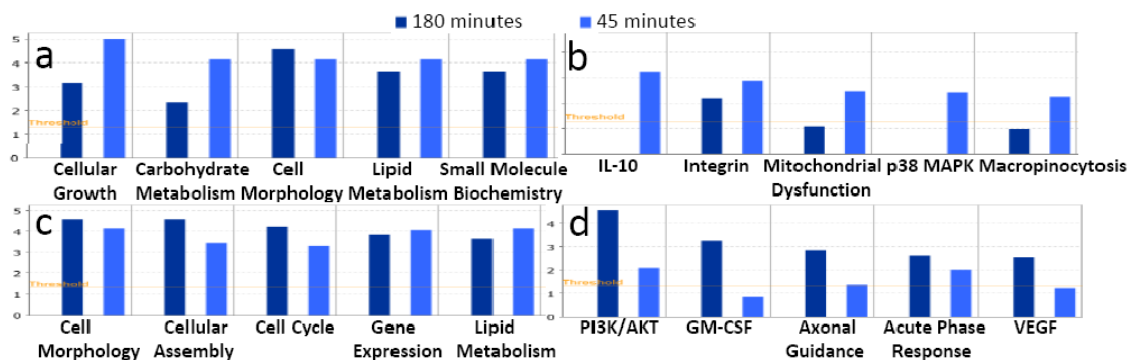


Figure 4: Cellular functions and pathways identified to be altered in the adaptive response *in vivo*. (a) Top five cellular functions identified at 45 minutes ranked by their p-values (light blue bars). The p-values of the same functions at 180 minutes are also plotted (deep blue bars). (b) Top five pathways identified at 45 minutes ranked by their p-values. (c) Top five cellular functions identified at 180 minutes. (d) Top five pathways identified at 180 minutes. Y: $-\log(p\text{-value})$, orange threshold line has a p-value of 0.05.

A genome-wide investigation was further performed using Gene Set Enrichment Analysis (GSEA, Broad Institution MIT [79]). Instead of using selected lists of genes, GSEA utilizes the transcriptional levels of all genes in the array, thus bypassing the FDR control for individual genes, to determine whether specific a priori defined gene sets/pathways are significantly regulated. Two *a priori* defined gene sets, Biocarta pathways and biological process GO, were obtained from MSigDB (Broad Institution MIT, [79]). Using a suggested FDR cutoff of 25%, the enriched gene sets/pathways were identified and are shown in Table 4. Three shear-stress sensitive pathways, Rho [24], Wnt [80], NO1 [81], were up-regulated at both time points, suggesting their prolonged involvement in the adaptive response.

Table 4: Gene sets enriched in GSEA. red: up-regulated, green: down-regulated

Biocarta pathways	45'	Rho, EIF4, Wnt, NO1, fMLP, TCR and AT-1R pathways
	180'	Wnt, Rho, NO1, CARM, p38 MAPK and MAPK pathways
Bioprocess GO	45'	Cell-matrix adhesion, Cell-substrate adhesion, immune-system development, organ morphogenesis
	180'	Translation, Cellular biosynthetic process

Although the *in vivo* studies revealed interesting patterns of endothelial transcriptional regulation in response to increased shear stress, the inherent noise and variability of the *in vivo* studies make it difficult to pinpoint the critical genes and pathways involved in the adaptation process. Without FDR control, any interpretation of individual gene regulation will be only suggestive and inconclusive; discovery

studies cannot be carried out with great confidence. The animal surgery procedure also limited the ability to probe the early adaptation events, which are expected to be more informative since (1) the adaptation model [73] suggested a permeability peak at around 7 minutes after a shear increase, and (2) a large number of signaling pathways are able to respond rapidly to shear changes [82]. Therefore, a more well-defined study is necessary to confirm the patterns found *in vivo* and to characterize the adaptation responses with better precision and over a broader time range.

2.3 Rationale for Research Design of the *in vitro* Studies

The limitations of the *in vivo* animal study motivated this research project. This study seeks to dissect the adaptive dynamics of endothelial permeability and gene expression in well-defined *in vitro* settings. Although *in vivo* studies provide the most realistic data, *in vitro* flow chamber experiments can offer precisely-controlled flow environments. Different types of shear stress waveforms can be accurately generated and applied to endothelial cells; this is difficult, if not impossible, to do in animal studies. *In vitro* experiments also allow one to sample cells at selected time points and to capture the regulation events occurring in the early stages of the adaptive response. For transcriptomics study, *in vitro* experiments offer the benefit of less experimental variability than that seen in animals.

Figure 5 is the schematic of the experimental design. In both permeability and gene expression studies, endothelial cells were preconditioned at a basal level of shear

stress to reach an adapted state. The preconditioning time was determined experimentally. A changed profile of shear stress was then applied to trigger the adaptive responses. The basal shear stress was a 15 ± 15 dynes/cm² sinusoidal waveform at 1 Hz, which is physiologically relevant both in pig and human and is considered to be a healthy and atheroprotective shear stress profile [8, 10, 75]. Two types of waveforms were applied as altered shear stresses: (1) a magnitude step-up: 30 ± 15 dynes/cm² at 1 Hz; and (2) a frequency step-up: 15 ± 15 dynes/cm² at 2 Hz. These two step-up changes tested the separate responses of endothelial cells to the changes in magnitude and frequency of shear stress. The magnitude step-up experiment is the counterpart to the *in vivo* studies. After the shear stress step-up, endothelial permeability and gene expression were measured at sequential time points. Sampling time points were selected to capture both the rapid changes immediately after step-up and the prolonged process of adaptation.

We conducted all experiments using porcine aortic endothelial cells so that the results can be directly compared to those from the *in vivo* studies. The methods and protocol using porcine endothelial cells had been successfully developed and proven in our laboratory over the years. Furthermore, our laboratory has generated a collection of transcriptional profiles of porcine endothelial cells [36, 83, 84], both *in vitro* and *in vivo* using the same microarray platform, which were used directly for comparisons.

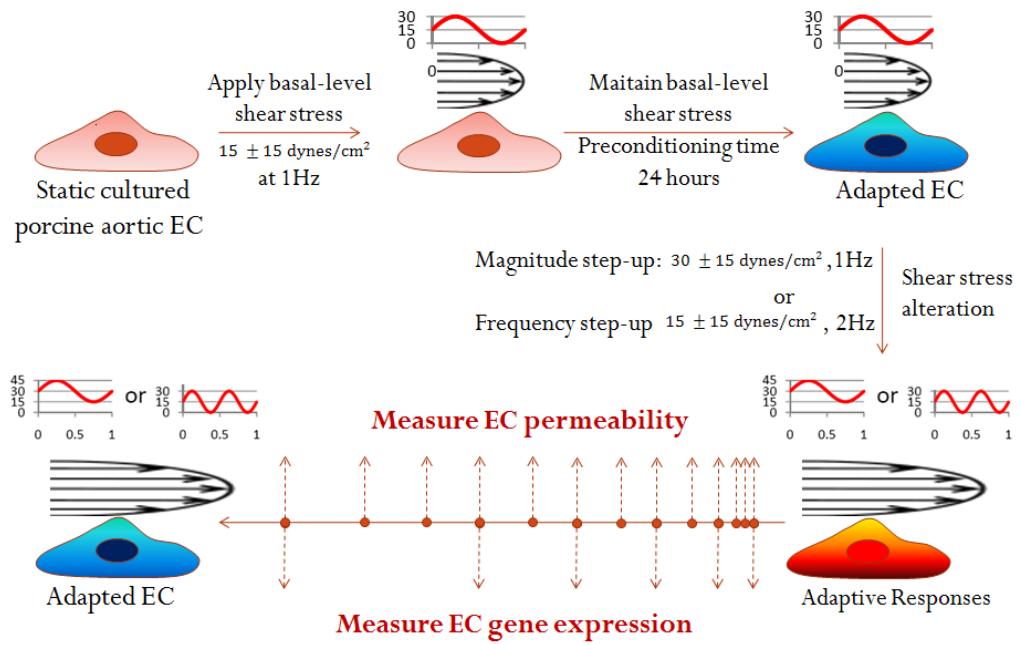


Figure 5: Schematic of the experimental design of the *in vitro* studies.

3. The Adaptive Dynamics of Endothelial Permeability

3.1 Experimental Design

The purpose of this study was to characterize the alteration of endothelial permeability during the adaptive response to changes in shear stress. The protocols to measure the endothelial permeability were developed based on the methods described by Lampugnani et al. (chapter 11 in [85]). Endothelial cells were cultured on a porous membrane inserted inside a custom designed two-chamber laminar flow chamber. The shear stress was applied to the endothelial surface in the luminal (upper) chamber, and fluorescein isothiocyanate-conjugated bovine serum albumin (FITC-BSA) was used as a molecular tracer in the perfusion media. Tracer concentration was measured in the abluminal (bottom) chamber to obtain the transendothelial mass flux. The abluminal chamber was a closed volume so that there was no pressure difference across the endothelium. Thus the convective mass transfer is negligible. The permeability of the membrane is magnitudes higher than the endothelium so its mass-transfer resistance is negligible [85]. We optimized the design of flow circuit to minimize the total volume of the perfusion media so that a higher concentration of molecular tracer can be used for better sensitivity at low cost.

Endothelial cells were cultured under static conditions until fully confluent. Preliminary studies showed confluent endothelial monolayer forms after 36 hours when seeded at 10^5 cell/cm², and the permeability to BSA stays constant after 36 hours at

around 3.5×10^{-6} cm/s up to 4 days. The permeability of static cultured endothelial cells measured in our study is consistent with previous studies [16, 86]. After reaching confluence, endothelial cells were conditioned at the basal level shear stress. The preconditioning time was determined by a pilot study, where the endothelial permeability was measured at 18 hours and 24 hours under basal level shear stress. No difference in permeability was found. This is consistent with a previous study, where endothelial permeability reached a stable level after 12 hours exposure to shear stress [23]. The preconditioning time of 24 hours was thus used in all subsequent permeability experiments. The step-up shear profiles were applied after preconditioning, and the tracer concentration was measured continuously for the first hour, then every 15 minutes for the second hour and every 30 minutes until six hours had elapsed. This sampling schedule was designed to capture the temporal change of permeability at high resolution. After flow experiments, endothelial cells were fixed and carefully examined under microscope for monolayer integrity. Data obtained from defective monolayers were excluded.

Four experiments were performed for each step-up condition. The permeability was calculated at each time point and normalized by the preconditioned value. One-sample t-tests were then used to identify the time points at which the permeability was significantly altered.

3.2 Materials and Methods

3.2.1 Flow Circuit and Apparatus Design for Permeability Studies

To characterize the dynamic adaptive response of the endothelial permeability, a major challenge is to measure endothelial permeability at a high temporal resolution. Previous *in vivo* [73] studies predicted that the permeability peaks at 7 minutes after shear stress step-up. Therefore, it is critical for the designed apparatus to have the ability to probe the permeability changes in a time span of minutes. However, as a natural barrier to bimolecular transport, endothelium has a low permeability to both albumin ($\sim 10^{-6}$ cm/s) and LDL ($\sim 10^{-7}$ cm/s), posing a major challenge to the design of the measurement system.

In the widely-used permeability assay for static endothelial cells (described in [85]), cells are cultured on a porous membrane that defines the luminal and abluminal volumes. The tracer molecules are injected to the luminal side of the membrane, and the concentrations of tracer molecules are measured in the abluminal space. The endothelial permeability, P , can be then calculated as $P = \frac{\Delta C_s}{\Delta t} \times V_s / C_l \times A$, where $\frac{\Delta C_s}{\Delta t}$ is the rate of change in tracer concentration in the abluminal chamber, V_s is the abluminal volume, C_l is the luminal concentration and A is the effective diffusion area of the membrane. The calculated permeability is the time averaged value during the period of Δt , and $C_s \ll C_l$ is assumed. This system can be used in this study when shear stress is applied to the cells. To accurately measure the permeability changes in a high temporal resolution, i.e.

to minimize Δt , high measurement sensitivity can be achieved by maximizing the luminal concentration C_1 and diffusion area A and minimizing the abluminal volume V , given that the measurement sensitivity of ΔC_s is limited by the detection instruments. In this study, both the flow loop and the permeability measurement chamber were designed and optimized to meet these requirements.

3.2.1.1 Design of Flow Circuit

The flow circuit was designed to meet the following criteria: 1. ability to generate a pulsatile flow with controlled mean, frequency and amplitude; 2. rapidly adjustable flow profile for step-up changes; and 3. employ a minimal flow volume.

The flow circuit is illustrated in the schematic Figure 6. The steady mean flow was provided by a peristaltic roller pump (ColeParmer). A dampener was custom designed to eliminate the high frequency pulses generated by the pump, and the liquid volume in the dampener was less than 2 ml. To superimpose the pulsatile flow, a computer-controlled stepping motor (Intelligent Motion System, Marlborough, CT) is used to drive a bellows pump connected to the flow loop. A flow-separation device was designed to separate the fluid in the bellows pump (with a volume of around 40 ml) from the perfusion media in the flow loop. This was achieved by using an enclosed volume of air to transmit the pressure pulse generated by the bellows pump to the flow circuit, thus avoiding the direct mix of fluids. Figure 7 shows the design of the pulse

dampener and flow separator. The dampener and flow separator were fabricated using translucent polycarbonate plastic in the Physics Staff Machine Shop at Duke University.

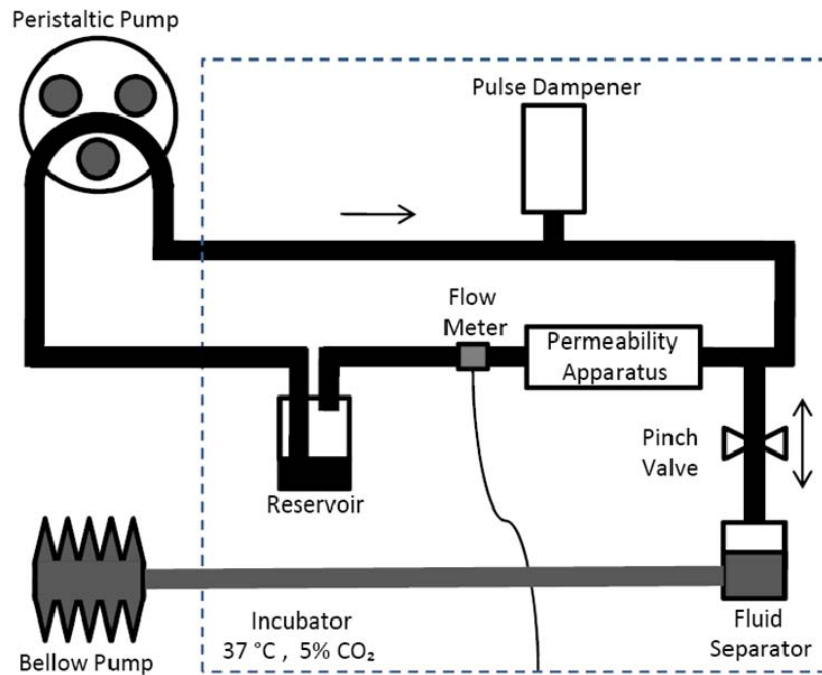


Figure 6: Schematic of the flow circuit for permeability measurement.

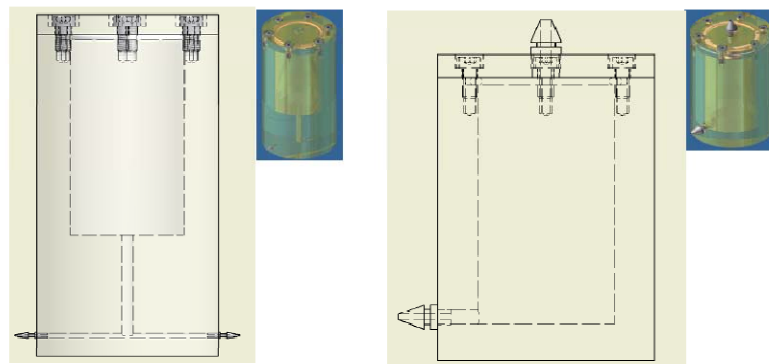


Figure 7: Schematics of custom designed flow dampener (left) and separator (right) with 3D representations.

The volumetric flow rate can be constantly monitored using transonic flow probes (Transonic Systems), which were connected to a computer through a National Instruments data acquisition (DAQ) board (NI PCI-6221). Real-time flow parameters, including mean flow rate, frequency and amplitude, were calculated by a LabView program. In step-up experiments, the peristaltic pump was adjusted to double the mean shear stress, and the step motor was reprogrammed to double the frequency. The flow circuit was placed in a cell culture incubator at 37 °C and 5% CO₂ during experiments. Figure 8 shows the photograph of the flow circuit assembled inside the incubator, with only pumps left outside.

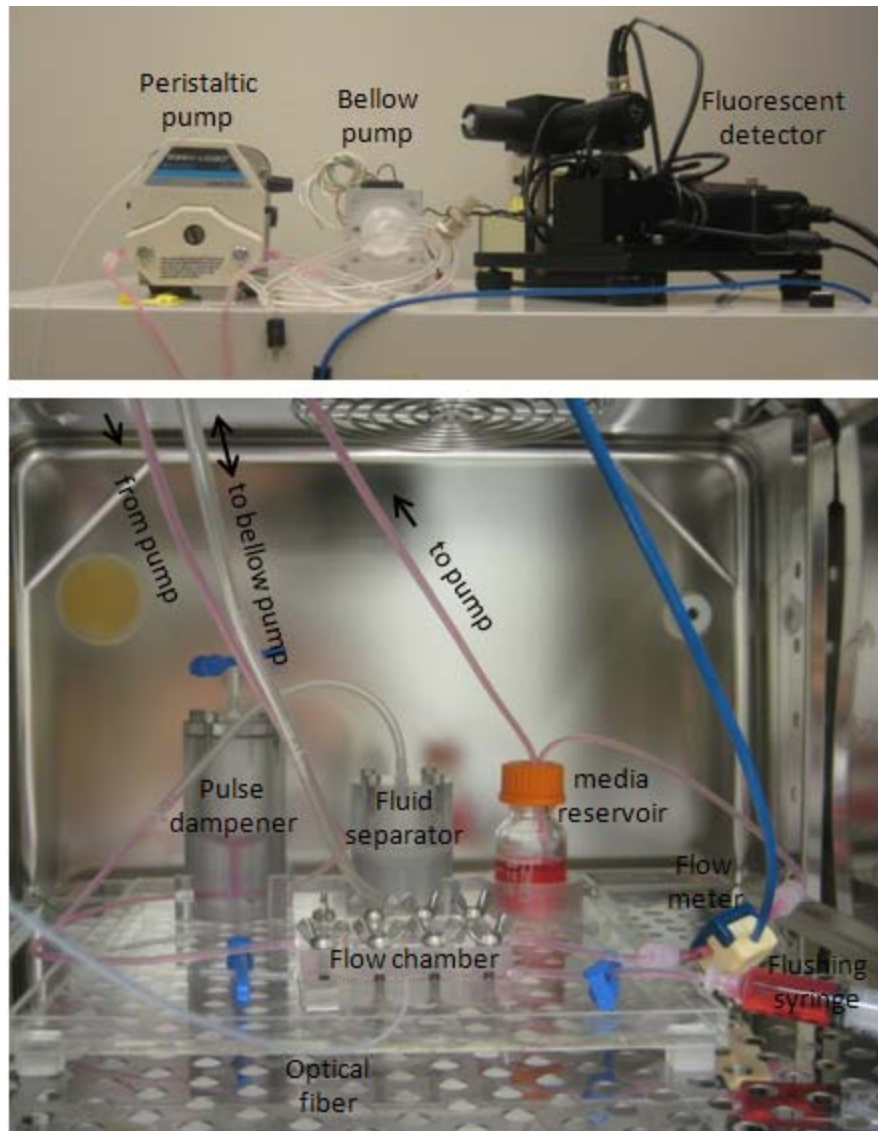


Figure 8: Photograph of the flow circuit for permeability studies assembled inside a cell culture incubator.

3.2.1.2 Design of the Two-chamber Permeability Apparatus

A laminar flow chamber apparatus was designed to apply the shear stress on the endothelial cells cultured on a Transwell™ filter (polyester membrane with 0.4 μm pore

size, 25 mm diameter, Corning). As illustrated in Figure 9, the Transwell™ filter was glued on top of a 20 mm diameter opening on an acrylic or stainless steel slide (1/8 inch thick or 1.5 mm thick respectively) using medical grade silicon adhesive (Dow Corning). A 1-mm diameter hole was drilled on the side of the slide, allowing a silica optical fiber access to the opening (the abluminal chamber) under the filter.

The apparatus was designed with two chambers sandwiching the filter, a luminal flow chamber for shear stress exposure and an abluminal one for fluorescence measurements. The size of the luminal chamber was defined by a silicon gasket (Specialty Manufacturing Inc, Saginaw, MI) with a width of 2 cm, a length of 5 cm and a depth of 0.0254 cm. The abluminal chamber was the 20 mm diameter opening on the slide. The luminal chamber was connected to the flow circuit to apply shear stress to the endothelial cells; while the abluminal one is an enclosed media reservoir with the optical fiber access and ports to allow media exchange.

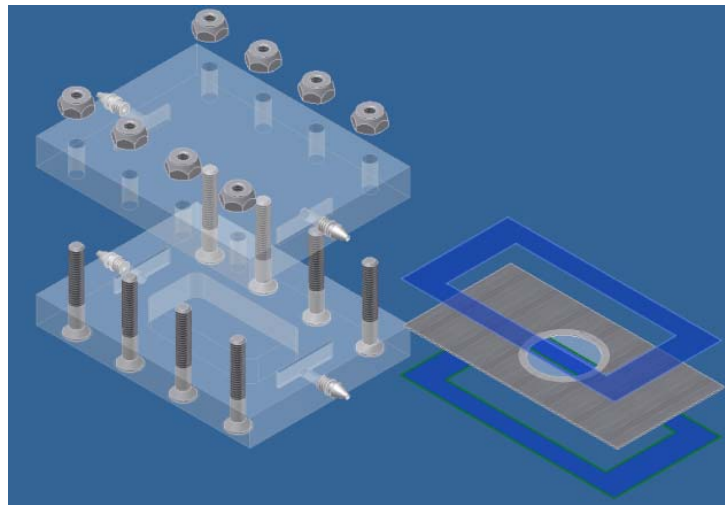
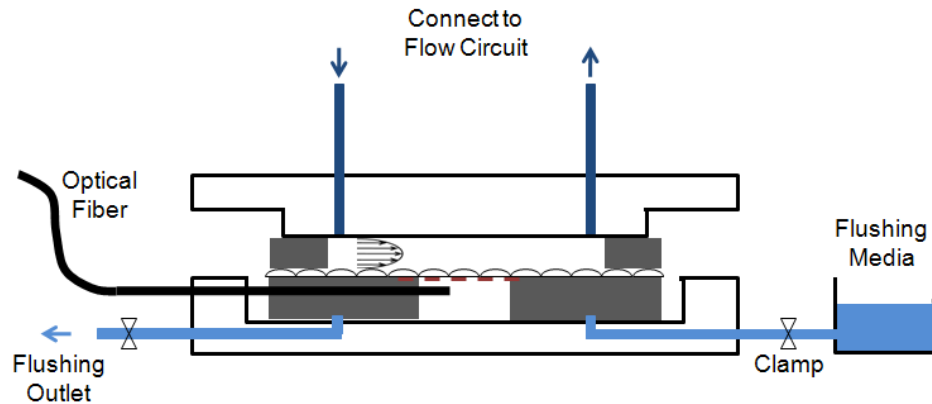


Figure 9: Schematic and 3D AutoCAD design of the permeability apparatus

During a test flow experiments, the pressure in the luminal chamber was measured by an ISOTECH™ transducer (Harvard Apparatus, Holliston, Massachusetts). The pressure was about 40 ± 40 cm H₂O (the outlet pressure as the reference point) when the baseline shear stress was applied. To eliminate the possible convective flux induced by the pressure difference across the cell monolayer, the abluminal chamber was kept

closed so that the pressure in the abluminal chamber is balanced with the luminal chamber.

The flow circuit designed in this study was able to generate various flow conditions with a volume of under 15 ml. In The three flow waveforms, the baseline and two step-up profiles were accurately and easily generated.

The mean and amplitude of the pulsatile shear stress τ can be predicted simply using the quasi-steady flow assumption [36, 87] by: $\tau = 6\mu Q/bh^2$, with μ =fluid viscosity, b =width and h =height of the luminal chamber, and Q is the flow rate.

3.2.2 Optical-Fiber Based Fluorescence Detection System

An optical fiber based fluorescence detection system was developed to measure the concentration of FITC-BSA in the abluminal chamber in real-time. This allowed fluorescence measurement without sample withdrawal, thus minimizing the disturbance to the flow circuit. Furthermore, a high temporal resolution of permeability measurement can be achieved by measuring in real time. This cost-effective and compact system used a light emitting diode (LED) as excitation light source and an ultra sensitive photodiode as photon detector, replacing commonly used expensive laser and photomultiplier tubes. The design was based on similar systems used in previous studies as described by Novak et al. [88], DeMaio et al. [89], Yang et al. [90] and in [91].

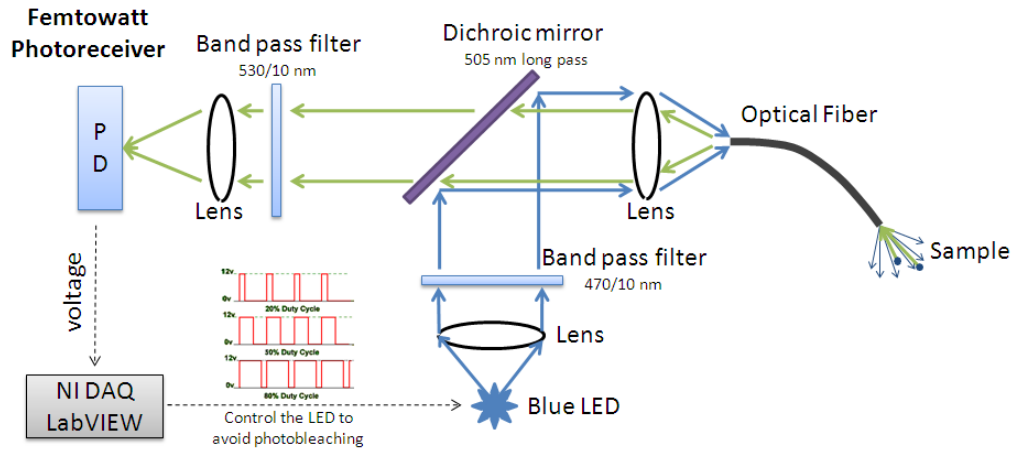


Figure 10: Schematic of the light path of the fluorescence detection system.

Figure 10 is the schematic of the light path of the fluorescence detector. Excitation lights from a high power blue LED (MBLED, peak wave length 470 nm, 625 mW, Thorlabs) were collimated by a plano-convex lens ($f=25.4$ mm, surface coated for 350-650 nm wavelength light transmission, Thorlabs). Blue excitation light was then filtered by a narrow bandpass filter (470 nm/10 nm, central wavelength/ full width at half maximum, Thorlabs), and reflected by a long pass dichroic mirror (Q505LP, Chroma) placed at 45 degree to the light path. Excitation light was finally focused by another plano-convex lens ($f=25.4$ mm, Thorlabs) to one end of the polymer clad multimode silica fiber (numerical aperture 0.48, 1 mm core diameter, Thorlabs). The other end, the measurement end, of the optical fiber was immersed in the abluminal solution. Both ends of the fiber were polished by $5\ \mu\text{m}$, $3\ \mu\text{m}$ and $1\ \mu\text{m}$ aluminum oxide polishing sheet (Thorlabs) sequentially to achieve the best transmission efficiency.

The emitted fluorescence light was collected by the same optical fiber and collimated by the same lens. The fluorescence light passed through the dichroic mirror, filtered by an emitter filter (530 nm/ 10 nm, Thorlabs) and was finally focused by another plano-convex lens ($f=25.4$ mm, Thorlabs) to the sensor of an ultra-sensitive femtowatt photoreceiver (PDF10A, Thorlabs). The photoreceiver combines a low noise silicon photodiode (detection wavelength range: 320 – 1100 nm, dimension: 1.1 mm by 1.1 mm) with a built-in ultra low noise transimpedance amplifier with a high gain of 10^{12} V/A. Thus, it has a comparable sensitivity to photomultiplier tubes and is able to detect optical powers down to 10 femtowatt.

All the optical components were enclosed in lens tubes (Thorlabs) and a special designed mirror holder was used to secure the dichroic mirror precisely at the 45 degree position. Thus, the entire optical path, except for the measurement end of the fiber, was shielded from stray light. The mirror holder and other adapters for assembling were fabricated in the Duke Physics Staff Machine Shop. Figure 11 shows the photograph of the fluorescence detector.

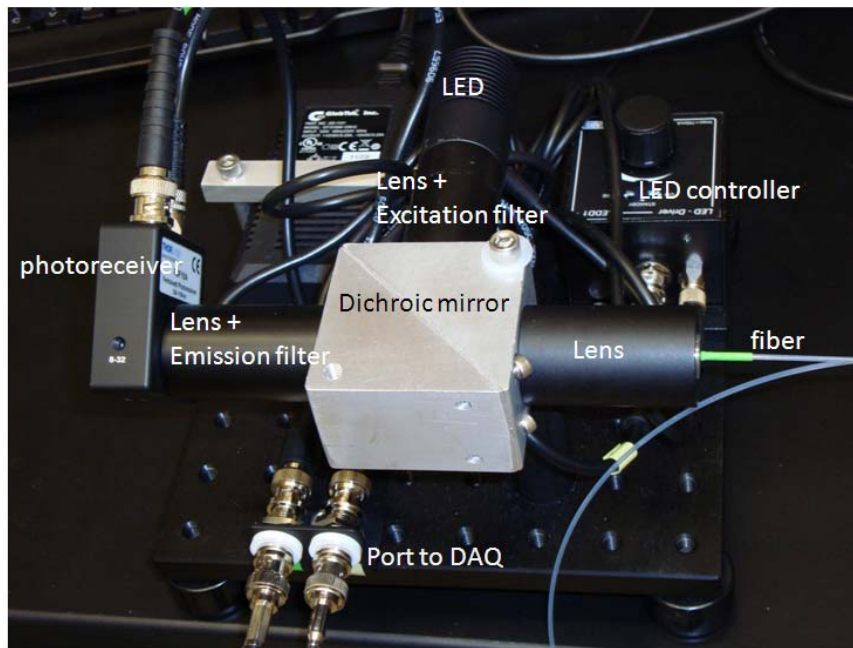


Figure 11: Photograph of the fluorescence detector.

The controllers of the LED and photoreceiver were connected to a DAQ board (NI PCI-6221, National Instruments) through BNC cables. The LED was turned on only during the measurement time to minimize photo bleaching. As shown in the diagram (Figure 12a), the output of the LED was controlled by a rectangular voltage signal at 20 Hz generated by the DAQ. The average excitation intensity can be modulated by altering either the duty cycle or peak voltage of the control signal. The DC voltage output from the photoreceiver was also transmitted to the computer via the DAQ board. A LabView (National Instruments) program was used for the LED control and data acquisition.

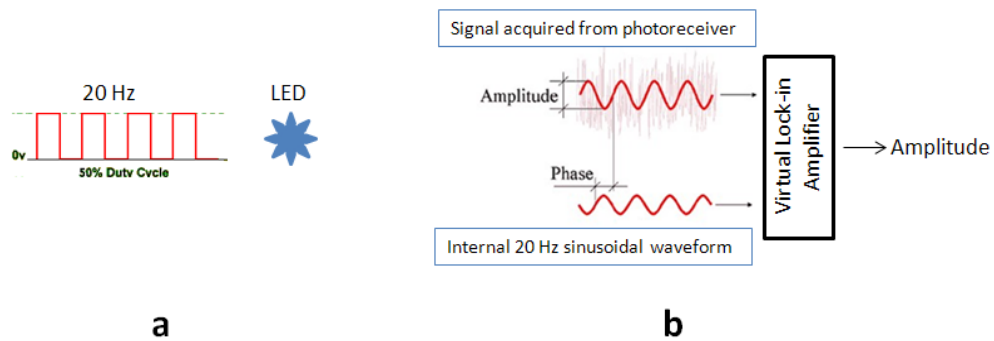


Figure 12: Schematic of LED control and virtual lock-in amplifier. a. a rectangular voltage waveform used to control the LED output. b. schematic of the virtual lock-in amplifier implemented in the LabView program.

To increase the detection sensitivity and minimize the noise from stray light that enter the measurement end of the fiber, a virtual lock-in amplifier was implemented in the LabView program [92]. As illustrated in Figure 12b, the fluorescence signal had a frequency of 20 Hz due to the frequency of the excitation lights. An internal sinusoidal waveform of 20 Hz was generated virtually in the LabView program. The virtual lock-in amplifier then acted as a narrow bandpass filter around the reference signal frequency, thus only amplifying the signal at 20 Hz. Therefore, the fluorescence measurement can be performed inside a conventional cell incubator without the effect of the ambient light.

During each measurement cycle, the LED was turned on for only 6 seconds. Two seconds after the LED was switched on and when the LED output was stable, the fluorescence signal was acquired for 4 seconds. The sampling rate was set to 100 kHz. Every 0.25 second, the sampled data was processed by the virtual lock-in amplifier to generate an output data point. The mean and standard deviation of the 16 data points

were recorded in files. Fluorescence measurements were fully automated, and the tracer concentration can be measured every minute to obtain $\frac{\Delta C_s}{\Delta t}$ for the permeability calculation.

Figure 13 shows the measurements of a series dilution of FITC-BSA solution from 100 ng/ml to 1 μ g/ml using three different excitation intensities. The peak voltages of the LED control signal were set to 0.5, 1.0 and 1.5V, respectively. The detection system demonstrated a good sensitivity and the R values of the linear regressions are greater than 0.998. Although 1.5V offered the best linearity and sensitivity, the high excitation intensity can lead to greater photobleaching and fluorescence signal saturation at lower concentrations, which limits the dynamic range of the measurements. Thus, the voltage of 1.0 V was used to control the LED output in the following experiments. We did not observe any photobleaching effect when 1.0 V was used. Our study also suggested that the fluorescence detection system has a sensitivity of at least 20 ng/ml for FITC-BSA (> 7 mol FITC / mol BSA, Sigma-Aldrich) at 1.0V LED control signal, which is sufficient for our study.

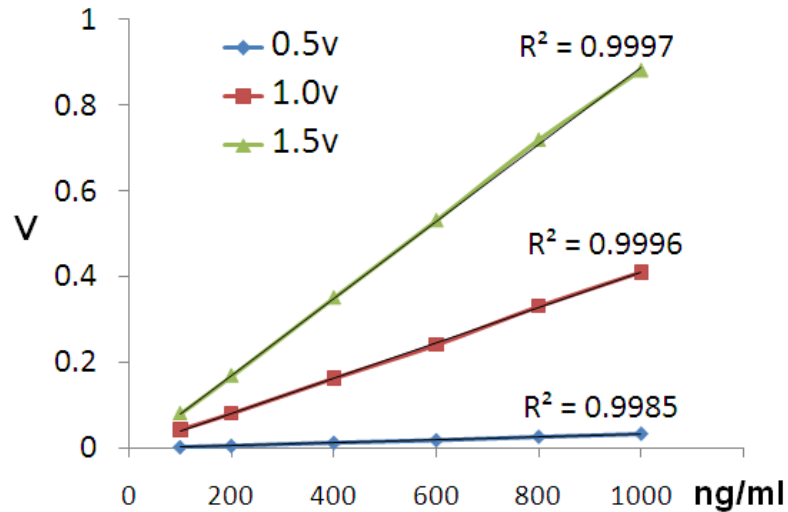


Figure 13: Measurement of a series dilution of FITC-BSA solution. X: concentrations of the FITC-BSA solution. Y: output voltages of the fluorescence detector. Excitation lights at three different intensity levels were generated by applying different driving voltage to the LED.

3.2.3 Cell Culture

Porcine aortic endothelial cells were harvested from swine aortae. All surgical procedures were approved by Duke Institutional Animal Care and Use Committee. Following euthanasia, the entire aorta was harvested and placed in ice-cold PBS. The aorta was cut open and pinned flat on a cell culture dish. The luminal surface was rinsed three times with PBS to remove blood and debris. The endothelial cells were scraped from the surface using a sterile rubber cell scraper, and then transferred to a 15ml conical tube containing cell culture media. The cells were finally transferred to a T75 cell culture flask.

The cell culture media was a solution of Medium 199 (Gibco), supplemented with 10% fetal bovine serum (FBS, Gibco) and antibiotic/antimycotic (Sigma-Aldrich).

Cultures were passaged using trypsin/EDTA. Endothelial cells were seeded at a density of around 10^5 cell/cm² on the Transwell™ polyester filter coated with collagen (sigma) at 10 µg/cm². Cells between passages 2 and 5 were used. Cells were cultured for 48 hours until tightly confluent, the media was then changed to a low serum formulation (Medium 199 with 2% FBS and antibiotic/antimycotic) to prevent overgrowth and condition endothelium for flow perfusion.

3.2.4 Permeability Experiments

After 12 hours in the low serum medium, endothelial cells were used in shear stress experiments. The low serum medium was used as the perfusion fluid. The viscosity of the low serum medium was 0.76 cp at T=37 °C measured by a falling ball viscometer (Gilmont).

The flow circuit was assembled and placed in a cell culture incubator, and 30 ml perfusion media was added to the reservoir. The perfusion fluid circulation was then started, and the flow rate was adjusted to the desired value to achieve the basal level shear stress of 15 ± 15 dynes/cm². The flow circulation was left to run for one hour until no air bubble remained in the tubing and the flow was stable. The step-up procedures were performed to obtain the precise parameters for the peristaltic pump (magnitude step-up) and bellows pump (frequency step-up) for later use. The permeability apparatus was finally assembled with the filter installed and the optical fiber inserted. Endothelial cells were preconditioned by basal level shear stress for 24 hours.

Around 20 minutes before step-up started, FITC-BSA (Sigma) was added to the perfusion media at a final concentration of 1000 $\mu\text{g}/\text{ml}$. The fluorescence detection system was turned on to measure the tracer concentration in the abluminal chamber. After obtaining the permeability of the preconditioned endothelial cells, shear stress magnitude or frequency was then doubled. During the first hour after step-up, the tracer concentration was measured continuously (every minute). Endothelial permeability was then measured every 15 minutes for the second hour and every 30 minutes until six hours had elapsed. The permeability was obtained by measuring the abluminal tracer concentration continuously for 5 to 10 minutes.

During the experiment, the concentration of FITC-BSA in the circulating media can be regarded as constant. Assuming a permeability of 5×10^{-6} cm/s and that the abluminal concentration remains zero at all time, only 340 μg of FITC-BSA (1.1% of the total amount) will be transferred across the endothelium in 6 hours. Thus, no more FITC-BSA needed to be added to the perfusion media.

After each flow experiment, the cell monolayer was fixed using Diff-Quick for 5 min (2 mg/l Fast green in methanol, VWR) and then Crystal Violet for 3 min (0.5% crystal violet in 20% methanol, VWR) as described in [85]. Monolayer integrity was examined under a microscope (Nikon).

3.2.5 Data Processing

A typical measurement dataset is plotted in Figure 14. The media used in our study had an auto-fluorescent signal of 2.25 V. After adding the tracer molecules to the perfusion media, the concentration in the abluminal chamber increased linearly. The permeability of the preconditioned endothelial cells was then obtained by calculating the rate of change in concentration, dC/dt , which is the slope (denoted as S_p) of the linear fit to the concentration plot over 5 minutes.

Since the focus of this study is to investigate the alteration of endothelial permeability during the adaptive response, the permeability values measured in all other time points were normalized to the preconditioned value. At each time point of permeability measurement, the rate of change in concentration, dC/dt , was calculated as the slope, S , of the linear fit to the concentration profiles during a time period of 5 minutes centered around the measurement time point. Thus, the normalized endothelial permeability at that time point was calculated as $\log_2(S/S_p)$. Two tailed one sample t-test was used to determine if the normalized permeability was significantly different than zero.

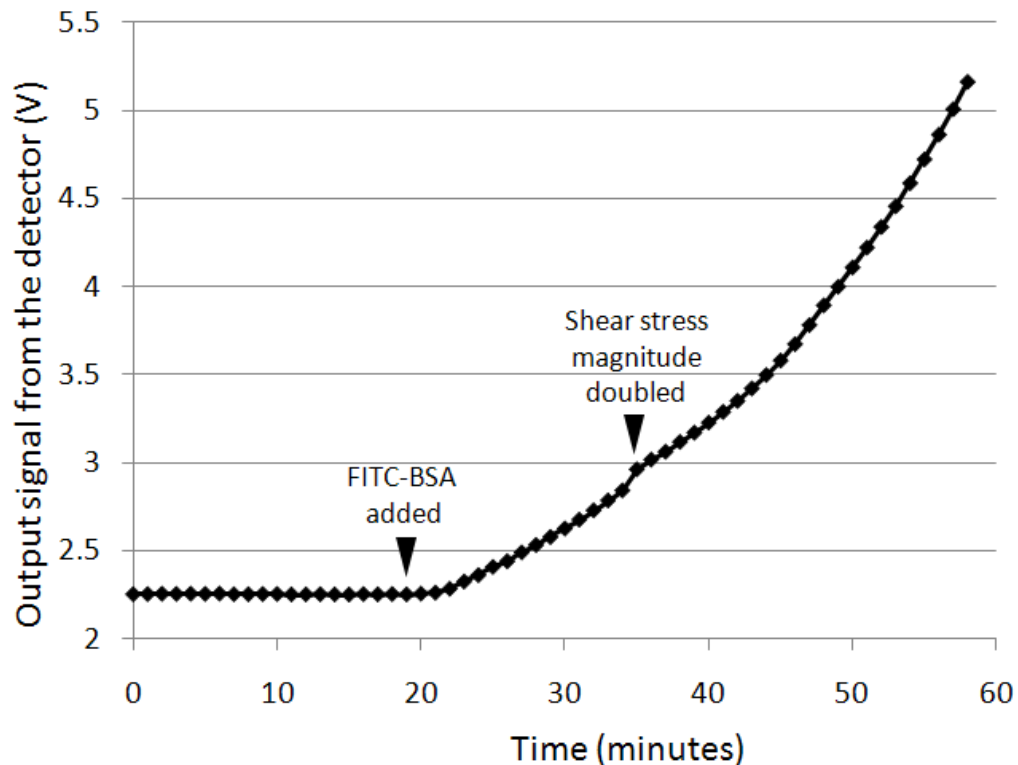


Figure 14: A typical concentration measurement plot. Fluorescent signal was measured every minute continuously. The perfusion media had an auto-fluorescent signal of 2.25 V. FITC-BSA was added to the fluid circulation around 20 minutes before the step-ups. The slopes of the concentration plot, dC/dt , were determined by linear fits in order to calculate the endothelial permeability.

3.3 Results

3.3.1 Endothelial Permeability in Response to Elevated Shear Stress Magnitude

Four shear stress magnitude step-up experiments were carried out to characterize the adaptive response of endothelial permeability. Figure 15 plots the normalized endothelial permeability at each time point during the adaptation process.

The permeability values at 40, 50, 75, 90, 105, 270, 300 and 330 minutes after shear stress step-up were identified to be significantly increased by the elevated shear stress ($p < 0.05$).

Our data demonstrated a dynamic response of endothelial permeability to changes in shear stress. Endothelial permeability increased immediately in response to the acute increase in shear stress magnitude. It peaked at 40 minutes, with a 1.9 fold increase comparing to the preconditioned value. Endothelial permeability then decreased slowly from 40 minutes to 150 minutes. It stayed at an elevated value, around 1.3 fold increase comparing to the preconditioned value, from 150 minutes to 360 minutes.

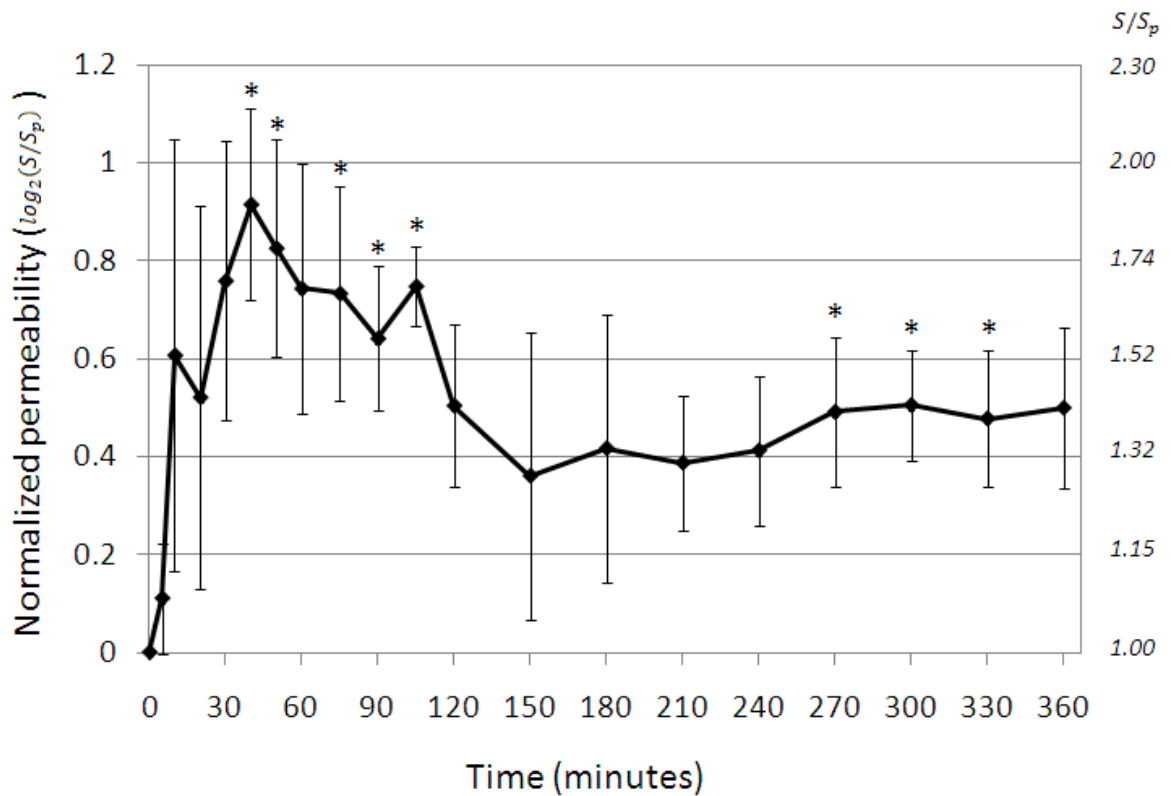


Figure 15: Plot of endothelial permeability during the adaptive response to elevated shear stress magnitude. Time 0: start of the magnitude step-up. Endothelial permeability values are normalized to the Time 0 value. Error bars: standard deviation of the mean, n=4. *: p<0.05

3.3.2 Endothelial Permeability in Response to Elevated Shear Stress Frequency

Four shear stress frequency step-up experiments were performed. Figure 16 is the plot of the normalized endothelial permeability at each time point during the adaptation process. The elevated shear stress frequency had a much smaller effect on the endothelial permeability. Only at 330 minutes, endothelial permeability was

significantly increased ($p < 0.05$) and the increase is relatively small (1.2 fold). At all other time points, the permeability was not significantly altered.

The apparent large increase in permeability at 20 minutes came mostly from one single measurement, and the peak disappeared when that data set was removed from the average. Although not statistically significant at each time point, a clear trend of increase in endothelial permeability was observed after 120 minutes exposure to the elevated shear frequency.

Therefore, different than the response to the elevated shear stress magnitude, the endothelial permeability to BSA does not have rapid increase phase; and it only increases slowly and gradually in response to the acute increase in shear stress frequency *in vitro*.

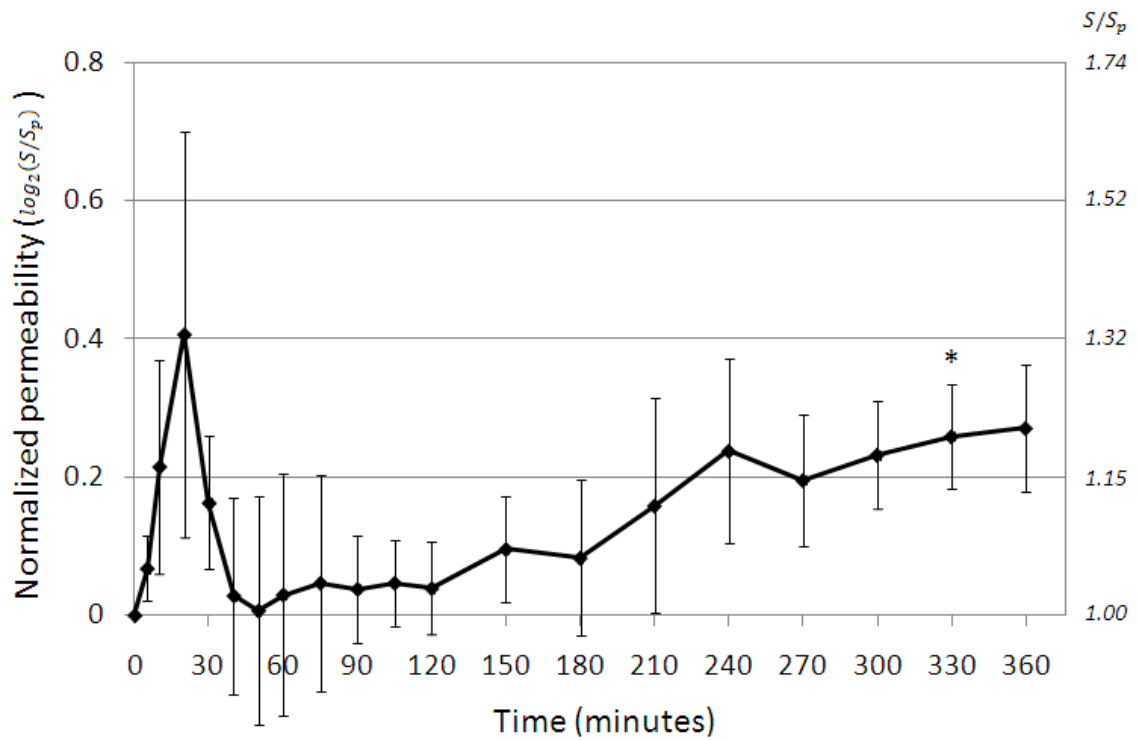


Figure 16: Plot of endothelial permeability during the adaptive response to elevated shear stress frequency. Time 0: start of the frequency step-up. Endothelial permeability values are normalized to the Time 0 value. Error bars: standard deviation of the mean, n=4. *: p<0.05

4. The Adaptive Dynamics of Endothelial Transcriptional Regulation

4.1 Experimental Design

The goal of this study was to determine the genome-wide transcriptional patterns of cultured endothelium during the adaptive response. A fully adapted endothelial monolayer was necessary to test the effect of adaptation; thus we first sought to determine the time necessary for cultured endothelial cells to reach the fully adapted state under the basal level shear stress. A control set of experiments was performed. Endothelial cells were exposed to the basal level shear stress, and sampled at 24 and 30 hours as shown in Figure 17a. The experiments were conducted with four replicates. Gene expression profiling was performed using DNA microarrays. Only two genes were identified as significantly differentially expressed between 24 hours and 30 hours at a false discovery level controlled at 20%. The preconditioning time of 24 hours was therefore used for the subsequent studies.

A flow system was developed to apply shear stress simultaneously to endothelial cells in multiple flow chambers in parallel. Endothelial cells were seeded into eight individual flow chambers, and were simultaneously preconditioned by the basal level shear stress for 24 hours using this flow circuit. This setting minimized experimental variability since all cells were from the same batch, had the same passage number, and were sheared by the same perfusion media. It also facilitated cell sampling, since individual chambers can be detached separately from the flow circuit. After

preconditioning, the step-up changes of shear stress were applied. Endothelial cells were sampled and subjected to gene expression measurements at the time points indicated in Figure 17b. These time points were selected to cover both the acute response phase and the more prolonged adaptation process. We matched the three time points used in the *in vivo* studies to facilitate comparisons.

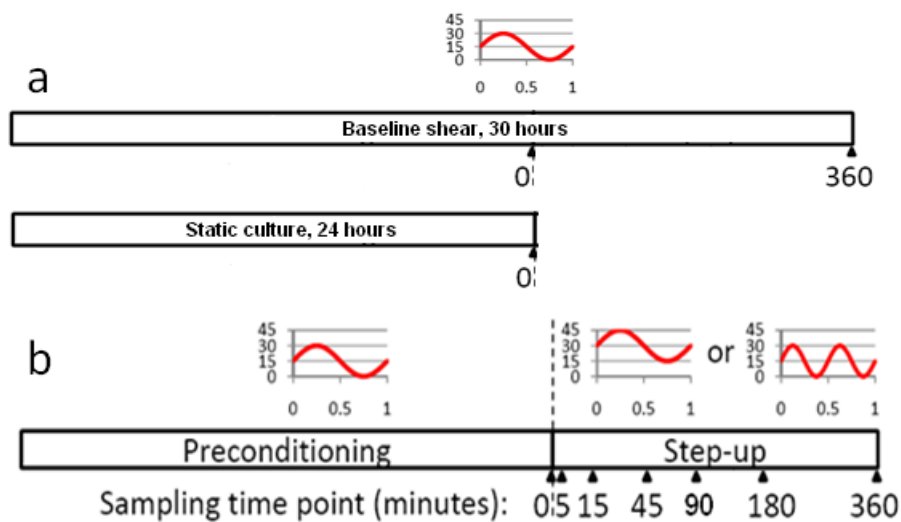


Figure 17: Sampling schedule for gene expression studies. a. Endothelial cells were subjected to baseline shear stress to determine the pre-conditioning time; b. Endothelial cells were sampled at multiple time points after step-ups. T=0: immediately before step-up.

Four biological replicates were performed for both magnitude and frequency step-up experiments. Microarrays were used to measure the global expression profiles. At each time point, the significantly differentially expressed genes were identified. Gene ontology and pathway analysis were carried out to investigate the adaptive response in the context of biological processes and pathways. The expression values of a subset of microarray identified genes were validated using quantitative real-time PCR. To

evaluate the inflammatory response, we also performed quantitative real-time PCR to measure the expression levels of the following genes: ICAM1, c-jun, KLF2 and eNOS.

4.2 Materials and Methods

4.2.1 Design of Flow System and Laminar Flow Chamber

A parallel flow system and laminar flow chambers were developed to apply controlled shear stress profiles to endothelial cells grown separately on eight glass slides. At designated time point, cells can be easily sampled by removing one of the chambers detached from the flow circuit.

The flow circuit used in the transcriptional studies is shown in Figure 18. Similar to the permeability flow circuit, the mean flow is driven by the peristaltic pump through a pulse dampener (Cole-Parmer) and the pulsatile components of the shear stress were superimposed by the computer controlled bellows pump (Intelligent Motion System, Marlborough, CT). Two eight-outlet Teflon® manifolds (Cole-Parmer) were used to distribute the flow evenly to the individual laminar flow chambers. The step-up of shear stress magnitude was performed by adjusting the speed of peristaltic pump, and the step-up of frequency was achieved by programming the bellow pump. The pinch valves were used to fine tune the flow rate for each chamber. The volumetric flow rate was monitored using transonic flow probes (C-Series, Transonic Inc., Ithaca, NY), which was connected to a computer through a National Instrument data acquisition (DAQ) board

(NI PCI-6221, National Instrument). Real-time flow parameters, including mean flow rate, frequency and amplitude, were calculated by a LabView program. During the experiment, the flow parameters were measured for each of the eight lines.

All the components with contact surface to the perfusion media were gas sterilized before experiments. During experiments, the flow circuit was placed inside a cell-culture incubator of 37 °C and 5% CO₂, with a port in the circuit allowing gas exchange through a sterile filter (0.4 um, Corning). Figure 19 shows the photograph of the flow circuit in use.

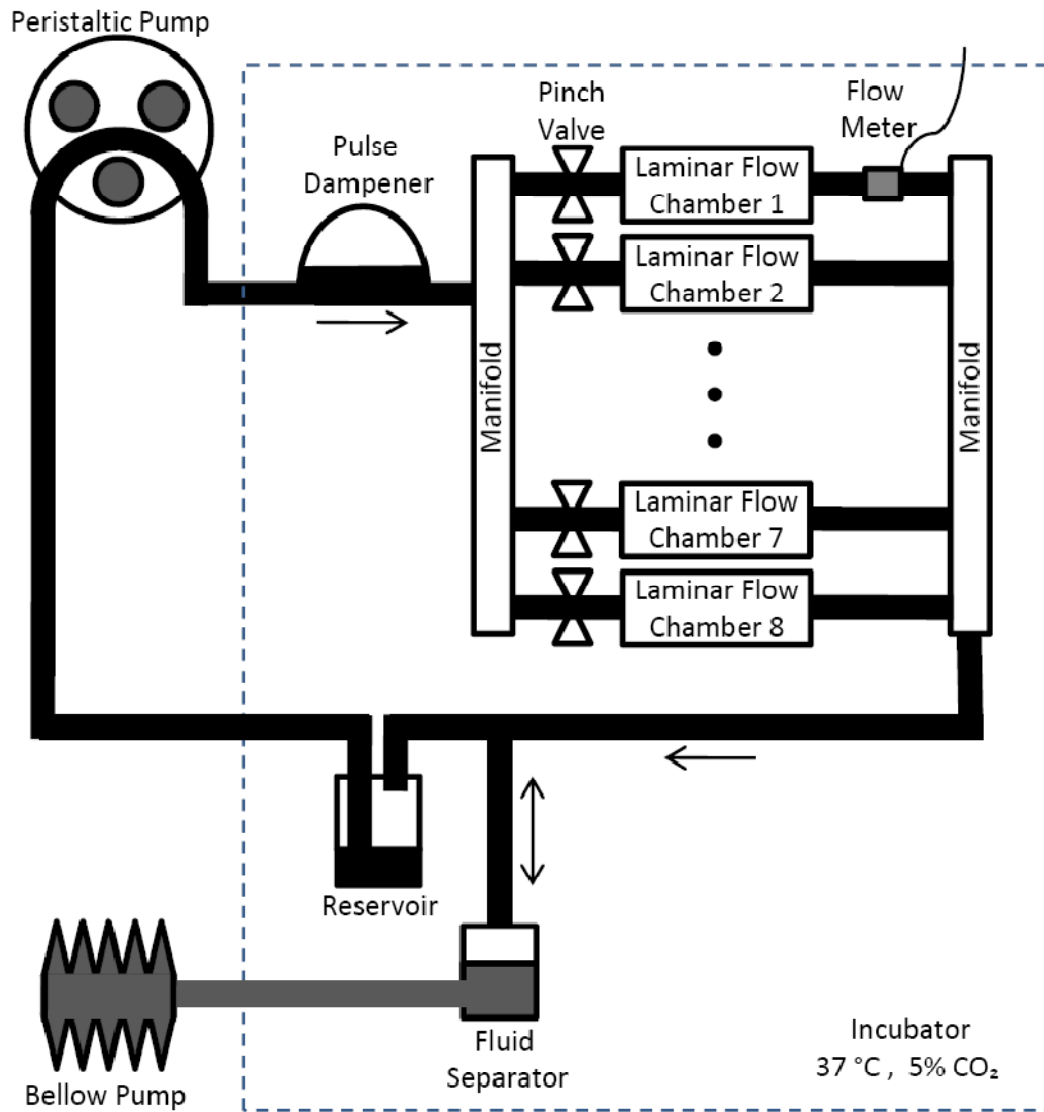


Figure 18: Schematic of flow circuit for transcriptional studies.

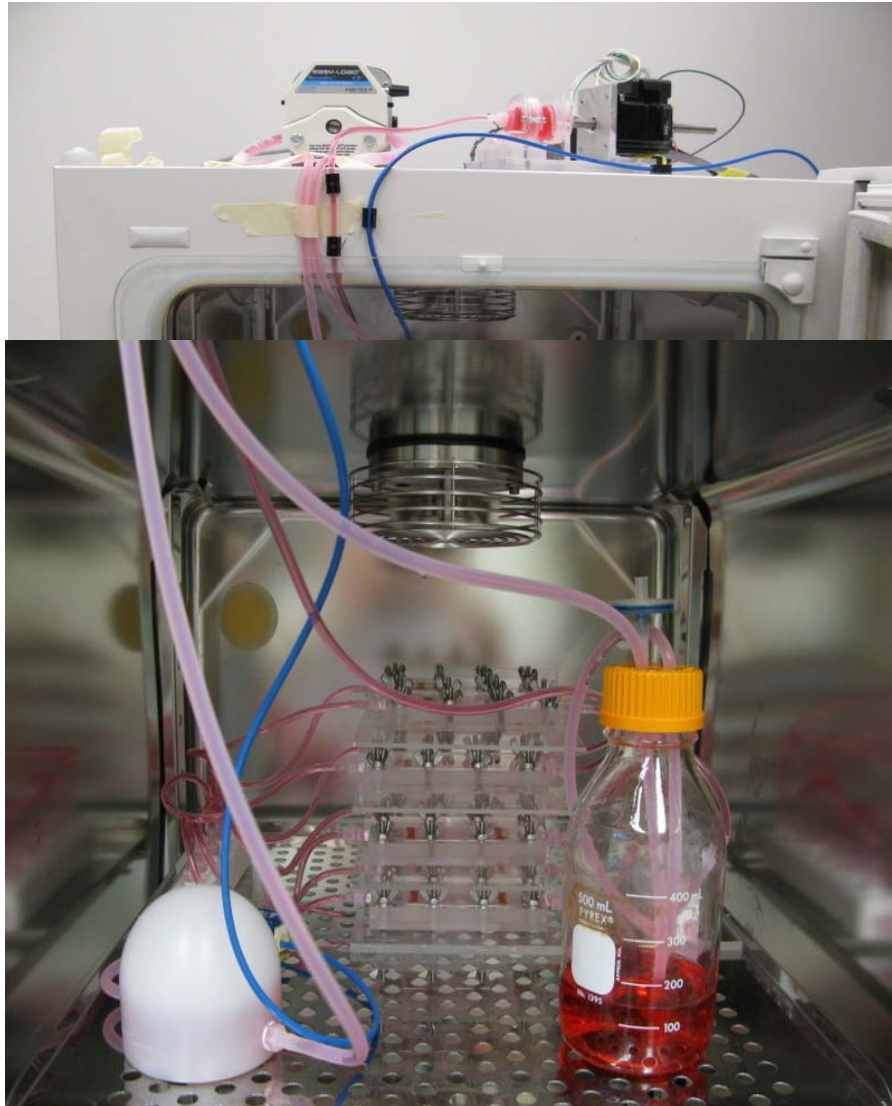


Figure 19: Photograph of flow circuit for transcriptional studies.

The laminar flow chambers used for transcriptional studies were similar to the ones used by Himburg et al. [36]. As illustrated in Figure 20a, two acrylic plates sandwich a silicone gasket that defines the flow region, and endothelial cells were cultured over a microscope glass slides sitting in the recess on the bottom plate.

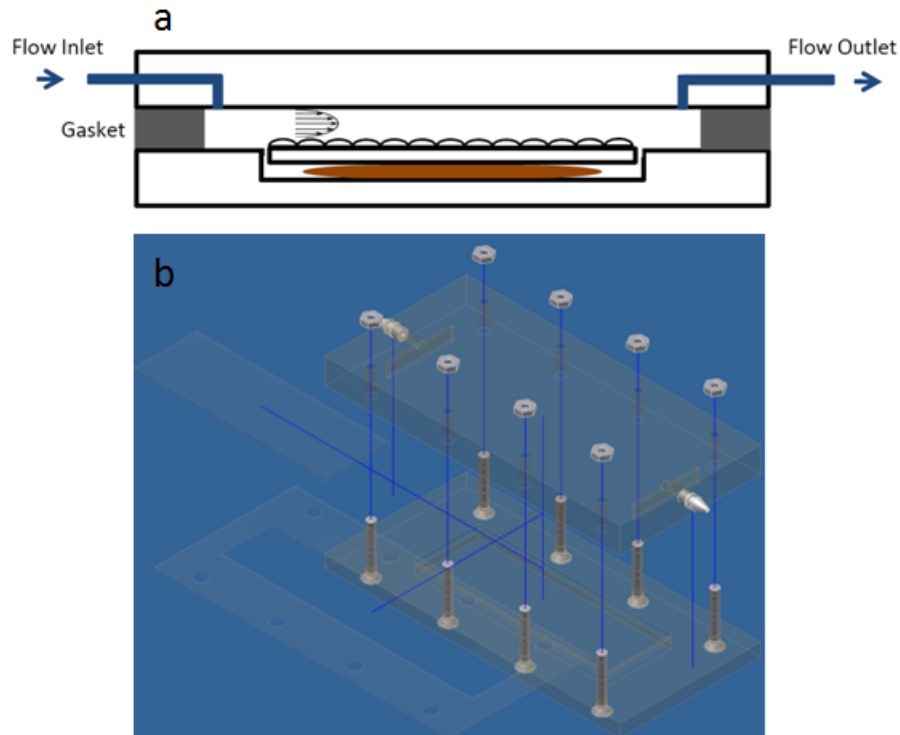


Figure 20: Schematic and 3D design of the laminar flow chamber

The height of the luminal space was defined by a silicone gasket of 0.01 inch. Controlling this height was critical to obtain an accurate shear stress, since a ten percent variation, 0.001 inch, would be transformed into a ~20% difference in shear stress. Although a thicker gasket could better tolerate the height variations, it was not used due to the high flow rate required for the nominal shear stresses. Considering the accuracy of the milling machine (0.001 inch) used to fabricate the chamber and the variations in the thickness of glass slides, previous chamber designs could not ensure an accurate control of heights over multiple chambers. A simple modification was made as shown in Figure

20a, where the recess holding the glass slides was fabricated deeper than the thickness of the glass slides (~1.0 mm). High compliance medical grade silicone sheet (McMaster-Carr) was glued down to support the glass slides using medical grade silicone adhesive (Dow Corning). The chamber can then be assembled with the silicone gasket partially overlapped with the glass slides to press the slide surface flush. Figure 20b shows a 3D representation of the flow chamber assembly.

All the flow chambers and components of the flow circuit were fabricated in the Duke University Physics Machine Shop, and a laser cutting machine (Universal Laser Systems, Scottsdale, Arizona) was used to cut the shape of all silicone gaskets to ensure the same accurate geometry.

In every experiment, the height of the luminal space of each flow chamber was measured before the chamber was installed in the flow loop. The height was measured optically using a Nikon inverted microscope. A 20X objective lens was used to focus on the cell monolayer and then the surface above. The distance between the two focal planes was recorded by a Z-positioning motor with a 0.2 μm step size (Prior Scientific, Rockland, MA) installed on the fine tune knob of the microscope. The Z-positioning motor was calibrated, and the height of the luminal space, h , can be calculated by $h = \Delta r \times 2 \mu\text{m}/\text{unit} \times 1.337$, where Δr is the reading from the Z motor and 1.337 is the refraction index of the perfusion media used in the experiments. In all experiments, the

heights of the flow chambers were consistently and accurately controlled within 5% of designed value (0.01 inch).

4.2.2 Cell Culture

Porcine aortic endothelial cells were harvested and cultured as described in Chapter 3. Endothelial cell cultures were passaged using trypsin/EDTA. Glass slides were coated with collagen (Sigma) at $10 \mu\text{g}/\text{cm}^2$. Cells between passages 3 and 5 were seeded on eight glass slides simultaneously. When the cells reached confluence (2-3 days), the media was changed to a low serum formulation (Medium 199 with 2% FBS and antibiotic/antimycotic) to prevent overgrowth and condition endothelium for flow perfusion.

4.2.3 Shear Stress Experiment

After 12 hours in the low serum medium, the cells were used in shear stress experiments. The low serum medium was used as the perfusion fluid. The viscosity of the low serum medium was 0.76 cp measured by a falling ball viscometer (Gilmont).

The flow circuit was assembled first in the cell culture hood. Eight segments of tubing, with the matching hydraulic resistance to the laminar flow chambers, were placed in the flow circuit. The flow circuit was then moved to the incubator, and 300ml perfusion media was added to the reservoir. The perfusion fluid circulation was then started, and the flow rate in each parallel line was adjusted to the desired value to achieve the basal level shear stress. The flow circulation was left to run for around one

hour until no air bubble remained in the flow circuit and the flow rate stayed constant. The step-up procedures were performed to obtain the precise parameters for the peristaltic pump (magnitude step-up) and bellow pump (frequency step-up). The laminar flow chambers were finally assembled with cell culture slides and were inserted into the flow circuit one by one, replacing the tubing segments.

The basal shear stress of 15 ± 15 dynes/cm² was applied to endothelial cells first. After 24 hours exposure, two randomly selected flow chambers were detached from the flow circuit and two tubing segments were placed in the circuit to maintain the flow rate for the remaining flow chambers. The integrity of the endothelial monolayer was confirmed under phase contrast microscope (Nikon), and the glass slide was then carefully removed from the flow chamber for RNA isolation. After obtaining these two preconditioned control samples (one extra for backup), the shear stress alteration was applied. At each designated time point as shown in Figure 17b, one randomly selected chamber was detached from the flow circuit and immediately disassembled for RNA isolation.

4.2.4 RNA Isolation and Microarray Protocol

Endothelial cells were immediately exposed to lysis solution. Total RNA was isolated and purified using the RNeasy mini kit (Qiagen). The quantity of the RNA was measured using a NanoDrop Spectrophotometers (Thermo Fisher Scientific) and the integrity was checked using an Agilent Bioanalyzer 2100 (Agilent).

Two micro gram of total RNA from each sample was amplified using the Ambion MessageAmpII kit (Applied Biosystems) following manufacture's protocols. Aminoallyl-UTP was incorporated into the amplified RNA products for dye-coupling. All seven samples from each single experiment, including the pre step-up control sample, were amplified at the same time to minimize amplifications variability. The amplified RNA samples were then labeled with Cy5 dyes. A reference RNA sample, derived from static cultured porcine aortic ECs, was labeled with Cy3, serving as the universal standard reference for all microarrays.

Samples were submitted to the Duke University Microarray Core Facility (DUMCF). Each sample and the standard reference were hybridized to custom printed *Sus Scrofa* DNA microarrays (version 1.0, Operon Biotechnologies). The arrays were scanned using GenePix (Molecular Devices) and the fluorescence intensity for each spot was quantified. Table 5 summarizes all the collected samples used in the microarray study. A total number of 68 microarrays were used.

Table 5: The summary of collected samples for microarray experiments

Control		Magnitude Step-up		Frequency Step-up	
Static condition	n = 4	-		-	
Preconditioned 24 h	n = 4	Preconditioned 24 h	n = 4	Preconditioned 24 h	n = 4
-		Step-up 5 minute	n = 4	Step-up 5 minute	n = 4
-		15 minute	n = 4	15 minute	n = 4
-		45 minute	n = 4	45 minute	n = 4
-		90 minute	n = 4	90 minute	n = 4
-		180 minute	n = 4	180 minute	n = 4
Preconditioned 30 h	n = 4	360 minute	n = 4	360 minute	n = 4
Total	n=12	n=28		n=28	

4.2.5 Microarray Data Analysis

4.2.5.1 Preprocess

The raw data digitalized using GenePix were imported into Genespring GX (Agilent). A quality check filter was first applied to eliminate the genes with signals lower than the averaged background noise in more than half of the total arrays.

Lowess normalization was performed to correct the systematic variances such as overall RNA quantities, labeling difference and other intensity-dependent artifacts. For each gene, the expression levels at all time points after step-up were normalized to the expression value of the preconditioned control samples. Unless specified otherwise, all the gene expression values presented in this chapter are normalized values in log₂ scale.

Thus, the expression values are zero for all genes of the preconditioned control samples. Genes that were upregulated by shear stress step-up have positive expression values, and genes downregulated have negative values.

4.2.5.2 Identify differentially expressed genes and other basic analysis

Significance Analysis of Microarrays [78] (SAM, Stanford) was used to identify the differentially expressed genes at each time point relative to the preconditioned controls. SAM uses a non-parametric statistic method to test if the expression value of each gene is significantly different than zero. SAM estimates the false discovery rate using a permutation-based method.

The lists of significantly differentially expressed genes were then subjected to clustering analysis using Genespring to identify the groups of genes regulated with the same temporal patterns. Principal component analysis was also carried to discover the regulation patterns of the global transcriptional profiles.

In addition to the discovery type of analysis, the expression values of a set of *a priori* selected genes were examined to understand how the inflammatory, oxidative responses, adhesive and cellular structure related genes were regulated during the adaptive response. Since only a limited number of genes were examined, the false discovery rate was not controlled and the standard one-sample t-test against zero was used.

4.2.5.3 Gene Ontology and network analysis

The gene lists generated from SAM or Genespring were imported into Ingenuity Pathways Analysis (IPA, Ingenuity) and GeneGo (GeneGo bioinformatics software, Inc.) for gene ontology, functional and pathway analysis. IPA was used to construct the networks of genes, which helped us understand how the differentially expressed genes interacted with each other at different times. GeneGo was used to perform the gene ontology and pathway analysis studies.

Briefly, IPA and GeneGo employ their large gene ontological database, where each gene was annotated with its function, gene ontology term, related pathways and diseases and relationship to other genes/proteins. The imported gene list was first annotated with the database, and then the program tests if genes related to any particular cellular function, disease or GO terms were over represented in this gene list. The Fisher's exact test is usually used to test if the overrepresentation is statistically significant.

4.2.5.4 Gene Set Enrichment Analysis

Gene Set Enrichment Analysis, GSEA [79], was used to identify significantly regulated pathways and compare the adaptive expression profiles with other transcriptional profiles. Instead of using a list of identified genes, GSEA utilizes the transcriptional levels of all the genes on the array to determine whether an *a priori* defined gene set is differentially expressed.

Since current version of GSEA does not support paired statistics, the analysis used in this study relied on a pre-ranked gene-list. All genes passed quality-check filter were included in the GSEA analysis. The normalization was done using Genespring as described previous, i.e., for each gene, the ratio of step-up sample/preconditioned-control was calculated. For each time point, all the genes were ranked based on a signal to noise metric, μ/σ , where μ is the mean expression levels and σ is the standard deviation (n=4). Thus, a ranked gene list was obtained at each time point, with the most significantly upregulated genes (relative to preconditioned control) on the top of the list and downregulated ones on the bottom of the list. For any *a priori* defined gene set, GSEA determines whether these genes were significantly presented, or “enriched”, on the top or the bottom of the ranked lists. A random-walk based statistics is used to calculate the p-value for each gene set, and a permutation based method is used to estimate the false discovery rate [79]. Therefore, it is possible to tell if any gene set is up or down regulated in the adaptive response using GSEA even when the microarray noise level is high. Furthermore, GSEA enable us to find the gene sets or pathways with great biological significances but cannot be identified by methods like IPA or GeneGo. For example, if a significant number of genes in a particular pathway are all upregulated slightly, e.g. by 20%, this pathway is highly likely to be activated. IPA and GenoGo will not detect this pathway since only a few or no gene would pass the statistic tests to be on

the gene list for analysis. However, GSEA may find a significant number of genes in this pathway are enriched on the top of the gene list.

Several *ad hoc* scripts were written in Matlab and R for data import/export and format translation.

4.2.6 Real-time quantitative-PCR

Microarray results were validated by real time quantitative-PCR methods. cDNA was synthesized from 100 ng RNA using the iScript cDNA Synthesis Kit (Biorad, Hercules CA) with a MyCycler (BioRad, MyiQ System) thermal cycler. A two-step quantitative Real-time RT-PCR (qPCR) reaction was carried out on a Bio-Rad MyIQ system (Bio-Rad Laboratories) using iQ SYBR Green kit (Bio-Rad). Triple replicates were performed for each gene. GAPDH gene was used as the housekeeping gene. Primers used in this study were designed and tested for efficiency previously in our lab [36, 38, 84, 93], and they were synthesized by Integrated DNA Technologies. Table 6 lists all the primers used in this study. The $2^{-\Delta\Delta CT}$ method was used to quantify expression levels of the target genes relative to the standard control sample.

Table 6: Primers for real-time quantitative-PCR

Gene	3' Primer	5' Primer
GAPDH	5'-GTC TTC TGG GTG GCA GTG AT-3'	5'-GGG CAT GAA CCA TGA GAA GT-3'
eNOS	5'-AGC ACA GC AGG TTG ATT TC-3'	5'-GGC TGG TAC ATG AGC ACA GA-3'
KLF2	5'-CAA AAT GCC ACC TGT CTT CC-3'	5'-AGC CCA CCG GGT CTA CAC TA-3'
VEGF	5'-AAG CTC ATC TCT CCT ATG TGC TG-3'	5'-ACG ACG AAG GTC TGG AGT GT-3'
c-jun	5'-TTC AGG GTC ATG CTC TGC TT-3'	5'-GAT GGA AAC GAC CTT CTA CGA C-3'
ICAM	5'-GGA GGT GGG AAG CTG TAG AA-3'	5'-TCA ATG GAA CCG AGA AGG AG-3'
Interleukin-1α	5'-CAT CAT TCA GGA TGC ACT GG-3'	5'-CAA GGA CAG TGT GGT GAT GG-3'

4.3 Results

4.3.1 Endothelial Gene Expression under Basal Level Shear Stress for 24 hours and 30 hours

In the control set of experiments, endothelial cells were exposed to the basal level shear stress (15 ± 15 dynes/cm², 1 Hz) for 24 hours and 30 hours. Gene expression profiles were measured by microarray to determine if the preconditioning time of 24 hours was sufficient for the static cultured endothelial cells to sufficiently adapt to the basal level shear stress. In each experiment, a control sample was kept in the perfusion media under static condition in the same incubator for 24 hours. Expression value of each gene under shear stress was normalized by the corresponding static controls.

A total number of 8268 genes, which had quality signals on at least half of the microarrays, were used in the statistical tests. Significance Analysis of Microarrays (SAM) was performed to identify genes that were significantly differentially expressed at 24 hours versus static, 30 hours versus static and between 24 hours and 30 hours. Table 7 summarizes the numbers of genes identified at different false discovery rates.

When the false discovery rates were controlled at 5%, 17.1% and 18.7% of total genes were identified to be significantly differentially expressed after exposed to the basal level shear stress for 24 hours and 30 hours, respectively. Figure 21 shows a great overlap between the lists of genes identified at 24 hours and 30 hours. This result demonstrated that a significant number of genes were regulated by shear stress when cultured endothelial cells were exposed to flow, and most of these genes were

consistently regulated after 24 hours and 30 hours exposure to shear stress. The 1838 genes, which were identified at either 24 hours or 30 hours at the false discovery of 5%, are regarded as shear sensitive genes in the following discussions.

Table 7: The numbers of identified genes in the control study.

	Estimated FDR 0%	Estimated FDR <5%
24 hours vs. Static	467 (111 up, 356 down)	1414 (534 up, 880 down)
30 hours vs. Static	560 (144 up, 416 down)	1565 (647 up, 982 down)
24 hours vs. 30 hours	2	2

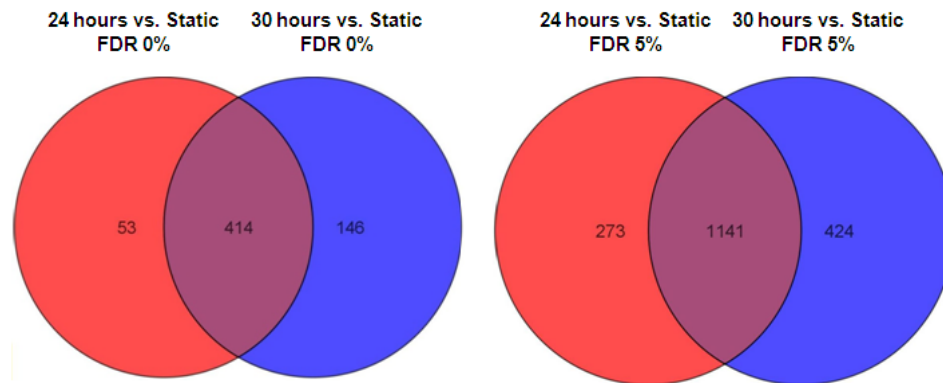


Figure 21: Venn diagram displaying the overlap of genes identified at 24 hours and 30 hours.

Only two genes, FLJ25476 and an unknown gene, were identified as differentially expressed genes between 24 hours and 30 hours. Even when the false

discovery rate was relaxed to 20%, there were no more genes identified. Figure 22 shows the overall comparison between the expression profiles of 24 hours and 30 hours. All 8268 genes are plotted. The x axis is the expression value at 24 hours and y axis is the expression value at 30 hours. All genes are tightly distributed around the diagonal line of $y=x$, suggesting these two expression profiles were highly similar. Therefore, we concluded that the gene expression of cultured endothelial cells is stable after exposed to the basal shear stress of 15 ± 15 dynes/cm². Thus, 24 hours was an appropriate preconditioning time for the following step-up studies.

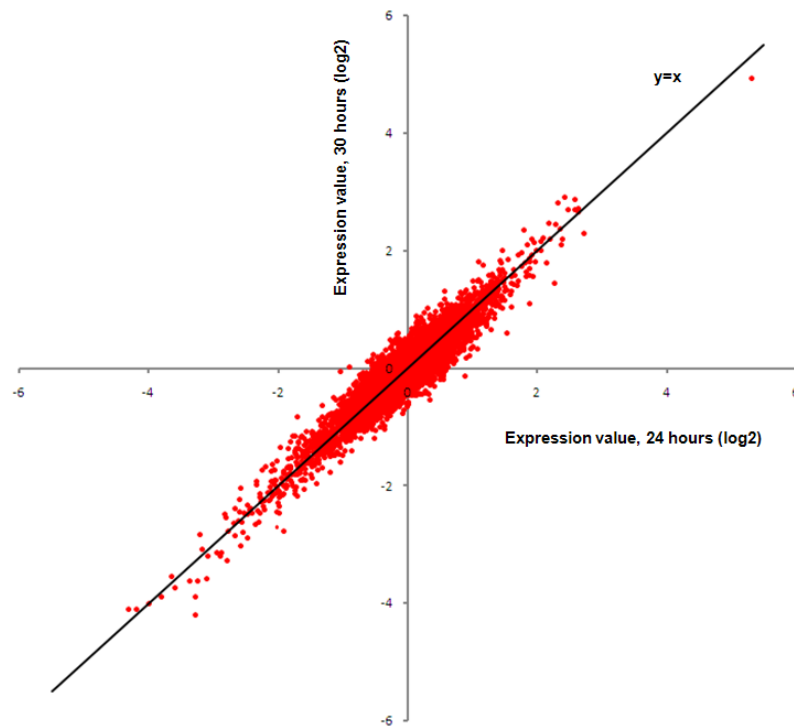


Figure 22: The scatter plot of gene expression profiles. Endothelial cells were exposed to 24 hours and 30 hours of basal level shear stress. The expression value of each gene was normalized by the corresponding static controls. X: the expression value after 24 hours of shear stress; Y: the expression value after 30 hours of shear stress.

4.3.2 Endothelial Gene Expression in Response to the Elevated Shear Stress Magnitude

In this set of experiments, endothelial cells were preconditioned under the basal level shear stress (15 ± 15 dynes/cm², 1 Hz) for 24 hours and the elevated mean shear stress (30 ± 15 dynes/cm², 1 Hz) was then applied. Samples were obtained immediately before the step-up (control) and at different time points after the step-up, as shown in Table 5.

4.3.2.1 Differentially Expressed Genes Identified at Each Time Point

The expression level of each gene of the step-up samples was normalized by the expression value of the corresponding control sample (before the step up). SAM was used to identify genes that were significantly differentially expressed at each time point comparing to the control sample.

Table 8 listed the number of genes identified at each time point at different levels of false discovery rate. Limited number of genes was called at earlier time points, and more genes were identified after 90 minutes. At FDR<10%, 86 genes were identified to be sensitive to the step-up at any time point. The size of this gene list is small and manageable comparing to the control study, where 1838 genes were found to differ between static cultured and preconditioned endothelial cells. Figure 23 shows that 40 of the 86 genes were called in the control set of experiments.

Table 9 is the complete list of genes identified at each time point at false discovery rate controlled at 10%. The expression values were normalized to the pre step-up controls, and they were presented in log2 scale. Several identified probes were not annotated with gene names since the corresponding porcine genes are unknown and no human or mouse gene is known with similar sequences.

Table 8: The numbers of identified genes at different time points in the magnitude step-up experiment.

Time	Estimated FDR < 5%		Estimated FDR < 10%	
	up-regulated	down-regulated	up-regulated	down-regulated
5 minute	0	2	0	2
15 minute	3	0	3	0
45 minute	2	0	9	0
90 minute	13	0	19	0
180 minute	16	6	20	7
360 minute	16	5	48	6

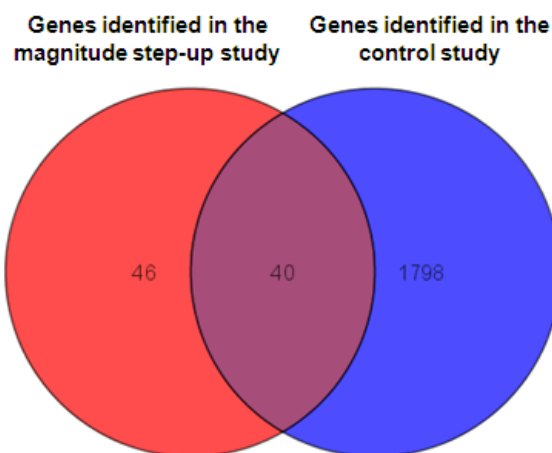


Figure 23: Venn diagram displaying the overlap of genes identified in the magnitude step-up study and control study.

Table 9: List of genes identified at different time points in the magnitude step-up experiments.

ID	Gene	Expression	Description
5 minutes			
SS00010196	IL1A	-0.60	interleukin 1, alpha
SS00010211		-0.41	
15 minutes			
SS00003206	ZFP106	0.59	zinc finger protein 106 homolog (mouse)
SS00003440	ACTC	0.45	actin, alpha, cardiac muscle
SS00010237		0.33	
45 minutes			
SS00009868	MYH9	1.00	myosin, heavy polypeptide 9, non-muscle
SS00000396	CCAR1	0.69	cell division cycle and apoptosis regulator 1
SS00007343	LMNB1	0.53	lamin B1
SS00009180	PCDH7	0.53	BH-protocadherin (brain-heart)
SS00008997	YAF2	0.51	YY1 associated factor 2
SS00006138	C3ORF17	0.49	Chromosome 3 open reading frame 17
SS00008956		0.48	
SS00001082	SCAMP1	0.40	secretory carrier membrane protein 1
SS00004979	KIAA1279	0.37	KIAA1279
90 minutes			
SS00000203	KLF2	1.50	Kruppel-like factor 2 (lung)
SS00006925	ID1	1.13	inhibitor of DNA binding 1, dominant negative helix-loop-helix protein
SS00004771	GADD45B	0.98	growth arrest and DNA-damage-inducible, beta
SS00007520	KLF4	0.92	Kruppel-like factor 4 (gut)
SS00007619	ID2	0.79	inhibitor of DNA binding 2, dominant negative helix-loop-helix protein
SS00006583	COL4A1	0.60	collagen, type IV, alpha 1
SS00003206	ZFP106	0.60	zinc finger protein 106 homolog (mouse)
SS00009712	TIMP3	0.58	tissue inhibitor of metalloproteinase 3 (Sorsby fundus dystrophy, pseudoinflammatory)
SS00000220	ID2	0.57	inhibitor of DNA binding 2, dominant negative helix-loop-helix protein
SS00003201	LOC51136	0.54	PTD016 protein
SS00008254	BHLHB2	0.54	basic helix-loop-helix domain containing, class B, 2
SS00010237		0.44	
SS00007441	KLF10	0.43	Kruppel-like factor 10
SS00001410	ID3	0.42	inhibitor of DNA binding 3, dominant negative helix-loop-helix protein
SS00007031	SGK	0.41	serum/glucocorticoid regulated kinase

SS00000868	PTTG1	0.40	pituitary tumor-transforming 1
SS00004979	KIAA1279	0.39	KIAA1279
SS00009988	TRPC3	0.35	transient receptor potential cation channel, subfamily C, member 3
SS00001680	CD83	0.32	CD83 antigen (activated B lymphocytes, immunoglobulin superfamily)
180 minutes			
SS00000203	KLF2	1.51	Kruppel-like factor 2 (lung)
SS00007520	KLF4	1.17	Kruppel-like factor 4 (gut)
SS00006925	ID1	0.99	inhibitor of DNA binding 1, dominant negative helix-loop-helix protein
SS00007619	ID2	0.87	inhibitor of DNA binding 2, dominant negative helix-loop-helix protein
SS00009975	KCNN4	0.79	potassium intermediate/small conductance calcium-activated channel, subfamily N, member 4
SS00003184	WASL	0.75	Wiskott-Aldrich syndrome-like
SS00006914	DSIPI	0.75	delta sleep inducing peptide, immunoreactor
SS00000220	ID2	0.72	inhibitor of DNA binding 2, dominant negative helix-loop-helix protein
SS00005051	LOC401137	0.63	hypothetical LOC401137
SS00008118	STK38L	0.63	serine/threonine kinase 38 like
SS00007835	LOC401137	0.54	hypothetical LOC401137
SS00009553	TEK	0.52	TEK tyrosine kinase, endothelial (venous malformations, multiple cutaneous and mucosal)
SS00000205	FAM26B	0.50	family with sequence similarity 26, member B
SS00000537	GJA4	0.46	gap junction protein, alpha 4, 37kDa (connexin 37)
SS00000587	HMOX1	0.45	heme oxygenase (decycling) 1
SS00001680	CD83	0.39	CD83 antigen (activated B lymphocytes, immunoglobulin superfamily)
SS00007712		0.37	
SS00008566	YWHAH	0.35	tyrosine 3-monooxygenase/tryptophan 5-monooxygenase activation protein, eta polypeptide
SS00009439		0.35	
SS00006985	DOK4	0.26	docking protein 4
SS00001142	KIT	-0.33	v-kit Hardy-Zuckerman 4 feline sarcoma viral oncogene homolog
SS00003482	TTC5	-0.36	tetratricopeptide repeat domain 5
SS00007051		-0.41	
SS00004185	RGS2	-0.69	regulator of G-protein signalling 2, 24kDa
SS00001048	HLA-A	-0.69	major histocompatibility complex, class I, A
SS00005446	CXCR4	-0.77	chemokine (C-X-C motif) receptor 4
SS00002290	CXCR4	-0.81	chemokine (C-X-C motif) receptor 4
360 minutes			
SS00000203	KLF2	1.56	Kruppel-like factor 2 (lung)
SS00006925	ID1	1.36	inhibitor of DNA binding 1, dominant negative helix-loop-helix protein
SS00007520	KLF4	1.30	Kruppel-like factor 4 (gut)
SS00009782	HTR2B	1.22	5-hydroxytryptamine (serotonin) receptor 2B
SS00009975	KCNN4	1.16	potassium intermediate/small conductance calcium-activated channel, subfamily N,

			member 4
SS00007619	ID2	1.08	inhibitor of DNA binding 2, dominant negative helix-loop-helix protein
SS00000510	NOS3	0.94	nitric oxide synthase 3 (endothelial cell)
SS00009004	13CDNA73	0.90	hypothetical protein CG003
SS00006583	COL4A1	0.86	collagen, type IV, alpha 1
SS00000220	ID2	0.85	inhibitor of DNA binding 2, dominant negative helix-loop-helix protein
SS00000587	HMOX1	0.77	heme oxygenase (decycling) 1
SS00001573	NPR1	0.77	natriuretic peptide receptor A/guanylate cyclase A (atriuretic peptide receptor A)
SS00007009	LOC57228	0.77	hypothetical protein from clone 643
SS00006949	EMILIN2	0.75	elastin microfibril interfacier 2
SS00006914	DSIPI	0.72	delta sleep inducing peptide, immunoreactor
SS00005801	HYAL2	0.68	hyaluronoglucosaminidase 2
SS00007835	LOC401137	0.67	hypothetical LOC401137
SS00009553	TEK	0.67	TEK tyrosine kinase, endothelial (venous malformations, multiple cutaneous and mucosal)
SS00009312		0.66	
SS00000205	FAM26B	0.65	family with sequence similarity 26, member B
SS00009154		0.64	
SS00003980	UPK3A	0.63	uroplakin 3A
SS00007236	FGFR3	0.60	fibroblast growth factor receptor 3 (achondroplasia, thanatophoric dwarfism)
SS00004694	PLEK2	0.60	pleckstrin 2
SS00005554	LOC401137	0.60	hypothetical LOC401137
SS00000499	DSTN	0.59	destrin (actin depolymerizing factor)
SS00008566	YWHAH	0.58	tyrosine 3-monooxygenase/tryptophan 5-monooxygenase activation protein, eta polypeptide
SS00000227	CXXC5	0.58	CXXC finger 5
SS00001921	SLC9A3R2	0.57	solute carrier family 9 (sodium/hydrogen exchanger), isoform 3 regulatory factor 2
SS00008590		0.55	
SS00008418	RAI17	0.55	retinoic acid induced 17
SS00006985	DOK4	0.53	docking protein 4
SS00007163	TMEPAI	0.53	transmembrane, prostate androgen induced RNA
SS00003206	ZFP106	0.52	zinc finger protein 106 homolog (mouse)
SS00010071	FAM26B	0.52	family with sequence similarity 26, member B
SS00009566	CLOCK	0.52	clock homolog (mouse)
SS00010488	C10ORF45	0.52	chromosome 10 open reading frame 45
SS00005569	PSAT1	0.51	phosphoserine aminotransferase 1
SS00000439		0.50	
SS00008883	SHCBP1	0.47	likely ortholog of mouse Shc SH2-domain binding protein 1
SS00002193	PSPH	0.46	phosphoserine phosphatase

SS00008822	ETS2	0.45	v-ets erythroblastosis virus E26 oncogene homolog 2 (avian)
SS00000711	PLK1	0.44	polo-like kinase 1 (Drosophila)
SS00003556	COBLL1	0.43	COBL-like 1
SS00002036	AK1	0.43	adenylate kinase 1
SS00009158	LOC401137	0.42	hypothetical LOC401137
SS00007829	RAMP2	0.42	receptor (calcitonin) activity modifying protein 2
SS00000616	TOP2A	0.34	topoisomerase (DNA) II alpha 170kDa
SS00000501	DCN	-0.57	decorin
SS00001142	KIT	-0.67	v-kit Hardy-Zuckerman 4 feline sarcoma viral oncogene homolog
SS00002946	AREG	-0.85	amphiregulin (schwannoma-derived growth factor)
SS00005446	CXCR4	-0.88	chemokine (C-X-C motif) receptor 4
SS00002290	CXCR4	-0.91	chemokine (C-X-C motif) receptor 4
SS00004185	RGS2	-0.93	regulator of G-protein signalling 2, 24kDa

Interconnected gene network

All these 86 genes were fed to the ingenuity pathway analysis (IPA) server to explore the interconnections among them. IPA constructed the most interconnected maps of the identified genes based on the knowledge database obtained from literature. The connection between any two genes is experiment-supported direct interaction between these two genes or proteins. The gene networks serves as a tool to navigate through the gene list and identify the “hub” genes. Figure 24 shows the top ranked gene network that contains 20 of all the 86 genes.

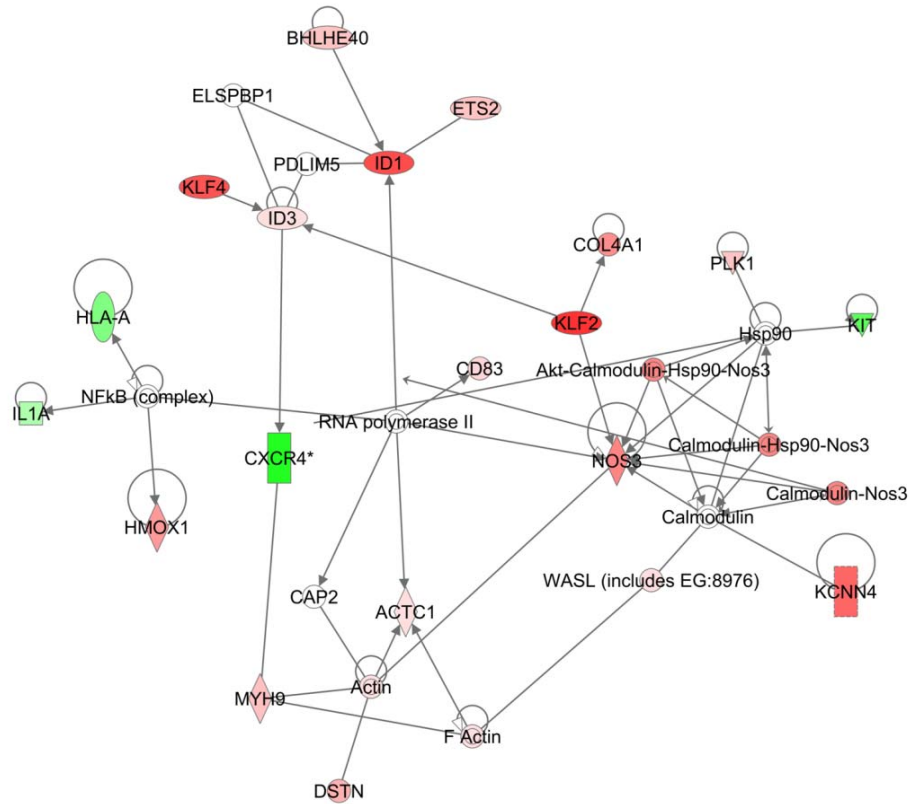


Figure 24: The top ranked gene network generated by IPA from genes identified in the magnitude step-up experiment. Each gene is color-coded by the expression value at 360 minutes. Red: overexpress; Green: underexpress.

This gene network contains four gene clusters centered on four hub genes , inhibitor of DNA binding 1 (top), eNOS (right), Actin (bottom) and NFκB (left). Three of the hub genes (eNOS, Actin and NFκB) have implications in maintaining healthy endothelial functions. Thus, the gene network suggests that a significant number of identified genes might play roles in regulating vascular functions.

Several previously known atherosclerosis-relevant genes appear in the identified gene list. The regulation pattern of these genes and their importance in endothelial functions are discussed below. Other genes with possible implications in atherogenesis or maintaining normal endothelial function are also discussed. The temporal expression profiles of the discussed genes are presented in Figure 25 in detail.

5 minutes and 15 minutes after step-up

During the early response period, only a few genes were identified as differentially expressed. The mRNA quantity of pro-inflammatory cytokine interleukin- 1α was reduced immediately after endothelial cells were exposed to increased shear stress for only 5 minute. Interleukin- 1α can induce the expression of endothelial-leukocyte adhesion molecules, such as E-selection and VCAM-1[94]. Thus, the elevated shear stress might have an immediate effect to inhibit endothelial-leukocyte adhesion.

Fifteen minutes after flow, the expression of actin α was increased. Although the function of this type of actin is unknown in endothelial cells, expression and distribution of actin proteins play important role in endothelial structure and barrier function [95]. This suggests endothelial cytoskeletal structure may start to change as earlier as 15 minutes after the step-up.

45 minutes after step-up

Forty-five minutes after the step-up, the mRNA level of myosin heavy chain (MHY9, non-muscle heavy chain-A), an actin-based motor protein, was doubled.

Myosin heavy chains are involved in reorganization of actin cytoskeleton and change of cell shape [96]. MHY9 was also reported to be upregulated in response to vascular injury [97]. Furthermore, MHY9 can bind and transport the angiogenic protein, nucleolin, playing a critical role in the modulation of angiogenesis [98]. Thus, the upregulation of MHY9 possibly indicates the remodeling of endothelial cytoskeleton and increased intracellular transport activity.

Brain-heart-protocadherin (PCDH7), a member of cadherin family, was also upregulated at 45 minutes. Although the function of PCDH7 in endothelial cells is still unknown, PCDH7 is thought to function in cell-cell recognition and adhesion [99]. Interestingly, single nucleotide polymorphism (SNP) of this gene is associated with coronary artery disease by a genome-wide association study [100].

Secretory carrier membrane protein 1 (SCAMP1), a Golgi membrane protein [101], was also upregulated at 45 minutes. SCAMP1 has been demonstrated to be an important Golgi vesicular trafficking protein [102] and has been implicated in both exocytosis and endocytosis activities [103-105]. As a ubiquitous component of recycling vesicles that shuttle between the plasma membrane and the Golgi complex, the upregulation of SCAMP1 gene can facilitate the trans-endothelial protein transport. It is also reasonable to hypothesize a possible involvement of SCAMP1 in nitric oxide synthesis because the Golgi association of eNOS and the trafficking of eNOS between Golgi and caveolae [98] are important in NO production.

90 minutes after step-up

Starting from 90 minutes, inhibitor of DNA binding 1, 2 and 3 (ID1, ID2 and ID3) were significantly upregulated. The proteins encoded by this family of genes are helix-loop-helix (HLH) protein. They can form heterodimers with basic HLH family of transcriptional factors, thus inhibiting the DNA binding and transcriptional activation ability of these transcriptional factors. ID family genes regulate cell cycle and cell fate, and they play an essential role in angiogenesis, both in vascular development and during the growth and metastasis of tumors [106-108]. Specifically, it has been demonstrated that ID1 can increase the proliferation activity of endothelial cells and participate in angiogenic processes [109, 110]. Overexpression of ID1 and ID3 in endothelial cells can increase the expression of ICAM-1 and E-selectin, and induce matrix metalloproteinase-2 and -9 transcription, endothelial migration and tube formation [109]. Furthermore, Ling et. al. [111] suggested that ID1 is one of the upstream regulators of NF- κ B and can activate NF- κ B signaling pathway to promote cell survival against apoptosis induced by TNF α . Although not previously studied as shear-stress sensitive genes, the upregulation of ID1, ID2 and ID3 found in our study suggests a crucial role of these genes in mediation of endothelial activation and gene expression in responses to shear stress.

KLF2 and KLF4 were up-regulated at 90 minutes and later time points. KLF2 and KLF4 are shear stress sensitive genes [27, 30] and important regulators of endothelial

activation in response to proinflammatory stimuli [54]. Overexpression of KLF2 in endothelial cells induces eNOS expression and increase eNOS activity. KLF2 can inhibit the induction of VCAM-1 and E-selectin in response to various proinflammatory cytokines [54]. KLF2 also helps to maintain an antithrombotic endothelial function by regulating key factors including thrombomodulin (TM), tissue factor (TF) and plasminogen activator inhibitor-1 (PAI-1) [55].

Other atherosclerosis related genes, including the cytoprotective and growth arrest gene, GADD45 β [31] and basement membrane protein, COL4A1 (collagen type IV α) [112], were also upregulated at 90 minutes.

180 minutes after step-up

Gene KCNN4, encoding the intermediate-conductance calcium-activated potassium channel, was upregulated at 180 and 360 minutes. KCNN4 is a critical mediator of endothelial hyperpolarization and endothelium-derived hyperpolarizing factor (EDHF)-mediated dilation [113, 114]. Specifically, upregulation of KCNN4 can increase the endothelial and smooth muscle cell hyperpolarization and EDHF signaling in response to the dilation cues, including increased shear stress [115-117]. One study even demonstrated that KCNN4-mediated EDHF signaling contributes dominantly to the flow-induced vasodilatation in coronary arterioles in patients with cardiovascular disease [118]. Thus, two important vascular dilation mediators, KCNN4 and eNOS (upregulated at 180 minutes, but only statistically significant at 360 minutes) were both

upregulated by the prolonged exposure to the elevated shear stress. In response to increased blood flow *in vivo*, endothelial cells employ NO and EDHF mediated pathways to dilate the blood vessels, thus reducing the shear stress. However, in our *in vitro* setting, endothelial cells were unable to regulate the shear stress. Therefore, endothelial cells attempted to adapt to the altered hemodynamic environment by producing more flow-induced dilation mediators.

Heme oxygenase-1 (HMOX1), an inducible enzyme in response to oxidative stress, was also upregulated at 180 and 360 minutes. HMOX1 has been recently recognized as an important anti-oxidative, cytoprotective and anti-inflammatory gene [68, 69]. Free heme catalyzes the production of reactive oxygen species (ROS), leading to endothelial dysfunction. Thus, HMOX1, which converts heme to carbon monoxide and biliverdin/bilirubin, is protective against the development of atherosclerosis and has been proposed as a novel therapeutic target [119, 120]. Overexpression of HMOX1 in endothelial cells also inhibits the expression of inflammatory adhesion molecules E-selectin and VCAM1 by inhibiting the activation of NF κ B [121], possibly through the reaction product bilirubin [122]. Indeed, the expressions of E-selectin and VCAM1 in our study were decreased at both 180 and 360 minutes although not significantly. Therefore, the upregulation of HMOX1 during the endothelial adaption can be a critical atheroprotective mediator that can reduce the oxidative and inflammatory level of endothelial cells.

Chemokine (C-X-C motif) receptor 4, CXCR4, was downregulated at both 180 minutes and 360 minutes. As a chemokine receptor, CXCR4 modulates endothelial inflammatory states. Low expression level of CXCR4 was able to inhibit endothelial apoptosis, and overexpression of CXCR4 induces the transcription of cytokines MCP-1 and IL-8. High levels of CXCR4 expression was also found in endothelial cells from atherosclerotic lesions, relative to healthy arteries [123].

Regulator of G-protein signaling 2, RGS2, was a novel mediator of vascular function [95, 124-126], acting as GTPase activating proteins for G α subunits of heterotrimeric G proteins. The downregulation of RGS2 by increased shear stress could attenuate the kinetic regulation of vasoconstrictor signaling and lead to the prolonged response of G protein-coupled receptors to vasoconstrictors [126]. Sun et. al. further demonstrated that RGS2 is an important downstream effector of NO-cGMP pathway to promote vascular relaxation [124]. Recently, Anger et. al. suggested a role of RGS2 in endothelial inflammation by mediating ERK 1/2 activation [127]. Although G protein-coupled receptors has been identified as an important mechanosensor for shear stress [128], regulation of RGS2 by shear stress is unknown previously and its implication in endothelial response to shear stress deserves further investigation.

360 minutes after step-up

Most of atherosclerosis-related genes that were regulated at 360 minutes has already been identified and discussed at earlier time points. This includes the continued

overexpression of KLF2, KLF4, ID1, ID2, eNOS, KCNN4, COL4A1 and downregulation of CXCR4 and RGS2.

At 360 minutes, two extracellular matrix related genes, elastin microfibril interfacier2 (EMILIN2) and hyaluronoglycosaminidase 2 (HYAL2) and an actin depolymerizing protein, destrin (DSTN), were upregulated. Although the functions of these proteins in endothelial cells remain unknown, their upregulation may suggest the process of the remodeling of extracellular matrix, cell adhesion to the matrix and cell migration after prolonged exposure to elevated shear stress.

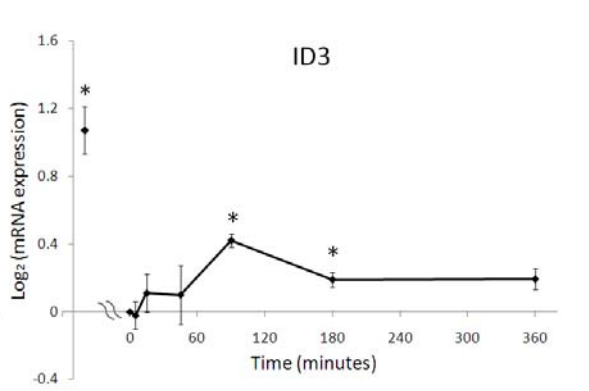
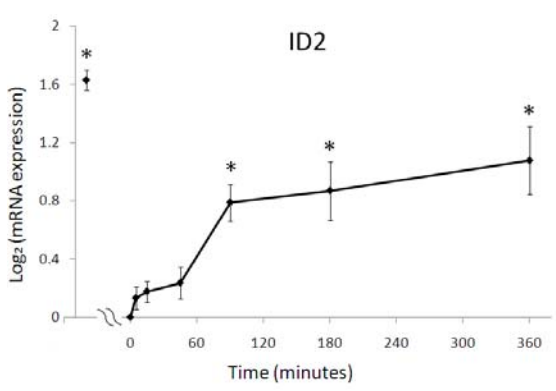
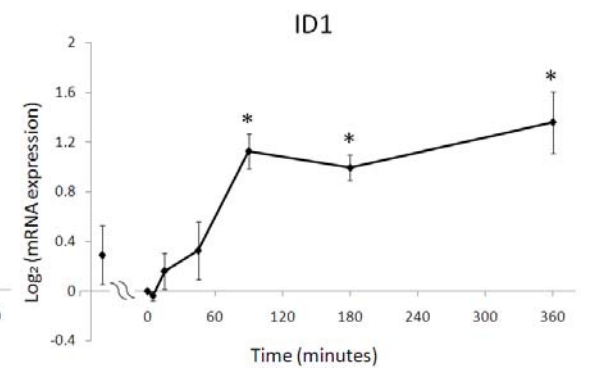
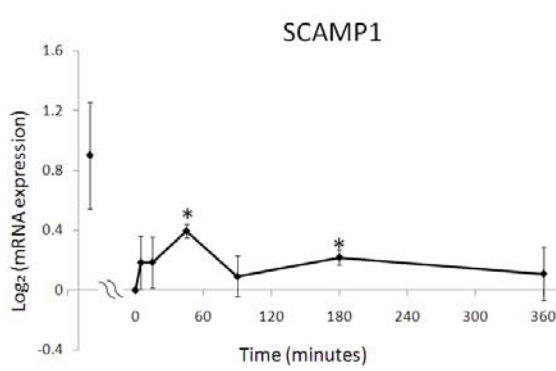
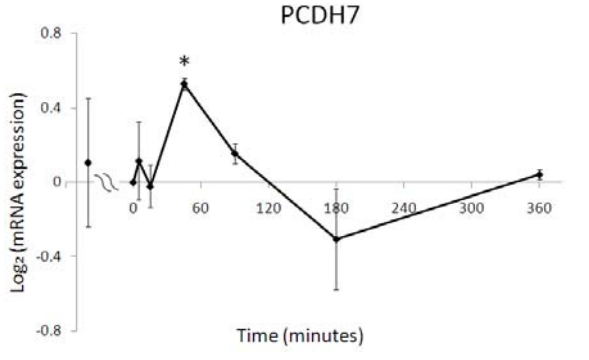
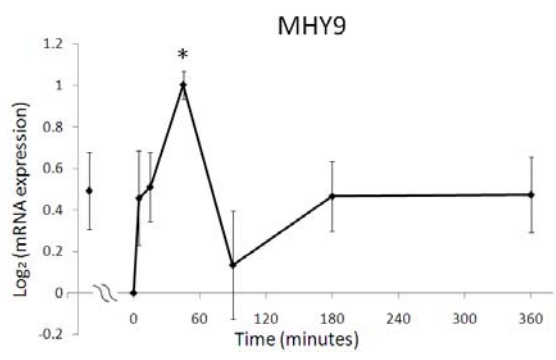
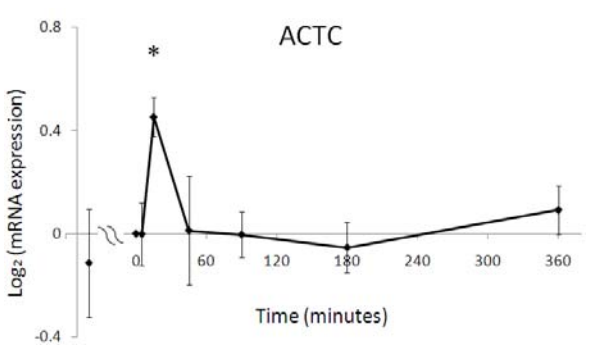
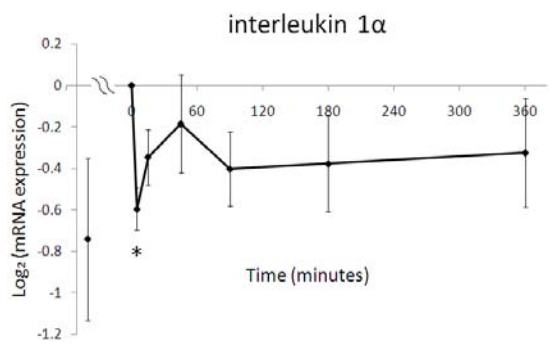
Summary

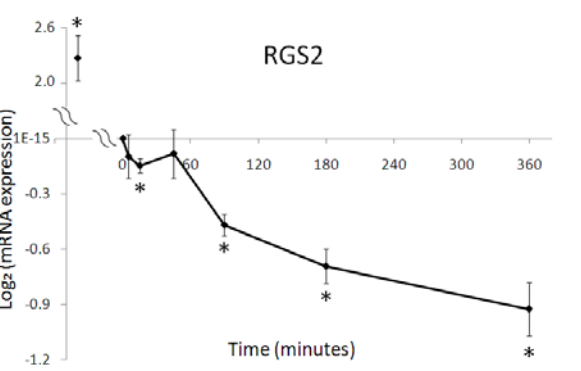
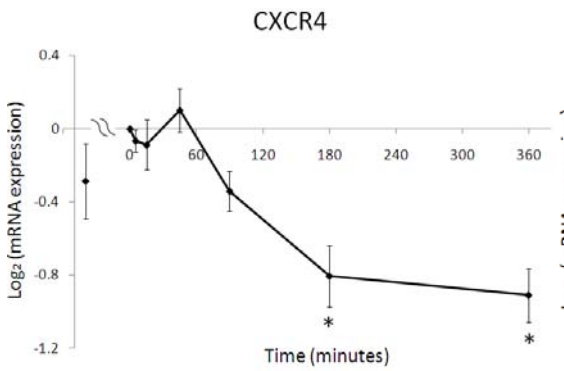
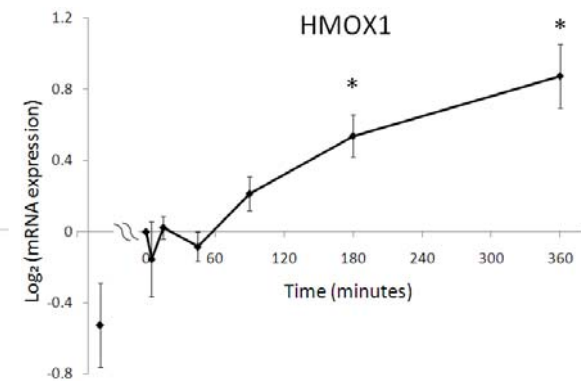
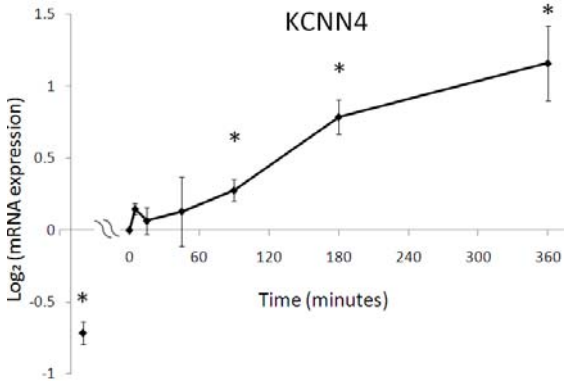
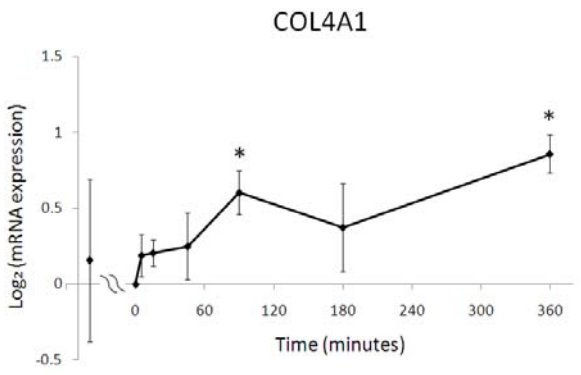
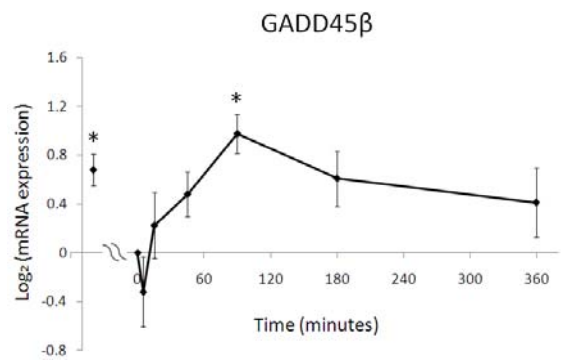
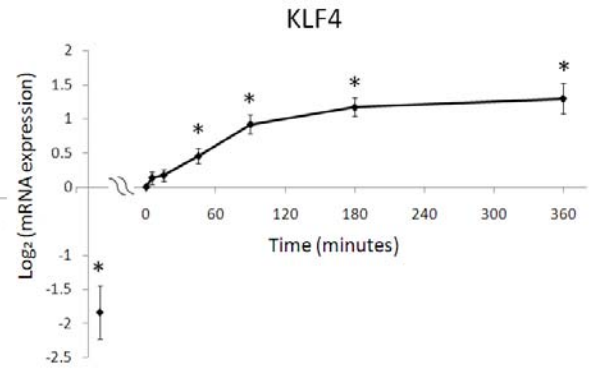
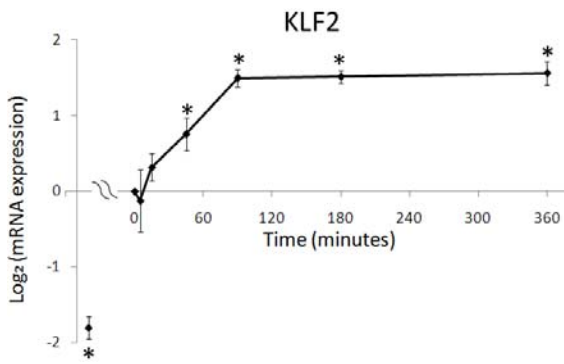
The temporal expression profiles of the 20 genes discussed above are plotted in Figure 25. Although all these genes were identified to be differentially regulated during the adaptive response, only eight of them showed significantly different expression levels in endothelial cells sheared by 24 hours basal level shear stress, relative to the static cultured controls. Furthermore, for four of the eight genes regulated by basal shear stress (ID2, ID3, GADD45 β and DESTN), the directions of gene regulation caused by the basal level shear stress and the elevated shear stress were opposite to each other. For example, 24 hours exposure to basal level shear stress significantly inhibited the expression of ID2 relative to static control; however, continued exposure to a higher level of shear stress for 90 minutes increased the expression level of ID2. Thus, the result suggests that either the mechanisms by which shear stress regulate these genes are

different in the static cultured cells than in the shear-stress preconditioned cells or, more likely, the gene expression patterns during the adaptive response are only transient and the prolonged shear stress (24 hours) may invoke other regulation mechanisms to counteract the early response.

Taken together, only four genes, KLF2, KLF4, KCNN4 and RGS2, were significantly regulated in the consistent directions by the basal level shear stress (relative to static cells) and the elevated shear stress (relative to shear stress preconditioned cells).

Indeed, we have identified several previously unknown shear stress sensitive genes, such as ID1, which may be important regulators in atherogenesis and can serve as potential therapeutic targets.





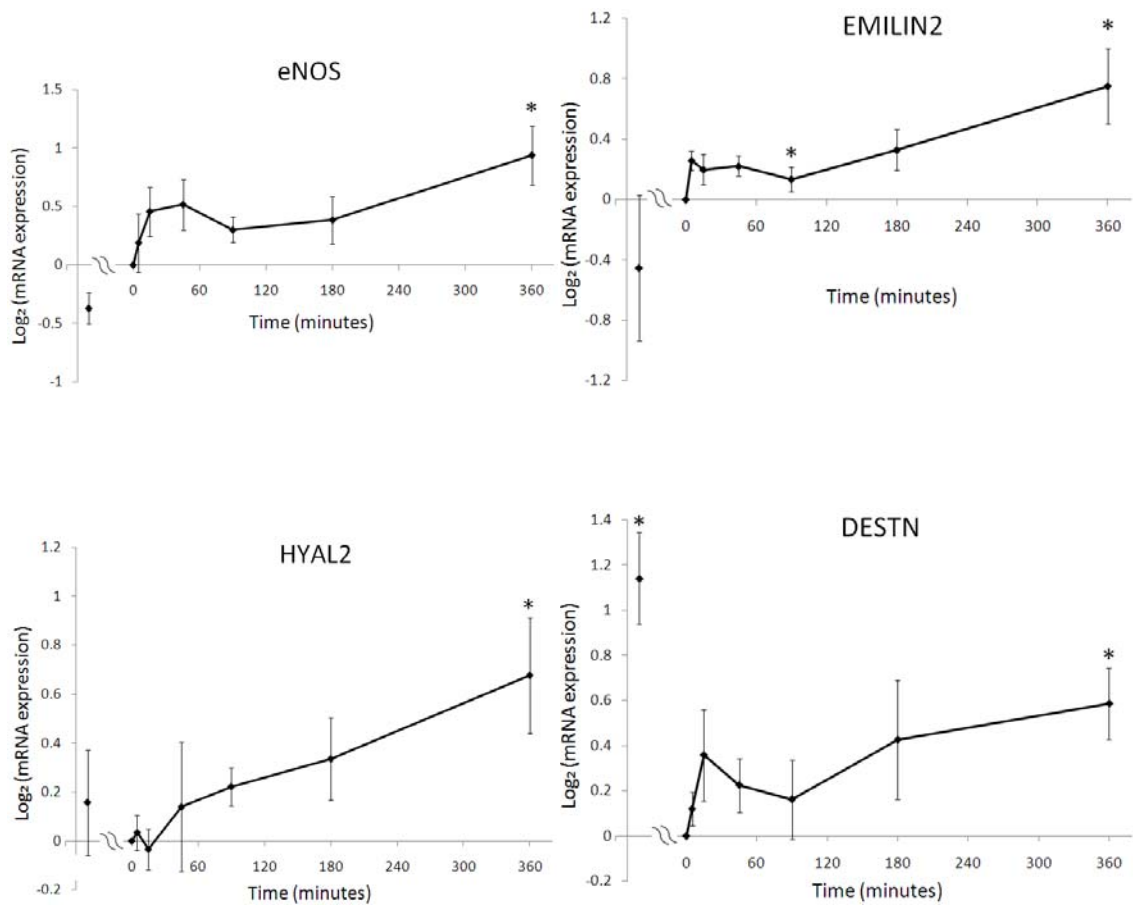


Figure 25: Expression profiles of the selected genes in the magnitude step-up study. The temporal regulation patterns of atherosclerosis-related genes are plotted. All expression values were normalized to Time 0 (the pre-step-up controls). In each panel, the first data point represents the expression value of the static cultured endothelial cells and the value was obtained from the control set experiments. *, p-value < 0.05, one-sample t-test against zero without false discovery controls.

Hierarchical clustering

All the 86 identified genes were pooled together and clustered as shown in Figure 26. The expression of a single gene at different time points is represented as one horizontal row of the heat map, and each row is the transcriptional profile of the 86 genes at each time point. The color scale represents the mean expression level (n=4) relative to the corresponding pre-step-up control. Yellow indicates an expression ratio of unity. Red and green indicate upregulation and downregulation, respectively.

The dendrogram on top of the heat map clustered the time points that had the most similar expressional profiles. As shown in Figure 26, for these 86 genes, the expressional profiles at 5 minutes and 15 minutes are similar and the expressional profiles of 90 minutes and 180 minutes are close to each other. Time point 360 minutes had the most distinct expression profile. However, it should be expected since more than half of the clustered 86 genes were identified at 360 minutes.

The dendrogram at left of the heat map clusters genes with similar temporal expression profiles. Based on the gene tree, the heat map can be subdivided into seven regions, region A to G as shown in Figure 26. Each region is a cluster of genes with similar temporal regulation patterns. Panels A to G in Figure 26 plot the expression values of genes random sampled from the corresponding regions.

The gene tree revealed that there are at least five distinct temporal gene expression patterns among the 86 genes. The expression levels of genes in clusters A and

G increased immediately upon shear stress increase and continued to rise gradually throughout the adaptive process. KLF2, KLF4, ID1, ID2, eNOS and COL4A1 are among those genes.

Genes in cluster B responded slower and were up-regulated around 180 hours after step-up, suggesting possible downstream positions in the signaling cascade. EMILIN2, HYAL2, DSTN and HMOX1 are in this cluster.

Transcriptional levels of genes in clusters C, D and E were not changed monotonically. The time course of expression in clusters C and E suggests possible roles for those genes as intermediates in signal transduction.

Genes in cluster D only participates in the adaptive responses transiently, and their expression levels fell back to the control level after a burst between 45 to 90 minutes. These genes would be easily overlooked if expression levels were only measured at the end points. These genes include SCAMP1, KLF10 and ACTC.

A small portion of genes were down regulated during adaptation (cluster F), most of which were significantly under-expressed after 180 minutes exposure to increased shear stress. CXCR4, RGS2 and HLA-A are among those genes.

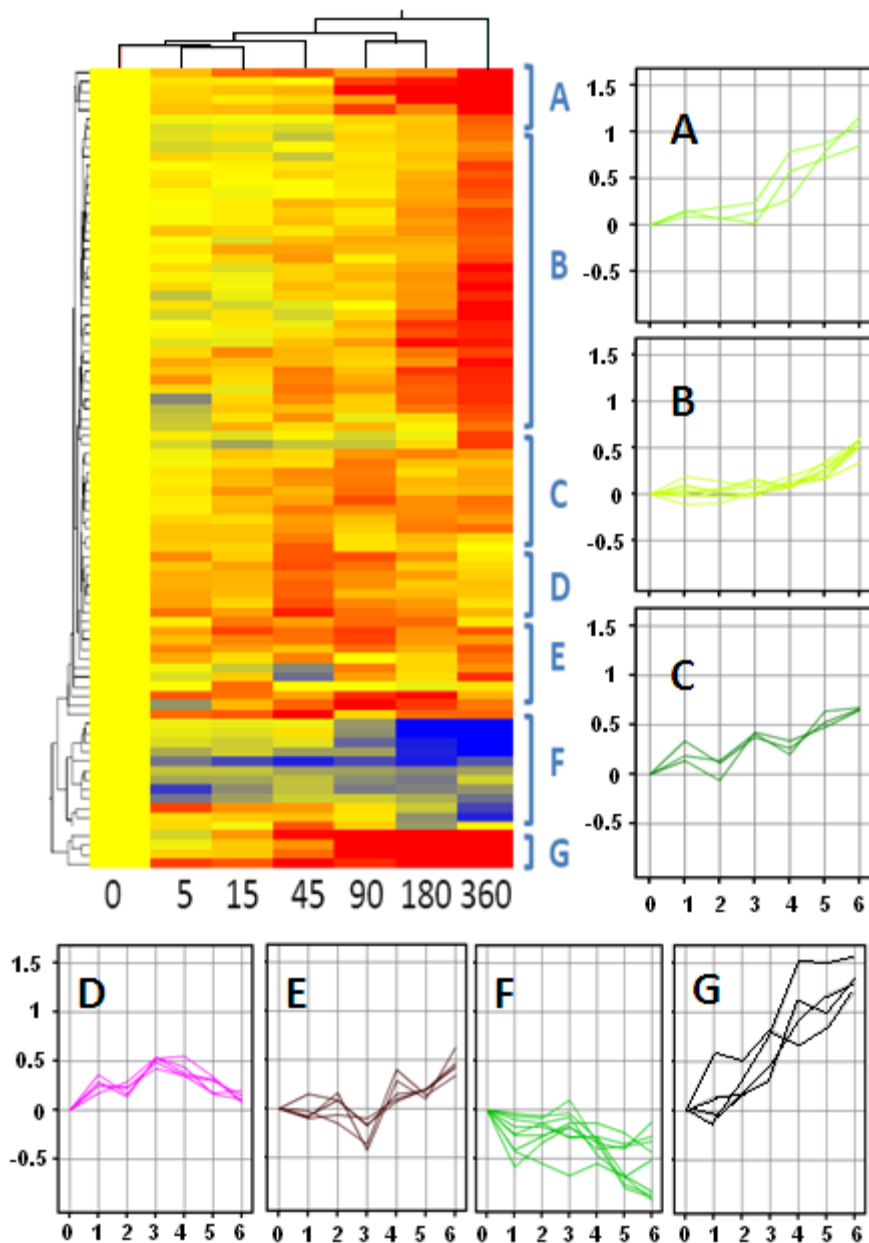


Figure 26: Identified genes clustered to show the temporal gene regulation profiles. . Panels A to G plot the expression values of genes random sampled from the corresponding regions from the heat map.

4.3.2.2 Expression of an *a-priori* Selection of Atherosclerosis-related Shear-Sensitive Genes

To further understand how the adaptive response of endothelial gene expression affects arterial atherosusceptibility, we next examined an *a-priori* selected set of genes that are known to participate in atherogenesis. These genes are listed in Table 10. Extensive studies have demonstrated their participants in maintaining normal endothelial function and in the development of atherosclerosis. Literature discussing the function of each selected gene is cited in the table. Some of these genes have already been discussed in the previous section and are included here for completeness. Paired t-test was used to test if the expression value is different than zero. No false discovery rate control was applied. Genes with a p-value less than 0.05 are marked in red and ones with p-value less than 0.1 are marked in blue.

We first examine how these genes were regulated in the control set of experiments. Previous studies have shown that, for most of these genes, the expression levels are regulated by shear stress. The known effects of shear stress are noted in the table with references, and the up or downregulation by laminar shear stress (LSS) or disturbed shear stress (DSS) is relative to static cultured cells. As shown in Table 5, data from the control set of experiments are consistent with the previous studies for all the genes, except for two, MCP1 and GADD45 β . In our study, MCP1 (CCL2) was upregulated by basal level shear stress relative to static cells. Although two studies showed the opposite result [45, 50], Shyy et al. [51] demonstrated a biphasic response of

MCP1 expression to shear stress where mRNA level increases upon the onset of the shear stress and then decreases to the static value or lower. This suggests a complex regulation mechanism of MCP1 expression by shear stress and further study is necessary. Our study also suggested a decreased mRNA level of GADD45 β in the shear preconditioned cells as compared with the static cells. Lin et al. found 24 hours of laminar shear stress increased GADD45 β promoter activities and protein expression [70]. However, GADD45 β mRNA level was slightly decreased by shear stress in another study [31]. Thus, the mechanism by which shear stress regulates GADD45 β expression warrants further investigation. Actually, our step-up study offered a potential explanation. As shown in Table 10, upon the increase of shear stress, the mRNA level of GADD45 β started to increase. The expression value was almost doubled at 90 minutes, and then decreased slowly afterwards. This suggests that this cytoprotective gene is induced temporally by the external stimuli, and the mRNA production stops once enough mRNA copies were transcribed in the initial response phase. After the cells adapted to new environments, lower level of mRNA quantity was maintained, which explains the seemingly contradicted previous results.

Although most of these genes were differentially expressed under shear stress relative to static cells, only part of them responded to increased shear stress after being preconditioned by the basal level shear stress. Besides the previously discussed upregulation of KLF2, KLF4, eNOS, GADD45 β and HMOX1, the expression of two

inflammatory genes, bone morphogenetic protein-4 (BMP4) and interleukin-8 (IL8), were repressed at one or more time points ($p < 0.05$) by the increased shear stress. The expression of the *a priori* selected genes suggests the elevated shear stress has a predominantly anti-inflammatory and anti-oxidative atheroprotective effect on endothelial cells. Furthermore, these seven genes, which are able to respond to shear stress in the preconditioned endothelial cells, may be more significant in the development of atherosclerosis *in vivo* since the regulation of the other genes is likely an *in vitro* response to the onset of flow from static conditions.

Table 10: The expression of *a-priori* selected genes in response to the elevated shear stress. Red: p<0.05; blue: p<0.1. LSS: laminar shear stress, DSS: disturbed shear stress.

	Preconditioned cells	During adaptation (normalized to preconditioned cells)					
	(normalized to static cells)	5	15	45	90	180	360
Inflammatory and adhesion genes							
ICAM1	-0.50	-0.12	0.01	0.10	-0.03	0.01	0.17
	Inflammatory adhesion molecule [46-49]. LSS: ↓ [45].						
VCAM1	-1.98	0.00	0.14	0.07	-0.19	-0.32	-0.31
	Inflammatory adhesion molecule [46-49]. LSS: ↓ [27, 45]; DSS: ↑ [45]						
CCL2	1.18	-0.21	0.15	-0.02	0.01	-0.01	0.23
	MCP1, Inflammatory molecule [47-49]. LSS: ↓ [45, 50] or biphasic [51]; DSS: ↑ [45]						
SELE	-0.25	-0.37	-0.16	-0.06	-0.26	-0.18	-0.07
	Adhesion molecule, E-selectin [46-49]. LSS: ↓ [45]; DSS: ↑ [45]						
FOS	-0.24	0.21	0.21	0.00	-0.18	0.92	-0.22
	c-fos gene, activating protein-1, inflammatory [52, 53]						
JUN	-1.69	-0.04	0.17	0.27	0.26	0.02	0.08
	c-jun gene, activating protein-1, inflammatory [52, 53]. LSS: ↓ [36]						
KLF2	1.81	-0.13	0.31	0.76	1.50	1.51	1.56
	Inflammatory regulation transcription factor [54-56]. LSS: ↑ [27, 54]						
KLF4	1.83	0.14	0.17	0.45	0.92	1.17	1.30
	Inflammatory regulation transcription factor [57]. LSS: ↑ [57, 58]						
BMP4	-2.17	-0.10	0.00	-0.04	-0.32	-0.23	-0.17
	Activates inflammatory [43, 60]. LSS: ↓ [50, 59]; DSS: ↑ [45]						
RELA	-0.11	-0.05	0.06	-0.02	0.03	0.07	0.11
	p65, NFκB [47-49]						
NFKBIA	-1.31	-0.07	0.08	0.01	0.11	0.10	0.13
	NFκB inhibitor, IκBα [47-49]. LSS: ↓ [61]						
IL8	0.95	-0.63	-0.54	-0.91	-0.80	-0.85	-0.87
	Inflammatory chemokine [47-49]. LSS: ↑ [62, 63]						
Vasomotion							
NOS3	0.37	0.19	0.46	0.52	0.30	0.38	0.94
	eNOS [11, 26]. LSS: ↑ [27]						
EDN1	-0.98	0.00	0.01	0.11	0.01	-0.14	0.01
	Endothelin-1 [26]. LSS: ↓ [50, 64]						
Caveolin-1	-1.39	-0.08	-0.01	0.08	-0.10	-0.25	-0.25
	Caveolin-1 [11, 26]. LSS: ↓ [27, 50, 59, 66]						
Oxidative state regulators							
SOD2	0.33	-0.36	-0.24	-0.51	-0.34	-0.27	-0.49
	cytoprotective, MnSOD [31]. LSS: ↑ [27]; DSS: ↓ [45]						
GADD45β	-0.68	-0.32	0.22	0.48	0.98	0.61	0.41
	cytoprotective gene [31]. LSS: ↑ [70] or slightly ↓ [31]						
HMOX1	0.53	-0.12	0.08	-0.13	0.12	0.45	0.77
	anti-oxidative, cytoprotective and anti-inflammatory gene [68, 69]. LSS: ↑ [50]						

4.3.2.3 Global Gene Expression Profiles during Adaptation

To understand how the endothelial transcriptome was dynamically controlled in response to the elevated shear stress magnitude, the expression of all genes were examined in this section.

Statistic summary of the transcriptional profiles at each time points are presented in Figure 27. The means and variance of the expression values (relative to the preconditioned cells) of all genes were calculated for each time point. The means are all close to zero, which is reassuring since the expression values of the majority of genes should not be affected by the elevated shear stress. The variance at time point 45 minutes is much larger than other time points, which is also shown by the histograms in Figure 27. This suggests, comparing to other time points, more genes were differentially expressed at 45 minutes. Thus, the endothelial transcriptome was greatly disturbed at 45 minutes by the elevated shear stress.

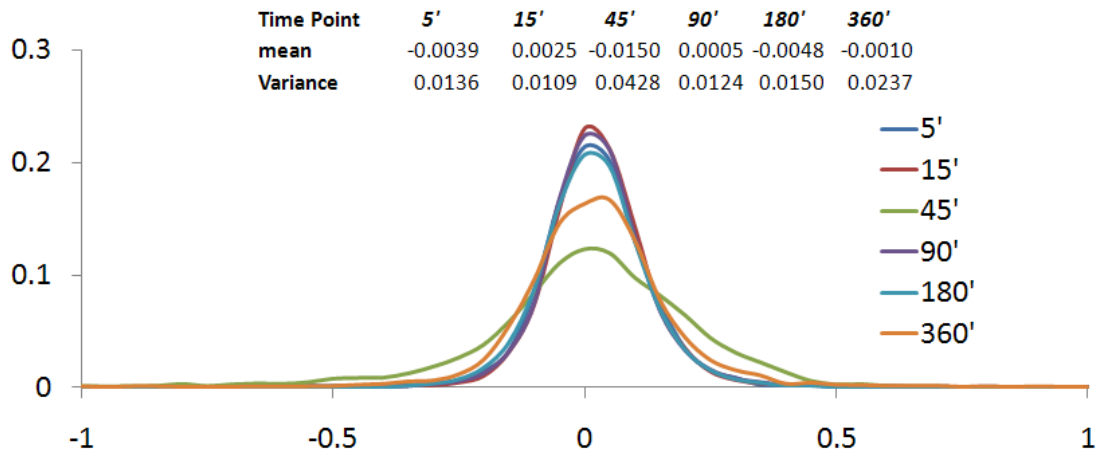


Figure 27: Statistic summary of the transcriptional profiles at each time points. Inserted table: the mean and variance of each time point over all genes. Histograms of all genes at each time point: x, expression value; bin size: 0.05; y, number of genes in each bin normalized by the total number of genes.

To understand how the expression profile at one time point is related to another, scatter plots in Figure 28 were used to visualize the comparison of transcriptional profiles between any two time points. All genes were plotted as individual data points in each panel. The x-axis is the expression value at the time point specified on top of the graph, and y-axis is the expression value at the other time point, specified on the left of the graph. If two time points have similar gene expression profiles, the data points will scatter along the diagonal line of $y=x$. As shown in Figure 28, three time points at the later stage of the adaptive response, 90, 180 and 360 minutes have relatively similar expression profiles. This is consistent with the observation made with individual genes as discussed in previous sections. After 90 minutes exposure to the elevated shear stress, endothelial cells seems to have passed the active response period and most genes

continue being up or down-regulated monotonically. This suggests the endothelial transcriptome is controlled by stable upstream regulation signals after 90 minutes and endothelial cells may enter the phase of being fully adapted to the new environment. On the contrary, the gene expression profiles show less similarity at the earlier adaptation stage (5, 15 and 45 minutes), indicating a dynamic early response phase. Especially, the transcriptional profile at 45 minutes is different than any other time points. As shown in the panels where 45 minutes is compared with other time points, a significant number of genes lie in the second and fourth quadrants, which indicates the opposite regulation directions at the two time points compared.

To further demonstrate this, all genes were clustered in Figure 29a. The hierarchical tree suggests time points 5 minutes and 15 minutes have similar transcriptional profiles, and so do the time points 90 minutes and 180 minutes. Time point 45 minutes branched out from all other time points at the root of the hierarchical tree, indicating a distinct global transcriptional profile.

The principal component analysis was applied to the six time points (Figure 29b), and further confirmed this finding. The expression profiles at six time points are projected onto the plane of the principal components (PC) 1 and 2 and the plane of PC1 and PC3. The first three principal components account for 80% of the total variability. As shown in Figure 29b, the 45 minutes time point is separated far from all other time points by PC1, confirming a unique endothelial expression profile at 45 minutes. Furthermore, the

path of the point moving over time in the projected plane was interesting. As shown in Figure 29b, from 5 minutes to 45 minutes, the coordinates along PC1 increase over time; however, after 45 minutes, the coordinates along PC1 decrease over time. This suggests that the time point 45 minutes is not only different but also a critical turning point.

The principal analysis showed in Figure 29b considered all genes as variables, so that each condition, i.e. time point, can be explained by the “principal gene components”. As suggested by Raychaudhuri et al. [129], principal component analysis can also be performed with time points as variables to summarize the patterns in which gene responses to each condition, i.e. how the genes were regulated over time. Figure 30a is the plot of the eigenvalues of all six principal components. Using the cutoff criterion that discards all components accounting for less than $(70/n)\%$, i.e. 11.67% , of the variability [129], we conclude that the gene expression data can be summarized by the first three principal components, which together contain more than 80% of the total variability.

The meaning of the three components can be understood from the loading plot of each component shown in Figure 30b. The first principal component accounts for 53.78% of the total variability. The coefficients of all time points are positive and almost constant. Thus, this component represents a time averaged expression value and distinguishes genes by overall expression. Genes with large positive values along this

component are upregulated at each time point during the adaptive response, while genes with negative values are downregulated.

The second component contains 17.65% of the total information. The loading coefficients of 15 and 45 minutes are highly positive, whereas 180 and 360 minutes have highly negative coefficients. Genes that are upregulated at 15 and 45 minutes and downregulated at 180 and 360 minutes will have a highly positive value along this component. Genes downregulated earlier and then upregulated will have a highly negative values. Thus, this component represents a flip of regulation direction at 45 minutes, and 17.65% of the dynamic gene regulation information can be explained by this pattern. This further confirms that 45 minutes is a tipping point.

The third component accounts for 11.69% of the total variability. This component has a highly negative coefficient at 5 minutes and positive one at 45 minutes. If a gene is downregulated at 5 minutes but immediately upregulated at 45 minutes, it has a highly positive value along this component. Thus, this component represents a rapid change of expression level within the first 45 minutes after shear stress step-up.

These three principal components contains more than 80% of the total variability, thus we can summarize most of the temporal expression information by the reduced set of three variables. They represent consistent expression over time, flip of regulation direction at 45 minutes, and dramatic change of expression before 45 minutes. The second and third components further demonstrate the biphasic response of endothelial

gene expression to increased shear stress, which includes an early response phase before 45 minutes and an adapting phase afterwards.

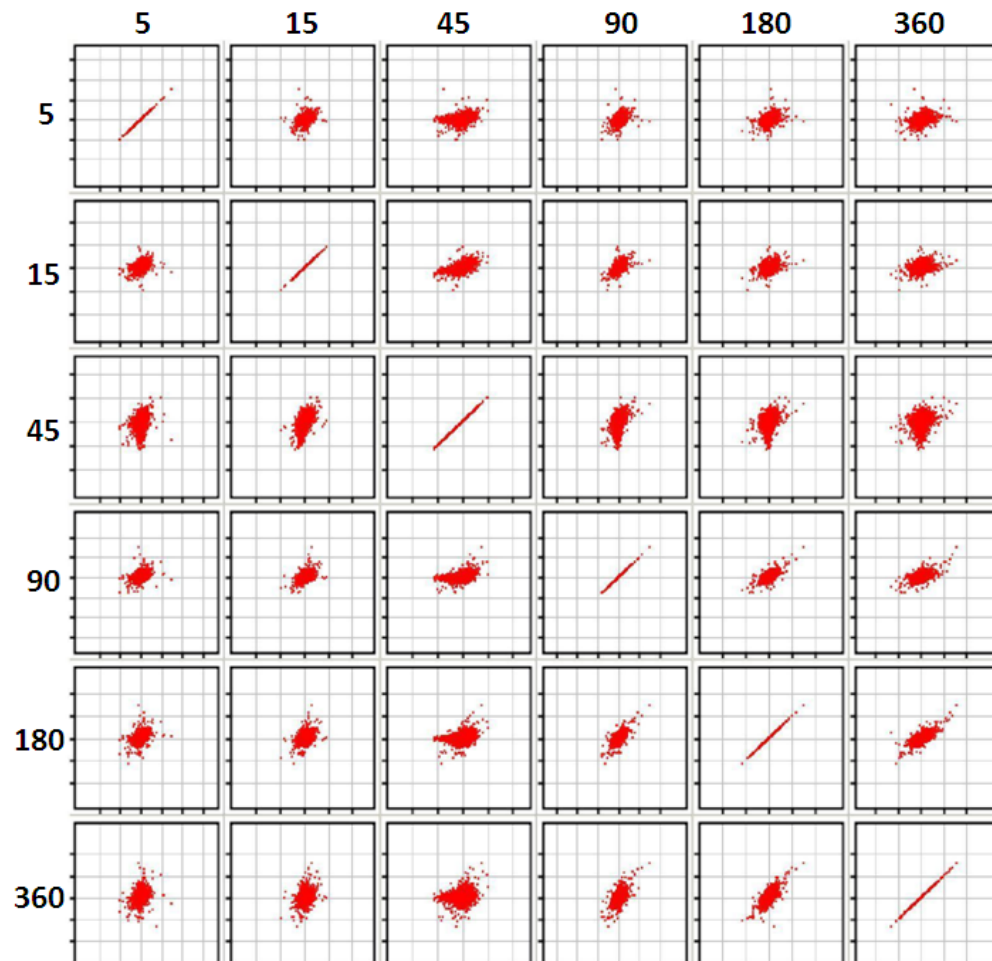


Figure 28: Matrix of scatter plots to compare the global expression profiles between different time points. Each panel compares transcriptional profile between two time points. Each gene is plotted as one data point, where x-axis is the expression value at one time point and y-axis is the expression value at the other time point.

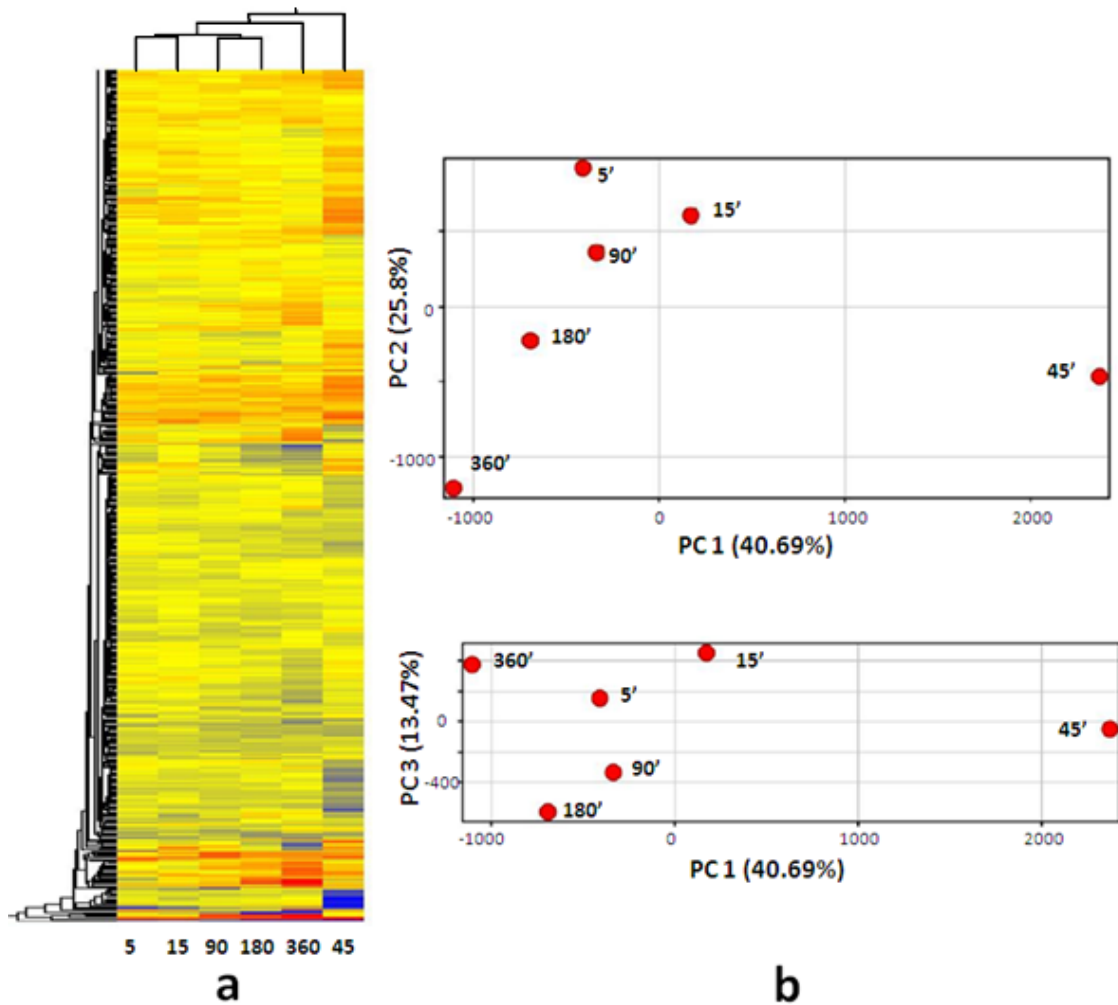


Figure 29: Clustering and principal component analysis of all genes. a. Hierarchical clustering of the global expression profiles of all time points. b. Principal component analysis. PC1: principal component 1, containing 40.69% of the total variance. PC2 and PC3 contain 25.80% and 13.47% of the total variance, respectively. Each time point is plotted in the projected planes of PC1 & PC2, and PC1 & PC3.

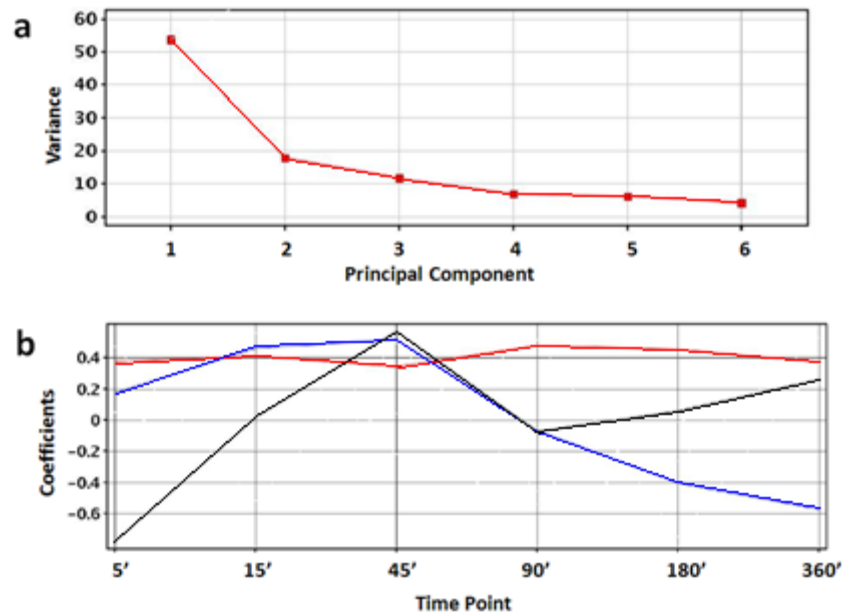


Figure 30: Principal component analysis. a. plot of eigenvalues of the principal components. b. Components loading. red: 1st component; blue: 2nd component; black: 3rd component.

4.3.2.4 Gene Ontology and Gene Functional Analysis

We have demonstrated that endothelial transcriptome was regulated dynamically in response to the increased shear stress. We next sought to understand how this may affect endothelial cellular function by performing gene ontology and gene functional analysis.

For each time point, one-sample t-test against zero was performed for each gene without false discovery rate controlled. A gene list was obtained for each time point using a p-value cutoff of 0.05. The numbers of genes used in the analysis were 323, 373, 372, 389, 400 and 420 at 5, 15, 45, 90, 180 and 360 minutes respectively. The gene lists were analyzed by GeneGo, which maps gene function, ontology and pathway

information onto the lists. The absence of false discovery control can be justified since this study analyzed the entire list of genes with no attempt to identify any individual gene. Furthermore, this type of study serves as a first step to discover potential important cellular processes and pathways that are involved in the adaptation process and guide further molecular biological analysis to dissect these pathways in detail. Therefore, the less strict statistical test is acceptable.

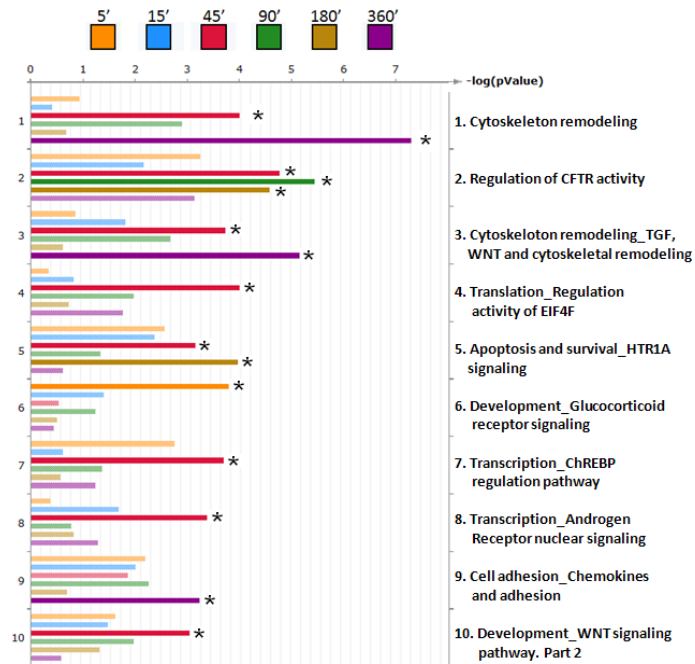
GeneGo results are presented in Figure 31. Two proprietary gene ontological (GO) databases were used: GeneGo curated pathways and cellular processes GO. Top ten enriched pathways, ranked by Fisher's exact p-value, are shown in Figure 31a. Top ten cellular processes are shown in Figure 31b. The x axis for each gene set is calculated as $-\log(p\text{-value})$. Since hundreds of pathways or cellular process GOs were tested simultaneously, the false discovery rate of gene sets was calculated and controlled by GeneGo. Highlighted bars indicate that the corresponding gene set was identified at a false discovery rate less than 5%.

As shown in Figure 31a, pathways involved in cytoskeleton remodeling (No. 1 and 3) were greatly affected by the elevated shear stress, with the strongest responses at 45 minutes and 360 minutes. However, the affected member genes in these pathways are not the same at 45 and 180 minutes, which might suggest the remodeling process has two distinct phases. Regulation of CFTR activity was turned on from 15 minutes to 180 minutes. The cystic fibrosis transmembrane conductance regulator (CFTR) is a member

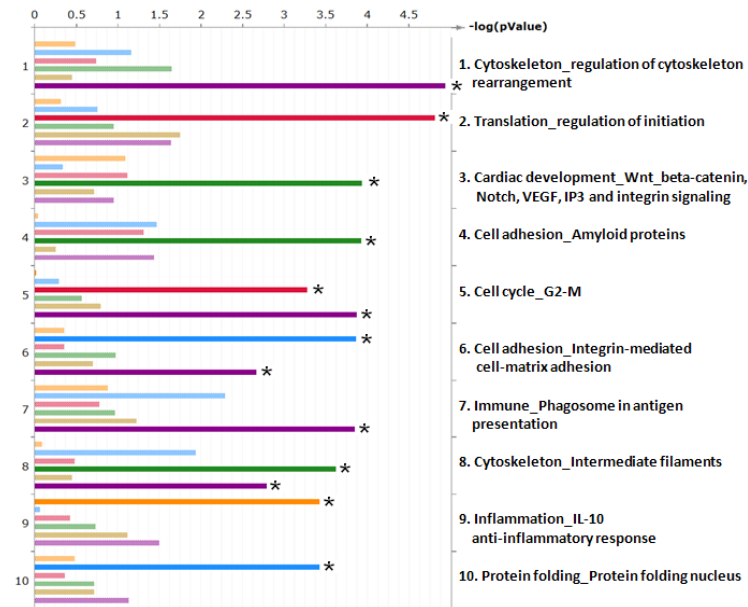
of ATP-binding cassette (ABC) transporter family, which acts as a cyclic AMP-activated chloride channel on endothelial cells [130]. Our result supports a role of CFTR pathway in shear stress-induced ATP release by endothelial cells as hypothesized in previous studies [131, 132]. Chemokine mediated adhesion pathway was also significantly altered at 360 minutes. Eight of the top ten pathways were significantly affected by the increased shear at 45 minutes (false discovery rates < 0.05), including several translation and transcription related signaling pathways and WNT signaling pathway. Interestingly, these pathways were not identified after 45 minutes, suggesting a transient switch on of these pathways. This further confirmed 45 minutes as a critical time point in the adaptation process.

The results of cellular processes analysis are in line with the pathway analysis. Cytoskeleton related processes were identified again at 360 minutes. Genes involved in translation regulation were altered at 45 minutes. IL10 mediated anti-inflammatory response was identified at 5 minutes.

Overall, the pathway/gene ontology study strongly suggests that endothelial cells undergo cytoskeletal remodeling during the adaption process. Cell adhesion was also affected by the increased shear stress. Around 45 minutes, several pathways were temporarily turned on to orchestrate the downstream adaptive response. The identified pathways/ontology provide potential candidate targets for further investigation.



a



b

Figure 31: GeneGo identified pathways and cellular processes that are sensitive to the elevated shear stress magnitude. Top ten pathways and processes were listed. a. canonical pathways; b. cellular processes. * indicates the false discovery rate < 5%.

4.3.3 Endothelial Gene Expression in Response to the Elevated Shear Stress Frequency

In this set of experiments, endothelial cells were preconditioned under the basal level shear stress (15 ± 15 dynes/cm², 1 Hz) for 24 hours and the frequency of the shear stress was then doubled (15 ± 15 dynes/cm², 2 Hz). As in the magnitude step-up studies, a control sample was obtained immediately before the step-up and other samples were harvested at different time points after the step-up.

Since the data analysis methods used here have been discussed in detail in the previous section, we only present the results in this section. All gene expression values are the normalized values (by the pre-conditioned controls) in log₂ scale.

4.3.3.1 Differentially Expressed Genes Identified at Each Time Point

Table 11 lists the number of genes identified at each time point at different levels of false discovery rate. Only a handful of genes were identified at time points before 360 minutes, and a limited number of genes were identified at 360 minutes.

A total number of 37 genes were identified by SAM to be upregulated by the step-up of frequency at one or more time point when the false discovery rate is less than 10%. No gene was down regulated by the step-up of shear stress frequency at any time point. Figure 32 shows that only three genes were also identified in the magnitude step-up experiments and only eight genes were also identified in the control experiments. Table 12 is the complete list of genes identified at each time point. Some identified

probes were not annotated with gene names since the corresponding porcine genes are unknown and no human or mouse homologous sequence was identified.

Table 11: The numbers of identified genes at different time points in the frequency step-up experiment.

Time	Estimated FDR < 5%		Estimated FDR < 10%	
	up-regulated	down-regulated	up-regulated	down-regulated
5 minute	0	0	0	0
15 minute	2	0	2	0
45 minute	0	0	0	0
90 minute	5	0	5	0
180 minute	2	0	2	0
360 minute	12	0	33	0

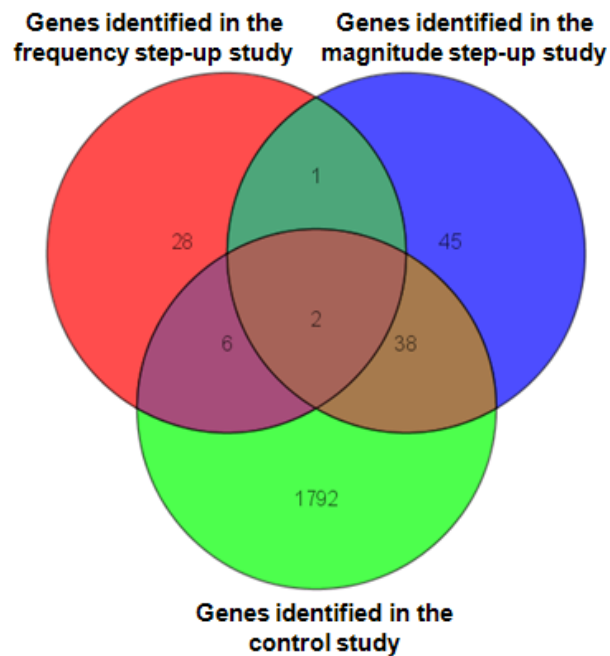


Figure 32: Venn diagram displaying the overlap of genes identified in the frequency step-up, magnitude step-up and control study.

Table 12: List of genes identified at different time points in the frequency step-up experiments.

ID	Gene	Expression	Description
15 minutes			
SS00008885	NUSAP1	0.59	nucleolar and spindle associated protein 1
SS00008707	NDRG4	0.41	NDRG family member 4
90 minutes			
SS00008707	NDRG4	1.08	NDRG family member 4
SS00009063	SERTAD4	1.07	SERTA domain containing 4
SS00009402	MBNL1	0.94	muscleblind-like (Drosophila)
SS00008885	NUSAP1	0.86	nucleolar and spindle associated protein 1
SS00006968	MGC17943	0.67	hypothetical protein MGC17943
180 minutes			
SS00009402	MBNL1	0.96	muscleblind-like (Drosophila)
SS00008883	SHCBP1	0.78	likely ortholog of mouse Shc SH2-domain binding protein 1
360 minutes			
SS00009479	MUM1L1	1.28	melanoma associated antigen (mutated) 1-like 1
SS00009156	CCNB3	1.17	cyclin B3
SS00008885	NUSAP1	1.16	nucleolar and spindle associated protein 1
SS00002311	CENPA	1.09	centromere protein A, 17kDa
SS00009039	DEK	1.08	DEK oncogene (DNA binding)
SS00008118	STK38L	1.08	serine/threonine kinase 38 like
SS00007619	ID2	1.05	inhibitor of DNA binding 2, dominant negative helix-loop-helix protein
SS00008745	HNRPLL	1.05	Heterogeneous nuclear ribonucleoprotein L-like
SS00000455	CCNB1	1.05	cyclin B1
SS00010453		1.02	
SS00008883	SHCBP1	0.95	likely ortholog of mouse Shc SH2-domain binding protein 1
SS00009037	FLJ20152	0.95	hypothetical protein FLJ20152
SS00009945	CDC2	0.93	cell division cycle 2, G1 to S and G2 to M
SS00005702	MGC13017	0.91	similar to RIKEN cDNA A430101B06 gene
SS00008689	VEGF	0.87	vascular endothelial growth factor
SS00000123	MCFP	0.87	mitochondrial carrier family protein
SS00009449	SRD5A2L	0.85	steroid 5 alpha-reductase 2-like
SS00009189	ZCCHC8	0.82	Zinc finger, CCHC domain containing 8
SS00009946	NEK2	0.82	NIMA (never in mitosis gene a)-related kinase 2
SS00010472	SNX16	0.80	sorting nexin 16

SS00007910	NCOA7	0.78	nuclear receptor coactivator 7
SS00009514	AMD1	0.78	adenosylmethionine decarboxylase 1
SS00003461	CCNA2	0.77	cyclin A2
SS00007681	FGFR2	0.76	fibroblast growth factor receptor 2
SS00004188	SCG2	0.76	Secretogranin II (chromogranin C)
SS00008006	ABCB1	0.74	ATP-binding cassette, sub-family B (MDR/TAP), member 1
SS00009066	ARG99	0.74	ARG99 protein
SS00010203		0.73	
SS00007312	PSIP1	0.70	PC4 and SFRS1 interacting protein 1
SS00009132	DNCL11	0.69	dynein, cytoplasmic, light intermediate polypeptide 1
SS00007957	APPL	0.69	adaptor protein containing pH domain, PTB domain and leucine zipper motif
SS00007539	USP1	0.65	ubiquitin specific protease 1
SS00009512		0.65	

The list of genes was first imported into IPA to generate gene networks. Interestingly, 11 of the 37 identified genes were found in a densely interconnected gene network (the top ranked one) as shown in Figure 33a. The genes are color coded by the expression values at 360 minutes. All the genes in this network were upregulated at 360 minutes as shown in the figure, and they were also upregulated at previous time points. These genes are highly interconnected and form a single dense cluster, indicating that they might participate in a unique cellular process. Indeed, almost all the genes in this network have important regulation roles in cell cycle control and mitosis process. This suggests that the elevated shear stress frequency may alter the proliferation state of endothelial cells.

All the 37 identified genes were clustered in Figure 33b. The regulation pattern is much simpler compared to that in the magnitude step-up study. As revealed in the figure, for most of the genes in the top portion of the heat map, the expression values increased throughout the time period. For a small number of genes in the bottom portion of the heat map, the expression values peaked earlier at around 90 minutes. No genes were downregulated at any time point, except gene MGC13017.

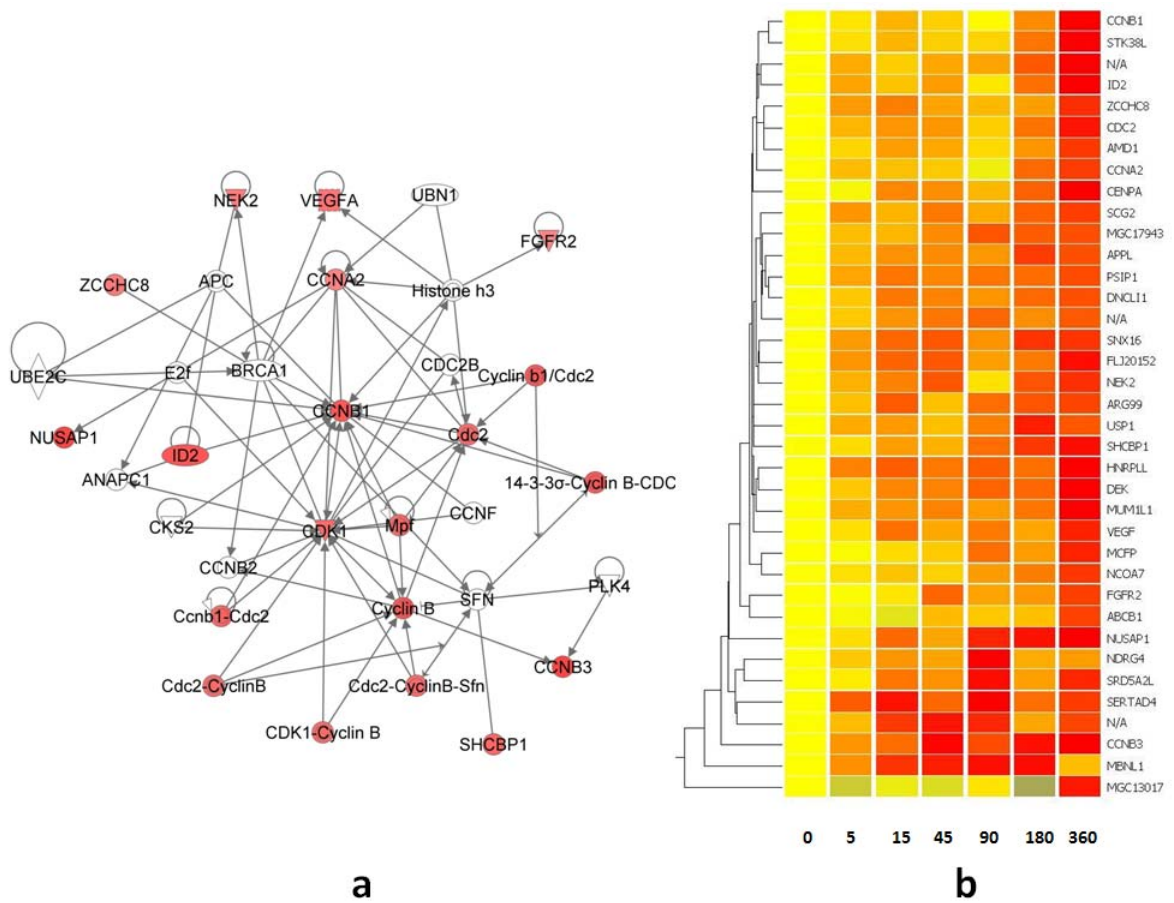


Figure 33: Gene network and clustering heat map generated from the identified genes in the frequency step-up study. a. The top ranked gene network generated by IPA from genes identified in the frequency step-up experiment. Genes are color-coded by the expression values at 360 minutes. b. Hierarchical clustering of the identified genes. Red: overexpressed; Yellow: unchanged; Blue: underexpressed.

The cell-cycle and mitosis related genes and other possible atherosclerosis-relevant genes in Table 12 are discussed below. The temporal expression profiles of these genes are presented in Figure 34.

Cell cycle and mitosis related genes

Nucleolar and spindle associated protein 1 (NUSAP1), a recently identified nucleolar-spindle-associated protein involved in spindle microtubule organization [133], was significantly overexpressed after 15 minutes exposure to elevated shear frequency. NUSAP1 protein localizes to nucleolus during interphase, and binds to central spindle microtubules during mitosis. Its function is critical for the formation of microtubule bundle. High level of NUSAP protein helps stabilize bundled microtubules against depolymerization, thus inducing longer and stronger microtubular spindles [134]. The expression of NUSAP1 in endothelial cells has not been reported before. However, in other type of cells, high mRNA level of NUSAP was found in highly proliferative cells [135]. Thus, NUSAP1 may be an important marker for endothelial proliferation and its role in regulating endothelial response to shear stress deserves further investigation.

Three cyclin genes, cyclins A2 (CCNA2) and B1 (CCNB1) and cyclin-dependent kinase 1 (CDK1 protein, a serine/threonine kinase encoded by gene CDC2) were significantly overexpressed at 360 minutes. In cell cycle control, CDK1 is activated by association with cyclin A and cyclin B. CDK1 association with cyclin B forms protein

kinase complex known as M-phase promoting factor (MPF), which is essential for G2/M phase transitions of eukaryotic cell cycle [2]. These three genes also had highly similar temporal regulation patterns as shown in Figure 34. The coordinated regulation of CDC2 and cyclin B indicates that endothelial cells may enter mitosis phase after 360 minutes exposure to elevated shear stress. Actually, recent studies demonstrated the increased proliferation of endothelial cells is associated with increased expression of cyclins A and B1 [136, 137]. Although the mechanisms by which cyclins regulate cell cycle is not fully understood in endothelial cells under shear stress, our result suggests the elevated shear frequency may activate the endothelial cells and drive endothelial cells out of the quiescence state.

Other cell cycle related genes upregulated by the elevated shear frequency includes ubiquitin specific protease 1 (UPS1), a positive regulator of DNA repair during G2 phase [138] and NEK2, another serine/threonine kinase regulating cell cycle. At the onset of mitosis, NEK2 plays important role in nuclear envelope breakdown and centromere separation [139]. Another centromere binding gene [140], centromere protein A (CENPA), was also overexpressed under elevated shear frequency after 15 minutes. Like cyclin B1, these three genes were all found to be overexpressed during the G2/M transition in animal cells [139, 141].

The temporal regulation patterns of the cell cycle related genes are highly similar. As shown in Figure 34, the expression levels of these genes were not altered

significantly before 90 minutes, and then increased greatly at 180 and 360 minutes. This coordinated expression suggests that these genes may be involved in a particular pathway that can sense the shear stress frequency and respond by regulating the endothelial cell proliferation.

Other interesting genes

Inhibitor of DNA binding 2 (ID2) was upregulated at 360 minutes by the frequency step-up. As discussed in previous section, ID2 was also upregulated by elevated shear stress magnitude, making it a potential important regulator of endothelial response to shear stress alteration. As an angiogenesis gene, ID2 can promote endothelial cell growth and migration [106, 142]. Overexpression of ID2 leads to a significant increase of smooth muscle cell proliferation in response to vascular injury [143]. Therefore, although current studies are mostly focused on its role in cancer, ID2 is also a critical player in the development of atherosclerosis, and may be a potential therapeutic target for both [144].

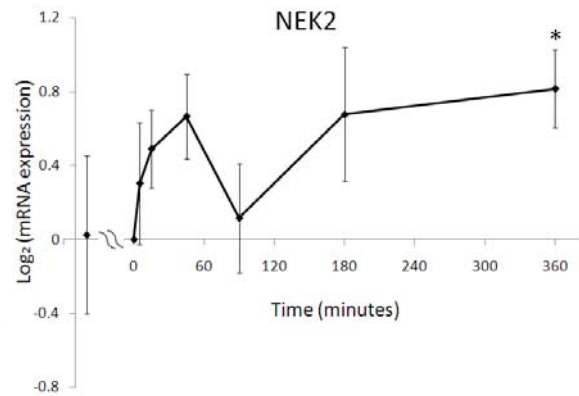
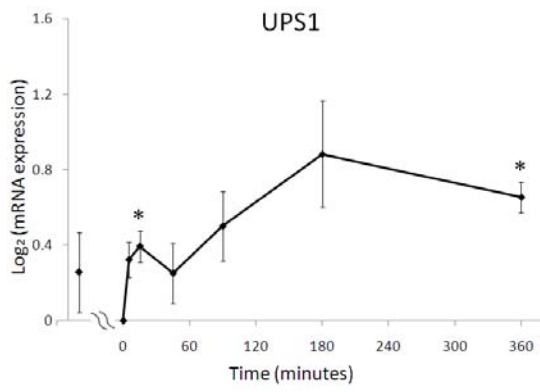
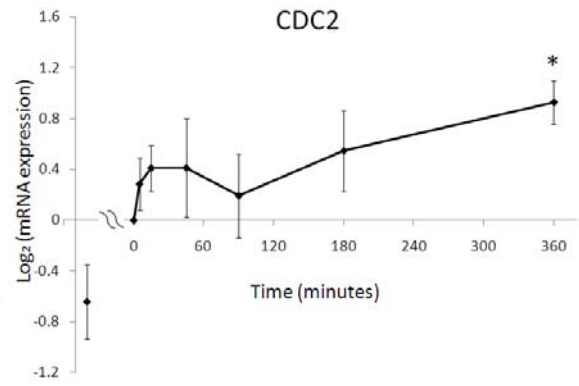
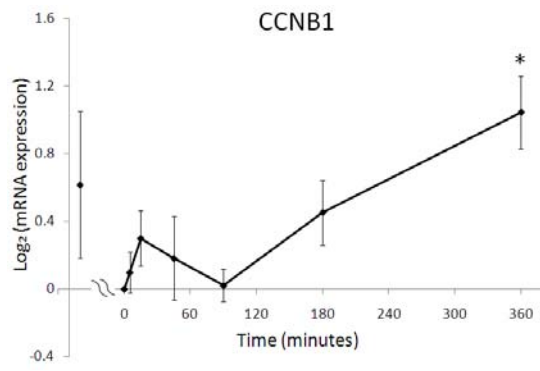
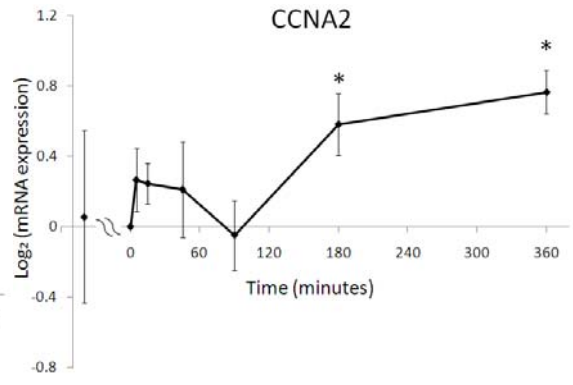
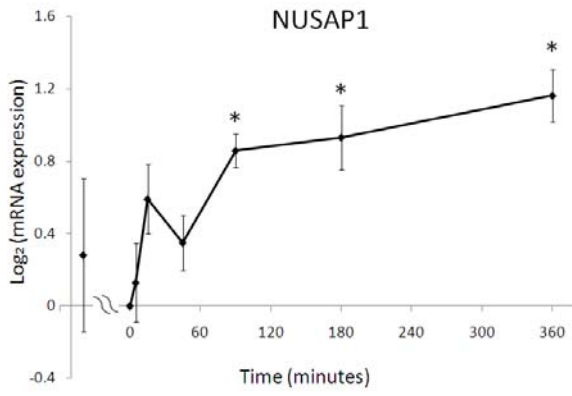
Several recent studies [107, 145-147] further linked ID2 to another master regulator of angiogenesis and atherogenesis, vascular endothelial growth factor (VEGF). Lasorella et al. demonstrated that overexpression of ID2 can induce the expression of VEGF [146]. Indeed, the expression level of VEGF is increased significantly by the step-up of shear frequency in our study. Although the exact role of VEGF in the atherogenic

process is still unclear and in debate, this important angiogenesis gene is known to participate in the initiation of atherosclerosis and in plaque formation and destabilization [76, 148-151].

Another potent angiogenesis gene, fibroblast growth factor receptor 2 (FGFR2), was also upregulated by the elevated frequency. Fibroblast growth factor (FGF) can stimulate angiogenesis, and the signal is transduced via FGFR tyrosine kinase [152, 153]. FGFR2 is also a potential participant in atherogenesis by regulating endothelial function [154, 155]. Together, upregulation of ID2, VEGF and FGFR2 genes suggests that elevated shear frequency may send strong angiogenesis signal to endothelial cells and mediate the development of atherosclerosis.

ATP-binding cassette B1 (ABCB1, encoding Multidrug resistance protein 1, MRP1) was another gene upregulated at 360 minutes. MRP1 is an active transporter for a variety of molecules. Increased mRNA level of ABCB1 was also found in atherosclerotic lesions, suggesting a role in atherogenesis [156, 157]. Current research suggests ABCB1 has an important role in modulation of oxidative stress and apoptosis of endothelial cells and smooth muscle cells [158, 159]. Inhibition of ABCB1 by siRNA allows endothelial cells to maintain their redox potential in response to oxidative stresses induced by oscillatory shear, thus promoting endothelial survival and function [159]. Thus, elevated shear frequency may predispose endothelial cells to increased oxidative level by upregulating ABCB1.

In summary, we found that elevated shear frequency can induce the expression of a group of cell cycle regulator genes and several angiogenesis genes. The upregulation of these genes may lead to endothelial activation and increased cell proliferation. Most of the identified genes are not previously known to be sensitive to shear stress. As shown in Figure 34, only two of the 11 identified genes, ID2 and ABCB1, were significantly downregulated by 24 hours basal shear stress in the control set of experiments. However, the elevated shear frequency upregulated these two genes. The expression levels of the other nine genes were not altered in the control experiment. Thus, our frequency step-up study discovered a new set of shear sensitive genes that are involved in cell cycle regulation of endothelial cells and angiogenesis. Some of these genes, such as ID2, CCNB1 and ABCB1, are potential novel therapeutic targets for atherosclerosis.



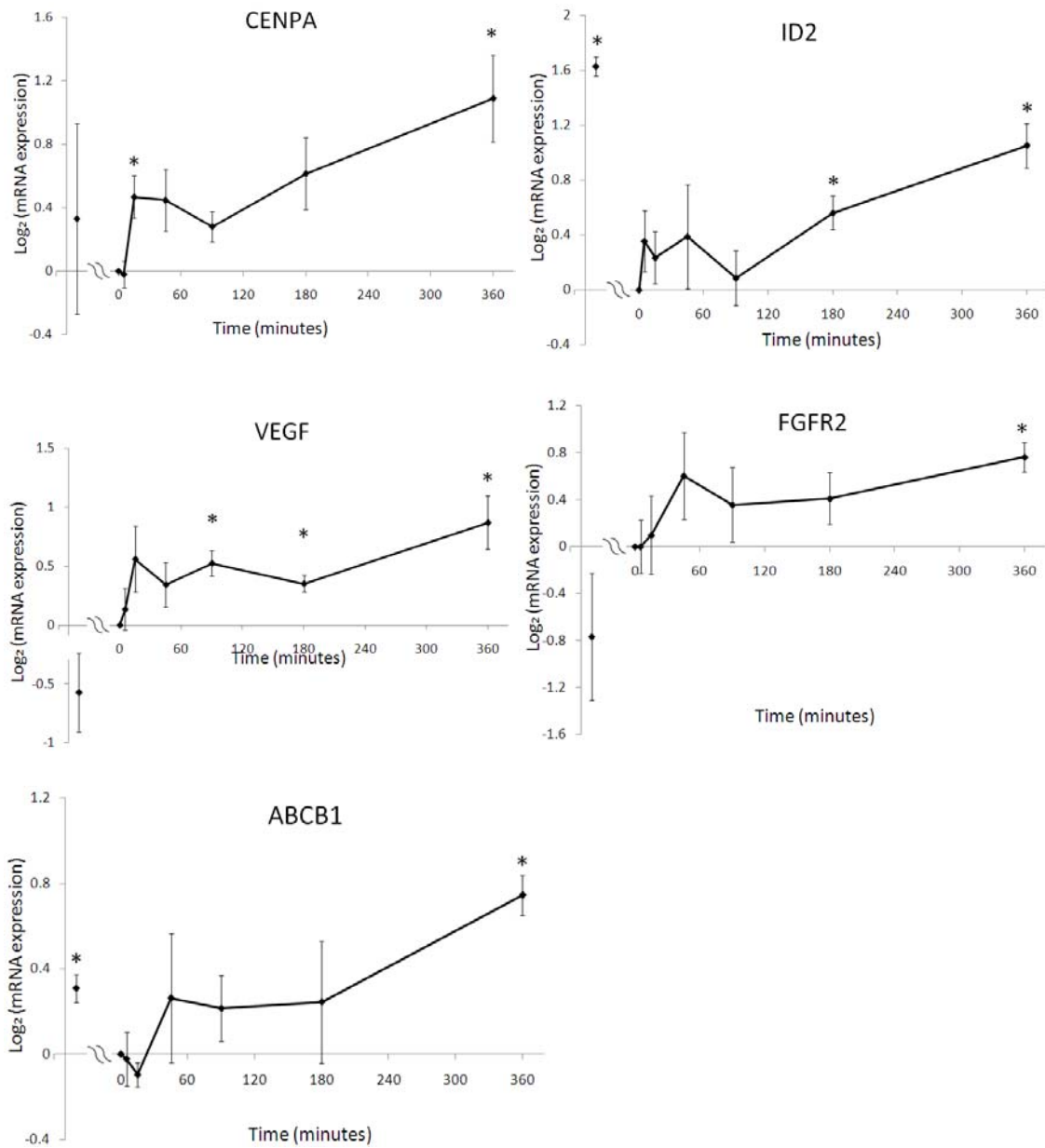


Figure 34: Expression profiles of the selected genes in the frequency step-up study. All expression values were normalized to Time 0 (the pre-step-up controls). In each panel, the first data point represents the expression value of the static cultured endothelial cells and the value was obtained from the control set experiments. *, p-value < 0.05, one-sample t-test against zero without false discovery controls. Error bar: standard error of the mean.

4.3.2.2 Expression of an *a-priori* Selection of Atherosclerosis-related Genes

The expression values of the *a-priori* selected genes were summarized in Table 13. Six genes were significantly differentially expressed in response to the elevated shear stress frequency, identified by t-test p value less than 0.05 at any time point. Proinflammatory adhesion molecule, ICAM and transcriptional factor, c-jun were both upregulated at 180 minutes. Caveolin-1 was upregulated at 90 minutes. These three genes showed no response to elevated shear stress magnitude.

Different than the response to elevated shear stress magnitude, proinflammatory cytokine BMP4 was upregulated at 15 minutes but downregulated at 360 minutes, and anti-oxidative gene HMOX1 was downregulated at 5 and 45 minutes. Although the anti-inflammatory gene KLF4 was overexpressed at 180 minutes, the increase was much less compared to the 2.5 fold increase in response to elevated magnitude.

Overall, 6 of the selected genes were sensitive to the elevated shear frequency and the induced fold changes were much smaller than in the magnitude step-up experiments. Therefore, the elevated shear frequency has a small effect in regulating these atherosclerosis related genes; overall, the elevated frequency predisposes endothelial cells to a proinflammatory and atheroprone phenotype.

Table 13: The expression of *a-priori* selected genes in response to the elevated shear stress frequency. Red: p<0.05; blue: p<0.1. LSS: laminar shear stress, DSS: disturbed shear stress.

	Preconditioned cells	During adaptation (normalized to preconditioned cells)					
	(normalized to static cells)	5	15	45	90	180	360
Inflammatory and adhesion genes							
ICAM1	-0.50	0.32	0.40	0.22	0.27	0.31	0.13
	Inflammatory adhesion molecule [46-49]. LSS: ↓ [45].						
VCAM1	-1.98	-0.18	-0.24	-0.20	-0.20	-0.50	-0.27
	Inflammatory adhesion molecule [46-49]. LSS: ↓ [27, 45]; DSS: ↑ [45]						
CCL2	1.18	-0.15	-0.01	-0.49	-0.32	-0.78	-0.12
	MCP1, Inflammatory molecule [47-49]. LSS: ↓ [45, 50] or biphasic [51]; DSS: ↑ [45]						
SELE	-0.25	0.25	0.11	-0.13	0.10	0.32	0.52
	Adhesion molecule, E-selectin [46-49]. LSS: ↓ [45]; DSS: ↑ [45]						
FOS	-0.24	-0.40	-0.02	-0.07	-0.30	0.01	0.17
	c-fos gene, activating protein-1, inflammatory [52, 53]						
JUN	-1.69	0.13	0.44	0.56	0.58	0.44	0.15
	c-jun gene, activating protein-1, inflammatory [52, 53]. LSS: ↓ [36]						
KLF2	1.81	0.09	-0.05	0.06	0.71	-0.02	-0.02
	Inflammatory regulation transcription factor [54-56]. LSS: ↑ [27, 54]						
KLF4	1.83	0.05	0.34	0.10	0.59	0.30	0.23
	Inflammatory regulation transcription factor [57]. LSS: ↑ [57, 58]						
BMP4	-2.17	0.03	0.33	-0.02	-0.06	0.01	-0.22
	Activates inflammatory [43, 60]. LSS: ↓ [50, 59]; DSS: ↑ [45]						
RELA	-0.11	0.07	-0.01	-0.03	0.30	-0.05	0.18
	p65, NFκB [47-49]						
NFKBIA	-1.31	-0.60	-0.61	-0.63	-0.59	-0.41	-0.26
	NFκB inhibitor, IκBα [47-49]. LSS: ↓ [61]						
IL8	0.95	-0.31	0.12	0.00	-0.31	-0.38	-0.12
	Inflammatory chemokine [47-49]. LSS: ↑ [62, 63]						
Vasomotion							
NOS3	0.37	0.15	0.22	-0.08	0.16	0.07	0.01
	eNOS [11, 26]. LSS: ↑ [27]						
EDN1	-0.98	0.11	0.48	0.13	0.64	0.68	0.26
	Endothelin-1 [26]. LSS: ↓ [50, 64]						
Caveolin-1	-1.52	0.26	0.48	0.43	0.44	0.45	0.49
	Caveolin-1 [11, 26]. LSS: ↓ [27, 50, 59, 66]						
Oxidative state regulators							
SOD2	0.33	-0.11	-0.25	0.04	-0.14	-0.38	-0.12
	cytoprotective, MnSOD [31]. LSS: ↑ [27]; DSS: ↓ [45]						
GADD45B	-0.68	-0.26	-0.16	0.06	-0.28	-0.13	-0.26
	cytoprotective gene [31]. LSS: ↑ [70] or slightly ↓ [31]						
HMOX1	0.53	-0.21	-0.21	-0.27	0.09	-0.16	-0.13
	anti-oxidative, cytoprotective and anti-inflammatory gene [68, 69]. LSS: ↑ [50]						

4.3.2.3 Global Gene Expression Profiles during the Adaptation

We next examine how the endothelial transcriptome was dynamically regulated in response to the elevated shear stress frequency. As previously described, both scatter plots and hierarchical cluster were used to compare the global expression profiles at different time points.

As revealed in Figure 35a, unlike in the magnitude step-up study where 45 minutes was found to have distinct gene expression pattern, the global transcriptional profiles at different time points are similar to each other in the frequency step-up study. No time point presents a noticeable unique transcriptional profile. The hierarchical clustering shown in Figure 35b confirms this observation. As suggested by the tree on top of the heat map, the distance, or the similarity, between any two time points is almost constant. The means and variance of the expression values of all genes were also calculated for each time point (Figure 35c). The means are all close to zero, and the variance at each time point is similar to each other. Furthermore, the principal component analysis revealed the same pattern, where no time point was apparently separated from others (data not shown).

Therefore, the degree of endothelial transcriptome disturbance by the frequency step-up is essentially the same at each time point. There is no apparent strong response of endothelial global gene expression to the elevated frequency, in contrast to the response to the elevated magnitude at 45 minutes. For the limited number of genes

identified to be significantly regulated, the expression levels increased along time and were the greatest at 360 minutes as shown in Figure 34.

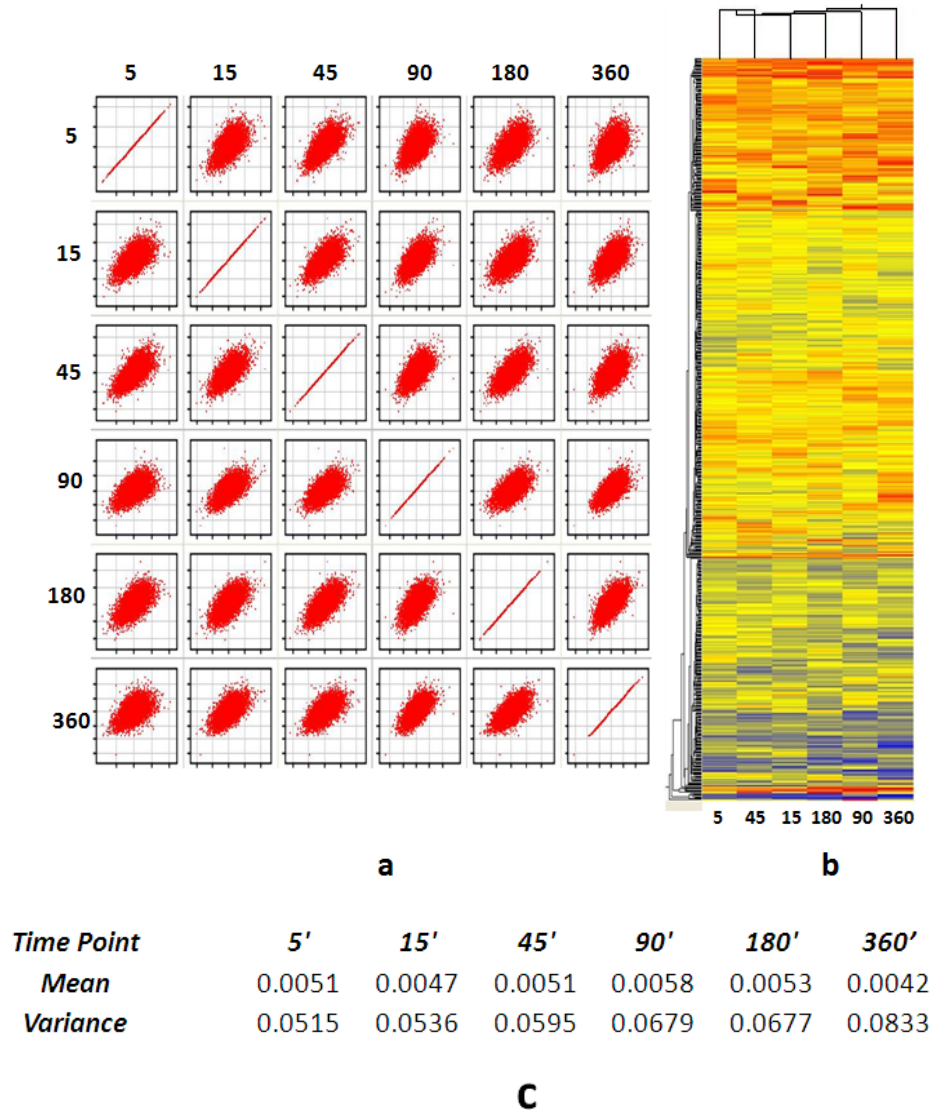


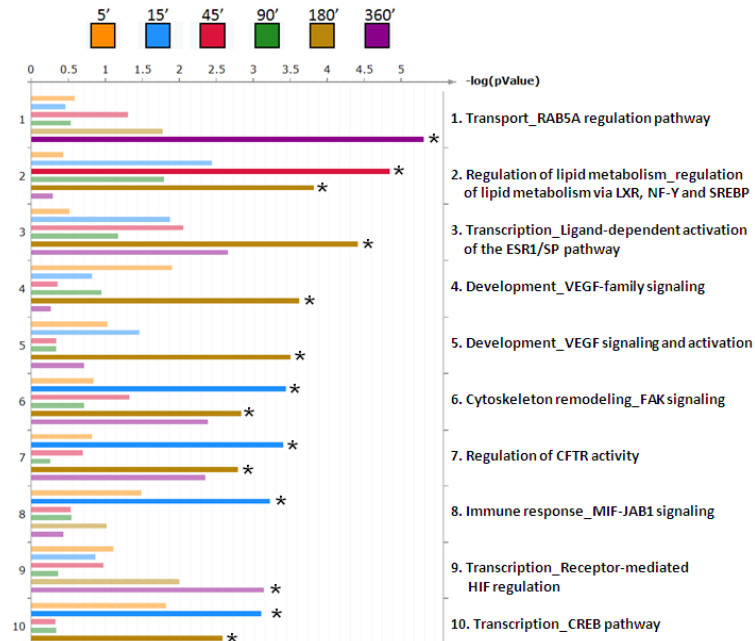
Figure 35: Matrix of scatter plots (a) and hierarchical clustering (b) to compare the global expressional profiles between different time points in the shear stress frequency step-up experiments. (c) Statistic summary of the expression values at each time point.

4.3.2.4 Gene Ontology and Gene Functional Analysis

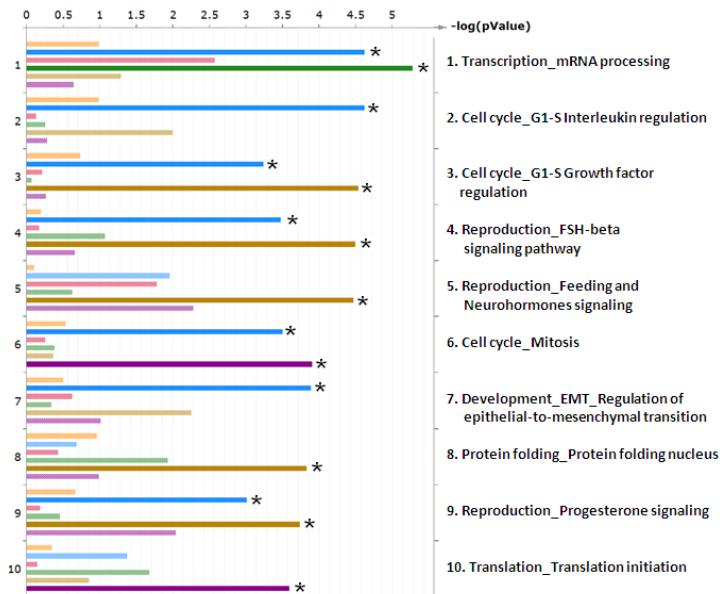
As described previously, a gene list was obtained for each time point using a one-sample t-test p-value cutoff of 0.05. The numbers of genes used in the GeneGo analysis were 326, 381, 372, 418, 506 and 499 at 5, 15, 45, 90, 180 and 360 minutes respectively.

Top ten enriched pathways are presented in Figure 36: GeneGo identified pathways and cellular processes that are sensitive to the elevated shear stress frequency. Top ten pathways and processes were listed. a. canonical pathways; b. cellular processes. * indicates the false discovery rates < 5%. Figure 36a. RAB5A (Ras-related protein Rab-5A) regulation pathway was significantly altered at 360 minutes. RAB5A pathway has an important role in endocytic pathway and protein trafficking [160]. In endothelial cells, RAB5A pathway regulates key events in VEGFR2 trafficking between the plasma membrane and early endosomes, thus regulating VEGF signaling pathway [161, 162]. Indeed, the VEGF signaling pathway was also identified as significantly affected at 180 minutes. This further supports the involvement of VEGF pathway in the endothelial adaptive response to increased shear frequency. Lipid metabolism pathway was identified at both 45 and 180 minutes, featuring the upregulation of caveolin-1 and downregulation of LDL-receptor. Macrophage migration inhibitory factor (MIF) mediated immune response signaling was turned on at 15 minutes; this pathway includes the upregulation of CDK2 and c-jun.

Top ten enriched cellular process GOs are shown in Figure 36b. As expected, cell cycle regulation GOs were identified at multiple time points. G1-S related genes were altered at 15 minutes and 180 minutes, and the mitosis regulation genes were affected at 15 minutes and later at 360 minutes. This suggests endothelial cells can sense the elevated shear frequency and decide to enter cell cycle as early as 15 minutes after the step-up. The relevance of other identified cellular processes to endothelial biology is unclear.



a



b

Figure 36: GeneGo identified pathways and cellular processes that are sensitive to the elevated shear stress frequency. Top ten pathways and processes were listed. a. canonical pathways; b. cellular processes. * indicates the false discovery rates < 5%.

4.3.4 Gene Expression Validated by Real-time Quantitative PCR

The mRNA expression levels of six genes were measured using real time quantitative PCR to validate the microarray results. The genes were selected because they were identified with a p-value less than 0.05 (without false discovery rate control) at one or more time points by microarray and also have important roles in endothelial function.

Expression levels of KLF2, eNOS and interleukin-1 α were measured for the magnitude step-up study. VEGF, c-jun and ICAM1 were measured for the frequency step-up study. The housekeeping gene for all experiments was GAPDH. The expression levels of each gene were normalized to the corresponding pre-step-up control sample. Expression value at each time point of each gene was obtained from four biological replicates. One-way t-test was applied to test if the expression value was different than zero.

Figure 37 is the side by side comparison of the expression values of KLF2, eNOS and interleukin 1 α measured by microarray and quantitative PCR (left and right panels, respectively). Consistent with the microarray findings, KLF2 was significantly upregulated at 45, 90, 180 and 360 minutes by quantitative PCR. Real-time qPCR also confirmed the up-regulation of eNOS at 360 minutes and down-regulation of interleukin 1 α at 5 minutes. Furthermore, the shapes of the temporal expression profiles revealed by real-time PCR matched the ones obtained from microarray measurements. The

expression values of KLF2 began to increase at 15 minutes, and then reached the plateau value at around 90 minutes. The mRNA quantity of eNOS did not start to increase significantly until 180 minutes after the exposure to elevated shear stress magnitude, and significant differences were only detected after 6 hours of step-up. Expression level of interleukin 1 α was immediately decreased at 5 minutes, and then bounced back quickly to the pre step-up levels.

Figure 38 shows the comparison of the expression values of VEGF, c-jun and ICAM1, measured by microarray and qPCR in the frequency step-up experiment. Microarray experiments identified the up-regulation of VEGF at 90, 180 and 360 minutes ($p < 0.05$). Although quantitative PCR only confirmed the significant overexpression at 360 minutes ($p < 0.05$), the directions of regulation at other time point were consistent with the microarray results. The overexpression of c-jun and ICAM1 at 180 minutes identified by microarray was validated by quantitative PCR ($p < 0.05$). The temporal expression profiles revealed by qPCR agreed well with the microarray data. The expression level of VEGF increased immediately upon the step-up of the frequency, and stayed at a higher level relative to the pre-step-up control. The mRNA level of c-jun and ICAM1 increased and peaked before 90 minutes, and then fell back to the pre-step-up control values.

Taken together, 11 data points, in Figure 37 and Figure 38 combined, were identified by microarray experiments with a p-value less than 5%. For all these 11 points,

qPCR confirmed the direction of the regulations, and for 9 of the 11 points, qPCR results also confirmed they were statistically significant with a p-value less than 5%. Therefore, we conclude the microarray data in this study is sufficiently accurate to capture the adaptive dynamics of endothelial gene expression.

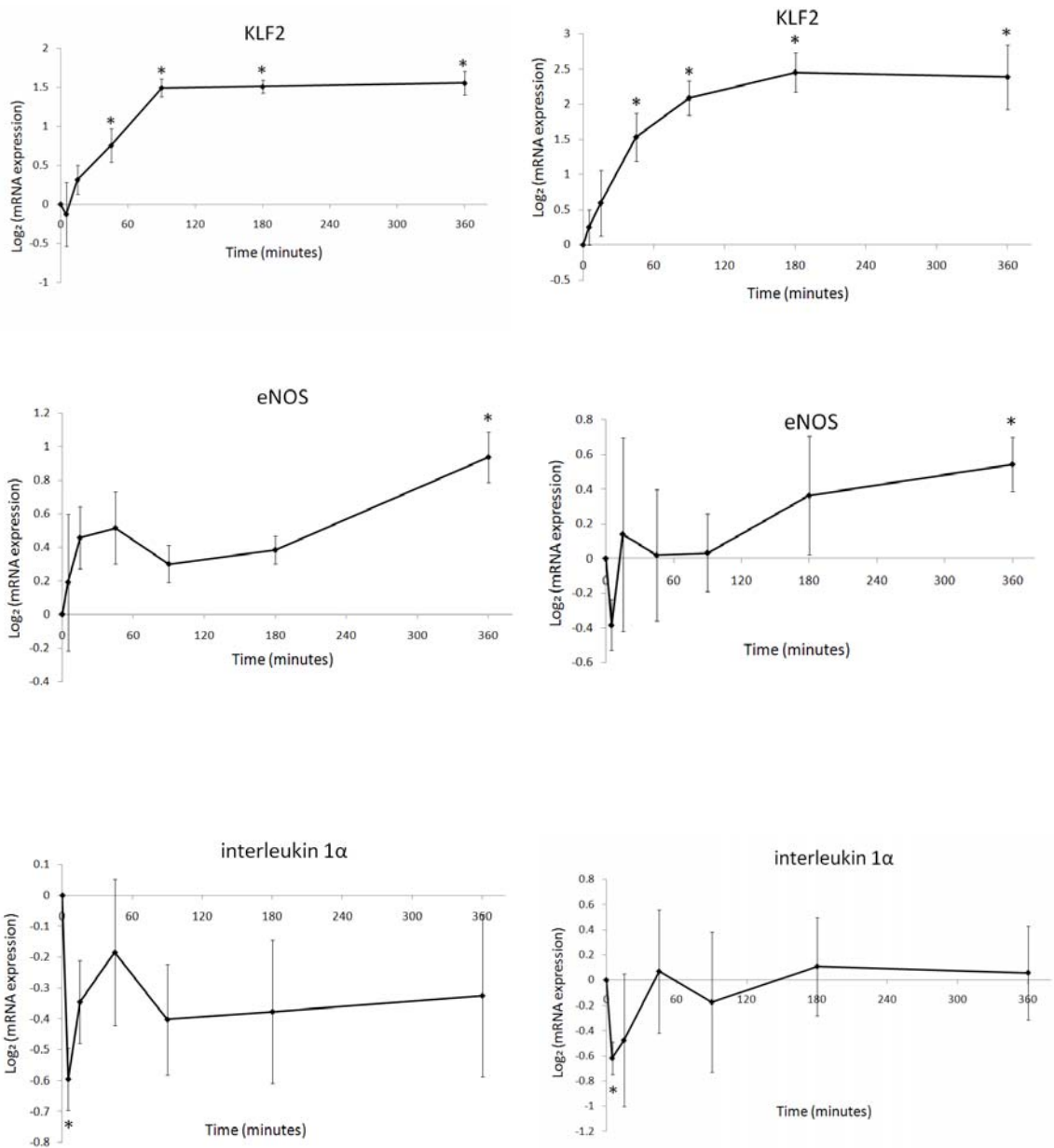


Figure 37: Real-time PCR validates the microarray results of the magnitude step-up experiments. Left: microarray measurements; Right: real-time PCR measurements. n=4 for each data point. Expression values were normalized by the pre step-up controls, and error bars indicates the deviation of the mean. *: p<0.05, one-way t-test against zero.

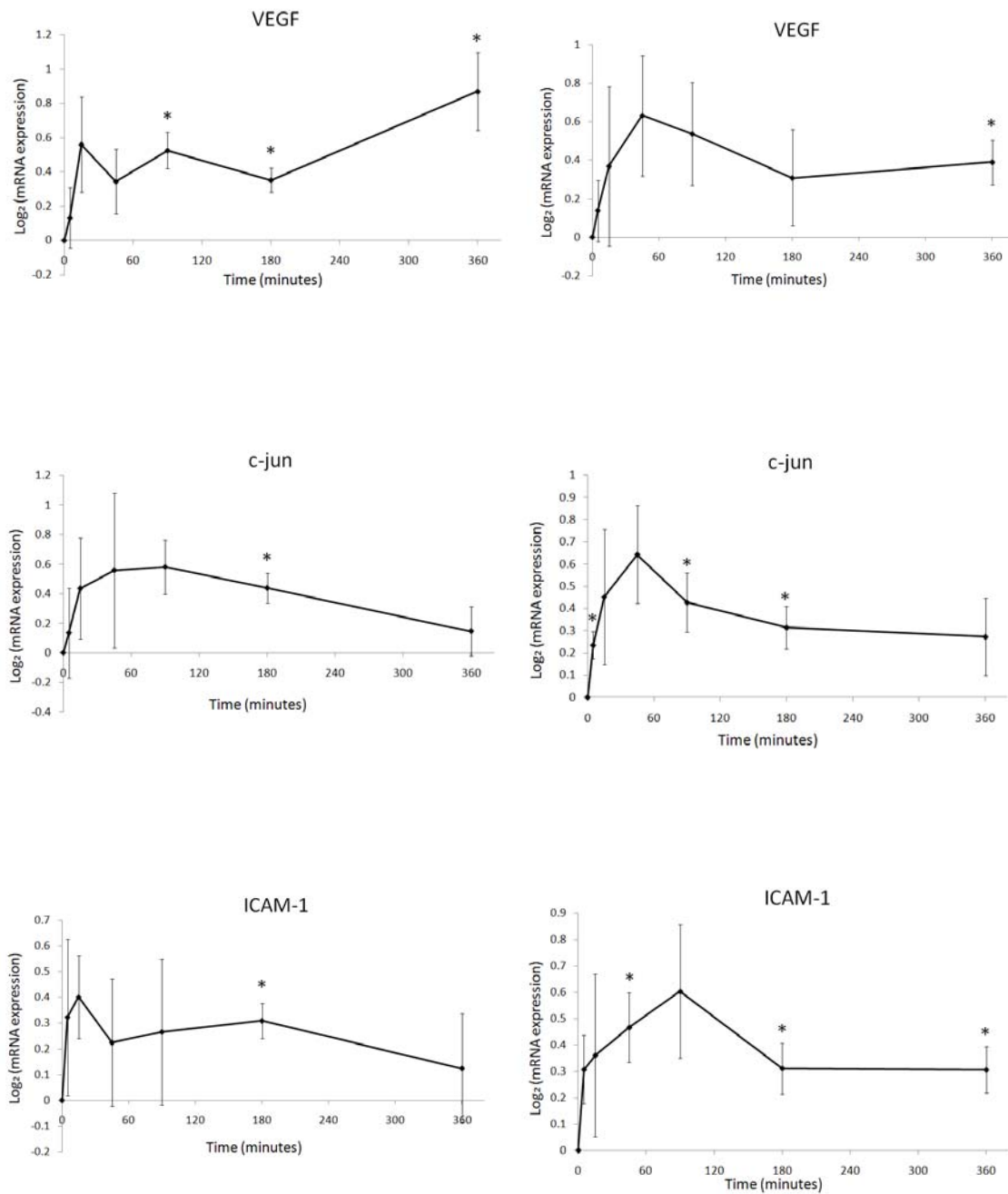


Figure 38: Real-time PCR validates the microarray results of the frequency step-up experiments. Left: microarray measurements; Right: real-time PCR measurements. n=4 for each data point. Expression values were normalized by the pre step-up controls, and error bars indicates the deviation of the mean. *: p<0.05, one-way t-test against zero.

5. Discussion

5.1 *The response of endothelial permeability to altered shear stress*

We have characterized the adaptive dynamics of endothelial permeability in response to acute changes in shear stress magnitude and frequency in well defined *in vitro* settings. Our results demonstrated that the step increase in shear stress magnitude immediately increased endothelial permeability to BSA; and the permeability nearly doubled after 40 minutes exposure to the elevated shear. This observation supports our hypothesis that an acute increase in endothelial permeability will occur when endothelial cells undergo cytoskeletal reorganization and junctional remodeling during adaptation to a new hemodynamic environment. Endothelial permeability started to decline after 40 minutes; however, it remained above the baseline (preconditioned) level until six hours after the shear stress step-up, which was the ending time of our experiments. Although it is not clear from this study whether endothelial permeability will eventually decrease to the baseline level, it is reasonable to believe so since several *in vitro* studies have associated lower permeability with higher shear stress magnitude following a relatively long term shear exposure [14-16]. Thus, the increased permeability at later times observed in our study is more likely a transient alteration of endothelial phenotype resulting from the onset of the elevated shear. A recently published study also supports this notion [16]. Warboys et al. demonstrated that an acute exposure (1 hour) to shear stress significantly increased porcine endothelial permeability to albumin

in vitro (relative to static cultured cells), while a chronic exposure (7 to 9 days) decreased the permeability.

Friedman et al. [72] and Hazel et al. [73] have investigated the adaptive response of endothelial permeability to shear stress alteration *in vivo*. As described before, an *ad hoc* mathematical model of adaptation was developed to fit the experimental data [72, 73]. Based on the mathematical model, in response to an acute increase in shear stress *in vivo*, endothelial permeability can be described as $P = 1 + k \delta(t)$, where P is the instantaneous permeability normalized by the permeability of fully adapted cells, k is a constant that depends on the imposed change in shear stress, and δ is a function of time. The variation of δ with time based on the results presented in [73] is shown in Figure 39. The mathematical model predicted a rapid increase in endothelial permeability upon the step increase in shear stress and a permeability peak at 7 minutes. Compared to our *in vitro* result, the increase in permeability is much steeper *in vivo*; endothelial permeability peaks much earlier (7 minutes *in vivo* vs. 40 minutes *in vitro*); and it decreases much faster *in vivo*. The differences are not too surprising since *in vitro* measurements of endothelial permeability usually differs greatly from *in vivo* measurements [25]. More importantly, the instantaneous endothelial permeability was measured directly in our study; however, the *in vivo* values were obtained from a mathematical model where numerous assumptions were made. Nevertheless, our *in vitro* study and the previous *in*

vivo study consistently confirm the transient increase in endothelial permeability in response to the acute increase in shear stress magnitude.

Our study did not find any statistically significant dependence of endothelial permeability on shear stress frequency during the first 6 hours after the frequency step-up. However, there was a clear trend of increase in endothelial permeability after 120 minutes exposure to higher shear frequency. Although the observed increase in permeability was relatively small (1.2 fold increase at 6 hours) and slow, it is possible that endothelial permeability would eventually increase to a significantly higher level after longer exposure to the elevated shear frequency. The dependence of endothelial permeability on the frequency of chronically applied shear stress is unknown both *in vivo* and *in vitro*. Himburg et al. [36] demonstrated that 24 hours exposure to shear stress at 2Hz evoked an endothelial proinflammatory response *in vitro*, which may compromise endothelial barrier function. The gradual increase in permeability in response to higher shear frequency may be a result of increased endothelial mitosis, as suggested by our microarray studies, since mitosis generates leakage sites for trans-endothelial biomolecular transport [163-165]. Compared to the dynamics of the permeability response to higher shear stress magnitude, the lack of a rapid increase in permeability immediately after the frequency step-up suggests that the increase in shear stress frequency was unable to induce sufficient endothelial cytoskeletal reorganization and junctional remodeling activity. This is certainly consistent with Himburg et al. [36], who

find no effect of shear stress frequency on endothelial cell alignment and the expression and localization of several structural proteins, including actin, tubulin, VE-cadherin and α -catenin.

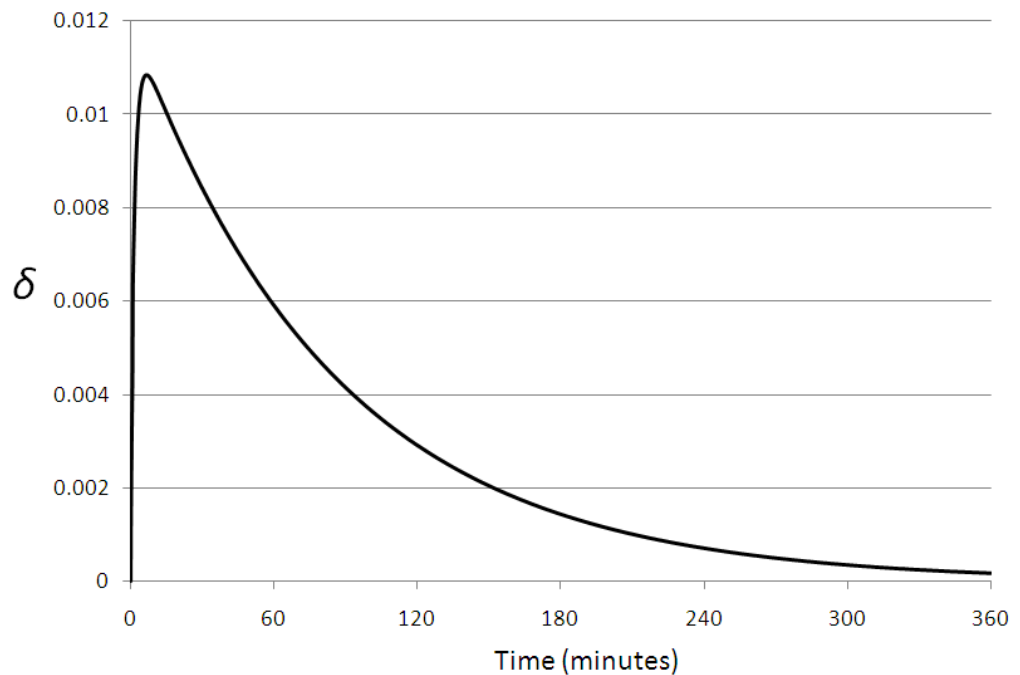


Figure 39: Plot of function δ in the mathematical model predicting endothelial permeability alteration in response to an acute increase in shear stress magnitude *in vivo*. The plot was generated based on the mathematical model describe in [73].

In summary, we demonstrated that the instantaneous endothelial permeability to BSA increased rapidly in response to acute increases in shear stress magnitude, but increased slowly and gradually in response to higher shear frequency. It is important to point out that the mechanism of the induced increase in permeability remains unknown. Further studies are necessary to find out whether the increase is due to endothelial cytoskeletal reorganization and junctional remodeling, as hypothesized in our study, or

is regulated by other mechanisms. Some clues can be found in the results of our transcriptomics study. As described in the previous chapter, the expression of several cytoskeletal and transport-related genes and pathways was altered by the increase in shear stress magnitude; and several cell-cycle and mitosis regulating genes were identified as sensitive to the elevated shear stress frequency.

5.2 The response of endothelial gene expression to altered shear stress

Our study provides the first detailed temporal map of endothelial transcriptional activity during the adaptive response to altered shear stress. We have identified 86 genes that are sensitive to elevated shear stress magnitude and 37 genes sensitive to elevated frequency. Only three genes, ID2, STK38L and SHCBP1, were identified as sensitive to both magnitude and frequency step-ups. This suggests that endothelial cells have different sensing mechanisms for shear stress magnitude and frequency.

The step increase in shear stress magnitude promoted the expression of a group of anti-inflammatory and anti-oxidative genes *in vitro*. Among these genes, KLF2, KLF4, HMOX1 and GADD45 β were upregulated; and BMP4, IL-1 α and IL-8 were downregulated. The vasomotion related genes eNOS and KCNN4 were also upregulated. Several cytoskeletal, junctional and cell adhesion genes, such as actin, MHY9, PCDH7 and COL4A1, were upregulated by the acute increase in shear stress, suggesting a possible cell remodeling process. The functions of these genes and their involvements in atherogenesis have been discussed in previous chapters. Overall, our

data suggests that the acute elevation of shear stress magnitude has a predominantly anti-inflammatory and atheroprotective effect on endothelial cells. This may have implications for the beneficial effects of exercise.

The acute increase in shear stress frequency upregulated a set of cell-cycle regulating genes and several angiogenesis genes. Among these genes are three cyclin genes (cyclin A2, B1 and B3), CDK1, angiogenic genes ID2 and VEGF. The upregulation of these genes may lead to endothelial activation and increased cell proliferation. Thus, elevated shear stress frequency may predispose endothelial cells to an atheroprone phenotype.

The global gene expression profile was regulated dynamically during the adaptive responses to increased shear stress. Clustering analysis showed that the transcriptional profile at 45 minutes after shear magnitude step-up clustered last with other time points, indicating a distinct global transcriptional profile at 45 minutes. Principal component analysis further suggested that 45 minutes was a critical turning point for global gene expression regulation. Pathway analysis demonstrated that the overall activity of the identified pathways was the greatest at 45 minutes and the activity of cytoskeleton remodeling pathways was the greatest at 180 minutes. These results suggest that the adaptive response of global gene expression to the acute increase in shear stress magnitude is triphasic, consisting of an induction period, an early adaptive response (ca. 45 minutes) and a late remodeling response.

In our *in vitro* adaptive model, endothelial cells were first preconditioned by the basal level shear stress and gene expression was then measured at multiple time points during adaptation. This experimental setting helped us to discover several previously unknown shear sensitive genes. This is because some of the genes respond to elevated shear stress in preconditioned cells but not in static cells; and other genes respond to shear stress only transiently. Therefore, they cannot be detected in conventional shear stress experiments, in which shear stress is applied to static cultured endothelial cells and gene expression is measured only at the end time point. Several novel shear sensitive genes identified in this study, such as ID1, ID2 and ABCB1, may be important regulators in atherogenesis and can serve as potential therapeutic targets.

One of the most important findings in our study is that static cultured cells and preconditioned cells respond differently to the same level of increase in shear stress (0 to 15 dynes/cm² for static cells and 15 to 30 dynes/cm² for preconditioned cells). More than a thousand genes were identified as differentially expressed in static cultured cells in response to the preconditioning shear stress. However, only 86 genes were identified to be sensitive to the further increase in shear stress magnitude in the step-up experiment, suggesting a much smaller response of the preconditioned endothelial cells. Of the 86 identified genes, only 40 were also found to be sensitive to the application of the preconditioning shear stress to static cultured cells. The expression values of these genes during the adaptive response are plotted in the heat map shown in Figure 40. All 40

genes were ranked by their expression values after 24 hours exposure to preconditioning shear stress, relative to the expression in static cultured cells. The top ranked genes were upregulated greatly when the static cultured cells were exposed to the preconditioning shear stress, and the genes at the bottom were downregulated significantly. As shown in the heat map, the expression levels of some genes, such as KLF2 and KCNN4, were consistently upregulated (or downregulated) by the preconditioning shear stress and then the elevated shear stress. However, for other genes, such as ID2, the preconditioning shear stress and the elevated shear stress have opposite effects on their expression. Thus, one cannot predict from the transcriptional response of static cultured cells how a particular gene will be regulated during the adaptive response to a changed shear stress.

The expression of the *a-priori* selected atherogenesis-relevant genes further confirmed this. Although most of these well-studied genes were sensitive to the preconditioning shear stress in static cells, only a few were responsive to the further increases in shear stress magnitude in our study. For some of these genes, the responses to the preconditioning and elevated shear stress are opposite in direction. Therefore, the regulation patterns of endothelial gene expression are different in the preconditioned cells than in static cultured cells. Since the preconditioned endothelial cells are more representative of *in vivo* cells than static cultured cells, we believe the genes and their

regulation patterns identified in our step-up studies are more significant in understanding the development of atherosclerosis *in vivo*.

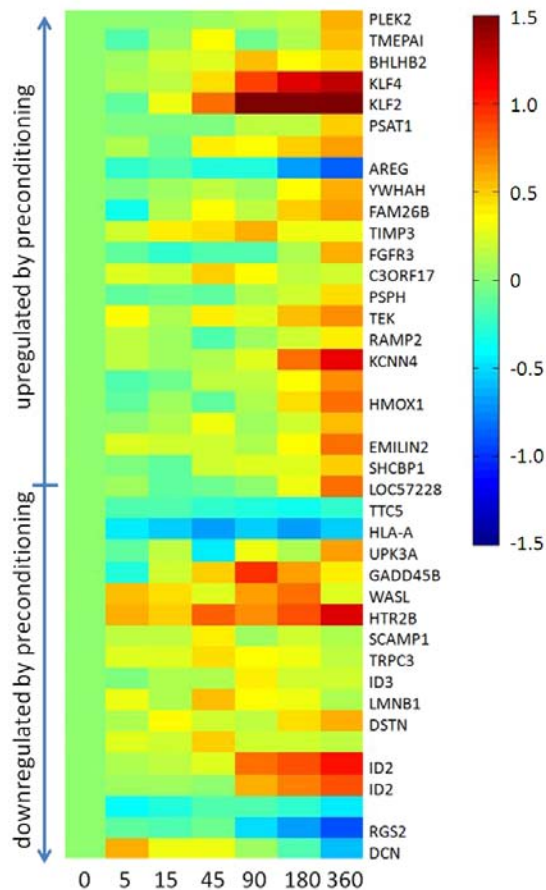


Figure 40: Heat map of the expression values of the genes that were sensitive to both the preconditioning and elevated shear stress. Each row is the time course of the expression value of one gene during the adaptive response. The expression values were normalized to the preconditioned value at time = 0, and are color coded. The genes were ranked based on their responses to preconditioning shear stress, i.e. the top ranked genes were upregulated by the preconditioning (relative to the static cultured cells) and the genes at the bottom were downregulated by the preconditioning.

5.3 Future Work

We have characterized the dynamic change of endothelial permeability to bovine serum albumin in response to altered shear stress. However, endothelial permeability to low density lipoprotein (LDL) is more relevant to atherogenesis, as described in Chapter 2. The mechanism of LDL transport across the endothelial monolayer is different than albumin. Albumin (4 to 10 nm in diameter) can easily diffuse through the endothelial cells and penetrate normal intercellular junctions (20 nm in width) [166]. However, due to the large size of LDL (21 to 26 nm in diameter), leaky junctions, transendothelial pores, and mitosis or apoptosis cells are the dominant pathways for LDL transport across endothelial cells [86, 163-165, 167]. Thus, one should use caution to apply what have been learned from albumin permeability in understanding trans-endothelial LDL transport. Therefore, an interesting follow-up study will be to investigate how the endothelial permeability to LDL is altered during the adaptation. Measurement of the permeability to LDL is more challenging since the endothelial permeability to LDL is one magnitude lower than to albumin and fluorescent labeled LDL is much more expensive to use in a high concentration. A computer-controlled cone-and-plate shear stress apparatus [168] may be better for the this experiment, since it uses smaller volume of perfusion media and higher tracer concentration can be applied. The optical-fiber based fluorescence detector developed in the dissertation can be incorporated directly to the cone-and-plate apparatus with a different set of band-pass filters and dichroic mirror

according to the wavelength of the labeled LDL. The results of such studies will increase our understanding of endothelial permeability to different molecules. It will be particularly interesting to see if there is any response of endothelial permeability to LDL to shear stress frequency since our transcriptomics study suggested that elevated frequency may induce mitosis, which could provide major paths for LDL transport.

The microarray studies suggested that elevated shear stress magnitude promotes the expression of a set of anti-inflammatory and anti-oxidative genes; and elevated shear stress frequency induces the expression of a set of cell-cycle regulating and angiogenesis genes. However, the regulation of these genes is not necessarily indicative of how the proteins encoded by those genes are regulated. Therefore, future work will include quantitative measurement of protein levels for proteins of interest. The limited selection of antibodies to porcine proteins poses a major challenging for using techniques such as western blotting or ELISA. Thus, human arterial cells may be used for protein studies, or alternatively, liquid chromatographs and mass spectrum (LC/MS) based proteomics techniques can be used to quantify protein levels without using antibodies. In addition to quantifying protein expression level, further experiments such as cell adhesion, reactive oxygen species production and cell mitosis assay will be carried out to confirm the transient change of endothelial phenotype during the adaptive response.

As discussed before, one interesting finding of the transcriptomics study is that static and preconditioned cells respond differently to the imposed increases in shear stress magnitude. It is reasonable to speculate the mechanisms by which shear stress regulates the expression of these genes are different in the static cultured cells than in the shear-stress preconditioned cells. However, one may argue that the regulation mechanisms are actually the same and the observed differences in gene expression were because of the differences in the duration of exposure to the shear stress increase (24 hours vs. 6 hours). A set of experiments can be designed to test this hypothesis. Static cultured cells will be exposed to preconditioning shear stress for a period of 5 minutes to 6 hours, and preconditioned cell will be exposed to elevated shear stress for 24 hours. The study will complement this dissertation and answer if the contradict regulation direction observed in this study is due to the differences in the regulation mechanisms or the duration of shear stress exposure.

Our study has identified several novel genes (e.g. ID1 and ID2) that are sensitive to shear stress and have potential implications in atherogenesis. We believe these identified genes/pathways are more significant in the development of atherosclerosis *in vivo* since the preconditioned cells used in our study are more realistic than static cultured cells comparing to *in vivo* cells. Thus, these genes deserve further studies to dissect the regulation mechanism or pathways and confirm their involvement in

atherogenesis using comprehensive molecular biology techniques. This effort may lead to the discovery of new therapeutic intervention for atherosclerosis.

In our adaptive model, the magnitude and frequency of shear stress were increased separately to dissect the endothelial responses to different shear parameters. Future studies could focus on the combined effect of elevated shear stress magnitude and frequency on endothelial functions. It will help to elucidate if the effects of these two shear stress parameters are additive or one has a more dominant effect. This will increase our understanding of the adaptive response of endothelial cells *in vivo*, since the increases of mean shear stress and frequency are usually coupled during several physiologic events, such as exercise. This research can be further extended by altering other parameters of shear stress to induce the adaptive response of endothelial cells. For example, the shear stress profiles used in current study are all unidirectional. It will be interesting to see how endothelial cells preconditioned under unidirectional shear stress respond to the shear stress profiles with reversal components. The experimental setup described in this dissertation is fully capable of generating various flow waveforms for such studies.

References

1. Fox, S.I., *Human physiology*. 7th ed. 2002, Boston: McGraw-Hill. xix, 728 p.
2. Lodish, H.F., *Molecular cell biology*. 6th ed. 2008, New York: W.H. Freeman. 1 v. (various pagings).
3. Kumar, V. and S.L. Robbins, *Robbins basic pathology*. 8th ed. 2007, Philadelphia, PA: Saunders/Elsevier. xiv, 946 p.
4. Ross, R., *The pathogenesis of atherosclerosis: a perspective for the 1990s*. *Nature*, 1993. **362**(6423): p. 801-9.
5. Ross, R., *Atherosclerosis--an inflammatory disease*. *N Engl J Med*, 1999. **340**(2): p. 115-26.
6. Lodish, H.F., *Molecular cell biology*. 5th ed. 2004, New York: W.H. Freeman. xxxiii, 973, [79] p.
7. Chien, S., *Molecular basis of rheological modulation of endothelial functions: importance of stress direction*. *Biorheology*, 2006. **43**(2): p. 95-116.
8. Chien, S., *Effects of disturbed flow on endothelial cells*. *Ann Biomed Eng*, 2008. **36**(4): p. 554-62.
9. Davies, P.F., *Hemodynamic shear stress and the endothelium in cardiovascular pathophysiology*. *Nat Clin Pract Cardiovasc Med*, 2009. **6**(1): p. 16-26.
10. Hahn, C. and M.A. Schwartz, *The role of cellular adaptation to mechanical forces in atherosclerosis*. *Arterioscler Thromb Vasc Biol*, 2008. **28**(12): p. 2101-7.
11. Cunningham, K.S. and A.I. Gotlieb, *The role of shear stress in the pathogenesis of atherosclerosis*. *Lab Invest*, 2005. **85**(1): p. 9-23.
12. Jo, H., et al., *Endothelial albumin permeability is shear dependent, time dependent, and reversible*. 1991. p. H1992-1996.
13. Phelps, J.E. and N. DePaola, *Spatial variations in endothelial barrier function in disturbed flows in vitro*. *Am J Physiol Heart Circ Physiol*, 2000. **278**(2): p. H469-76.

14. Kudo, S., et al., *Albumin permeability across endothelial monolayers under long-term shear stress*. *Jsm International Journal Series C-Mechanical Systems Machine Elements and Manufacturing*, 2005. **48**(4): p. 419-424.
15. Colgan, O.C., et al., *Regulation of bovine brain microvascular endothelial tight junction assembly and barrier function by laminar shear stress*. *Am J Physiol Heart Circ Physiol*, 2007. **292**(6): p. H3190-7.
16. Warboys, C.M., et al., *Acute and chronic exposure to shear stress have opposite effects on endothelial permeability to macromolecules*. *Am J Physiol Heart Circ Physiol*. **298**(6): p. H1850-6.
17. Conklin, B.S., R.P. Vito, and C. Chen, *Effect of low shear stress on permeability and occludin expression in porcine artery endothelial cells*. *World J Surg*, 2007. **31**(4): p. 733-43.
18. Himburg, H.A., et al., *Spatial comparison between wall shear stress measures and porcine arterial endothelial permeability*. *Am J Physiol Heart Circ Physiol*, 2004. **286**(5): p. H1916-22.
19. LaMack, J.A., et al., *Interaction of wall shear stress magnitude and gradient in the prediction of arterial macromolecular permeability*. *Ann Biomed Eng*, 2005. **33**(4): p. 457-64.
20. Buchanan, J.R., Jr., et al., *Relation between non-uniform hemodynamics and sites of altered permeability and lesion growth at the rabbit aorto-celiac junction*. *Atherosclerosis*, 1999. **143**(1): p. 27-40.
21. Conklin, B.S., et al., *Shear stress regulates occludin and VEGF expression in porcine arterial endothelial cells*. *J Surg Res*, 2002. **102**(1): p. 13-21.
22. Taddei, A., et al., *Endothelial adherens junctions control tight junctions by VE-cadherin-mediated upregulation of claudin-5*. *Nat Cell Biol*, 2008. **10**(8): p. 923-34.
23. Orr, A.W., et al., *Matrix-specific p21-activated kinase activation regulates vascular permeability in atherogenesis*. *J Cell Biol*, 2007. **176**(5): p. 719-27.
24. Tzima, E., *Role of small GTPases in endothelial cytoskeletal dynamics and the shear stress response*. *Circ Res*, 2006. **98**(2): p. 176-85.

25. Ogunrinade, O., G.T. Kameya, and G.A. Truskey, *Effect of fluid shear stress on the permeability of the arterial endothelium*. *Ann Biomed Eng*, 2002. **30**(4): p. 430-46.
26. Feletou, M. and P.M. Vanhoutte, *Endothelial dysfunction: a multifaceted disorder (The Wiggers Award Lecture)*. *Am J Physiol Heart Circ Physiol*, 2006. **291**(3): p. H985-1002.
27. Dekker, R.J., et al., *Prolonged fluid shear stress induces a distinct set of endothelial cell genes, most specifically lung Kruppel-like factor (KLF2)*. *Blood*, 2002. **100**(5): p. 1689-98.
28. Hwang, J., et al., *Pulsatile versus oscillatory shear stress regulates NADPH oxidase subunit expression: implication for native LDL oxidation*. *Circ Res*, 2003. **93**(12): p. 1225-32.
29. Hsiai, T.K., et al., *Monocyte recruitment to endothelial cells in response to oscillatory shear stress*. *FASEB J*, 2003. **17**(12): p. 1648-57.
30. Dekker, R.J., et al., *Endothelial KLF2 links local arterial shear stress levels to the expression of vascular tone-regulating genes*. *Am J Pathol*, 2005. **167**(2): p. 609-18.
31. Partridge, J., et al., *Laminar shear stress acts as a switch to regulate divergent functions of NF-kappaB in endothelial cells*. *FASEB J*, 2007. **21**(13): p. 3553-61.
32. Topper, J.N., et al., *Identification of vascular endothelial genes differentially responsive to fluid mechanical stimuli: cyclooxygenase-2, manganese superoxide dismutase, and endothelial cell nitric oxide synthase are selectively up-regulated by steady laminar shear stress*. *Proc Natl Acad Sci U S A*, 1996. **93**(19): p. 10417-22.
33. Malek, A. and S. Izumo, *Physiological fluid shear stress causes downregulation of endothelin-1 mRNA in bovine aortic endothelium*. *Am J Physiol*, 1992. **263**(2 Pt 1): p. C389-96.
34. Ziegler, T., et al., *Influence of oscillatory and unidirectional flow environments on the expression of endothelin and nitric oxide synthase in cultured endothelial cells*. *Arterioscler Thromb Vasc Biol*, 1998. **18**(5): p. 686-92.
35. Helderma, F., et al., *Effect of shear stress on vascular inflammation and plaque development*. *Curr Opin Lipidol*, 2007. **18**(5): p. 527-33.

36. Himburg, H.A., S.E. Dowd, and M.H. Friedman, *Frequency-dependent response of the vascular endothelium to pulsatile shear stress*. *Am J Physiol Heart Circ Physiol*, 2007. **293**(1): p. H645-53.
37. Bao, X., C. Lu, and J.A. Frangos, *Temporal gradient in shear but not steady shear stress induces PDGF-A and MCP-1 expression in endothelial cells: role of NO, NF kappa B, and egr-1*. *Arterioscler Thromb Vasc Biol*, 1999. **19**(4): p. 996-1003.
38. LaMack, J.A. and M.H. Friedman, *Individual and combined effects of shear stress magnitude and spatial gradient on endothelial cell gene expression*. *American Journal of Physiology-Heart and Circulatory Physiology*, 2007. **293**(5): p. H2853-H2859.
39. Yamawaki, H., et al., *Fluid shear stress inhibits vascular inflammation by decreasing thioredoxin-interacting protein in endothelial cells*. *J Clin Invest*, 2005. **115**(3): p. 733-8.
40. Mowbray, A.L., et al., *Laminar shear stress up-regulates peroxiredoxins (PRX) in endothelial cells: PRX 1 as a mechanosensitive antioxidant*. *J Biol Chem*, 2008. **283**(3): p. 1622-7.
41. Iiyama, K., et al., *Patterns of vascular cell adhesion molecule-1 and intercellular adhesion molecule-1 expression in rabbit and mouse atherosclerotic lesions and at sites predisposed to lesion formation*. *Circ Res*, 1999. **85**(2): p. 199-207.
42. Chappell, D.C., et al., *Oscillatory shear stress stimulates adhesion molecule expression in cultured human endothelium*. *Circ Res*, 1998. **82**(5): p. 532-9.
43. Jo, H., H. Song, and A. Mowbray, *Role of NADPH oxidases in disturbed flow- and BMP4- induced inflammation and atherosclerosis*. *Antioxid Redox Signal*, 2006. **8**(9-10): p. 1609-19.
44. Hwang, J., et al., *Oscillatory shear stress stimulates endothelial production of O₂⁻ from p47phox-dependent NAD(P)H oxidases, leading to monocyte adhesion*. *J Biol Chem*, 2003. **278**(47): p. 47291-8.
45. Brooks, A.R., P.I. Leikes, and G.M. Rubanyi, *Gene expression profiling of human aortic endothelial cells exposed to disturbed flow and steady laminar flow*. *Physiological genomics*, 2002. **9**(1): p. 27-41.

46. Galkina, E. and K. Ley, *Vascular adhesion molecules in atherosclerosis*. *Arterioscler Thromb Vasc Biol*, 2007. **27**(11): p. 2292-301.
47. Lusis, A.J., *Atherosclerosis*. *Nature*, 2000. **407**(6801): p. 233-41.
48. Libby, P., *Inflammation in atherosclerosis*. *Nature*, 2002. **420**(6917): p. 868-74.
49. Hansson, G.K. and P. Libby, *The immune response in atherosclerosis: a double-edged sword*. *Nat Rev Immunol*, 2006. **6**(7): p. 508-19.
50. McCormick, S.M., et al., *DNA microarray reveals changes in gene expression of shear stressed human umbilical vein endothelial cells*. *Proc Natl Acad Sci U S A*, 2001. **98**(16): p. 8955-60.
51. Shyy, Y.J., et al., *Fluid shear stress induces a biphasic response of human monocyte chemotactic protein 1 gene expression in vascular endothelium*. *Proceedings of the National Academy of Sciences of the United States of America*, 1994. **91**(11): p. 4678-82.
52. Ahmad, M., P. Theofanidis, and R.M. Medford, *Role of activating protein-1 in the regulation of the vascular cell adhesion molecule-1 gene expression by tumor necrosis factor-alpha*. *J Biol Chem*, 1998. **273**(8): p. 4616-21.
53. Nagel, T., et al., *Vascular endothelial cells respond to spatial gradients in fluid shear stress by enhanced activation of transcription factors*. *Arterioscler Thromb Vasc Biol*, 1999. **19**(8): p. 1825-34.
54. SenBanerjee, S., et al., *KLF2 Is a novel transcriptional regulator of endothelial proinflammatory activation*. *J Exp Med*, 2004. **199**(10): p. 1305-15.
55. Lin, Z., et al., *Kruppel-like factor 2 (KLF2) regulates endothelial thrombotic function*. *Circ Res*, 2005. **96**(5): p. e48-57.
56. van Thienen, J.V., et al., *Shear stress sustains atheroprotective endothelial KLF2 expression more potently than statins through mRNA stabilization*. *Cardiovasc Res*, 2006. **72**(2): p. 231-40.
57. Hamik, A., et al., *Kruppel-like factor 4 regulates endothelial inflammation*. *J Biol Chem*, 2007. **282**(18): p. 13769-79.

58. Villarreal, G., et al., *Defining the regulation of KLF4 expression and its downstream transcriptional targets in vascular endothelial cells*. Biochemical and biophysical research communications. **391**(1): p. 984-9.
59. Chen, B.P., et al., *DNA microarray analysis of gene expression in endothelial cells in response to 24-h shear stress*. Physiol Genomics, 2001. **7**(1): p. 55-63.
60. Sorescu, G.P., et al., *Bone morphogenic protein 4 produced in endothelial cells by oscillatory shear stress induces monocyte adhesion by stimulating reactive oxygen species production from a nox1-based NADPH oxidase*. Circ Res, 2004. **95**(8): p. 773-9.
61. Sun, H.-W., et al., *Involvement of integrins, MAPK, and NF-kappaB in regulation of the shear stress-induced MMP-9 expression in endothelial cells*. Biochemical and biophysical research communications, 2007. **353**(1): p. 152-8.
62. Cheng, M., et al., *IL-8 induces imbalances between nitric oxide and endothelin-1, and also between plasminogen activator inhibitor-1 and tissue-type plasminogen activator in cultured endothelial cells*. Cytokine, 2008. **41**(1): p. 9-15.
63. Cheng, M., et al., *IL-8 gene induction by low shear stress: pharmacological evaluation of the role of signaling molecules*. Biorheology, 2007. **44**(5-6): p. 349-60.
64. Eskin, S.G., N.A. Turner, and L.V. McIntire, *Endothelial cell cytochrome P450 1A1 and 1B1: up-regulation by shear stress*. Endothelium : journal of endothelial cell research, 2004. **11**(1): p. 1-10.
65. Garcia-Cardena, G., et al., *Biomechanical activation of vascular endothelium as a determinant of its functional phenotype*. Proc Natl Acad Sci U S A, 2001. **98**(8): p. 4478-85.
66. Zhao, Y., et al., *Improved significance test for DNA microarray data: temporal effects of shear stress on endothelial genes*. Physiological genomics, 2002. **12**(1): p. 1-11.
67. Okahara, K., B. Sun, and J. Kambayashi, *Upregulation of prostacyclin synthesis-related gene expression by shear stress in vascular endothelial cells*. Arterioscler Thromb Vasc Biol, 1998. **18**(12): p. 1922-6.
68. Wagener, F.A.D.T.G., et al., *Different faces of the heme-heme oxygenase system in inflammation*. Pharmacological reviews, 2003. **55**(3): p. 551-71.

69. Morse, D. and A.M.K. Choi, *Heme oxygenase-1: from bench to bedside*. American journal of respiratory and critical care medicine, 2005. **172**(6): p. 660-70.
70. Lin, K., et al., *Molecular mechanism of endothelial growth arrest by laminar shear stress*. Proceedings of the National Academy of Sciences of the United States of America, 2000. **97**(17): p. 9385-9.
71. Ohura, N., et al., *Global analysis of shear stress-responsive genes in vascular endothelial cells*. J Atheroscler Thromb, 2003. **10**(5): p. 304-13.
72. Friedman, M.H., et al., *Effect of periodic alterations in shear on vascular macromolecular uptake*. Biorheology, 2000. **37**(4): p. 265-77.
73. Hazel, A.L., D.M. Grzybowski, and M.H. Friedman, *Modeling the adaptive permeability response of porcine iliac arteries to acute changes in mural shear*. Ann Biomed Eng, 2003. **31**(4): p. 412-9.
74. Henderson, J.M., et al., *Effect of alterations in femoral artery flow on abdominal vessel hemodynamics in swine*. Biorheology, 1999. **36**(3): p. 257-66.
75. Himburg, H.A. and M.H. Friedman, *Correspondence of low mean shear and high harmonic content in the porcine iliac arteries*. Journal of Biomechanical Engineering-Transactions of the Asme, 2006. **128**(6): p. 852-856.
76. Friedman, M.H., H.A. Himburg, and J.A. LaMack, *Statistical hemodynamics: A tool for evaluating the effect of fluid dynamic forces on vascular biology in vivo*. Journal of Biomechanical Engineering-Transactions of the Asme, 2006. **128**(6): p. 965-968.
77. Benjamini, Y. and Y. Hochberg, *Controlling the False Discovery Rate - a Practical and Powerful Approach to Multiple Testing*. Journal of the Royal Statistical Society Series B-Methodological, 1995. **57**(1): p. 289-300.
78. Tusher, V.G., R. Tibshirani, and G. Chu, *Significance analysis of microarrays applied to the ionizing radiation response*. Proc Natl Acad Sci U S A, 2001. **98**(9): p. 5116-21.
79. Subramanian, A., et al., *Gene set enrichment analysis: a knowledge-based approach for interpreting genome-wide expression profiles*. Proc Natl Acad Sci U S A, 2005. **102**(43): p. 15545-50.

80. Shao, J.S., et al., *Vascular Bmp Msx2 Wnt signaling and oxidative stress in arterial calcification*. Ann N Y Acad Sci, 2007. **1117**: p. 40-50.
81. Alderton, W.K., C.E. Cooper, and R.G. Knowles, *Nitric oxide synthases: structure, function and inhibition*. Biochem J, 2001. **357**(Pt 3): p. 593-615.
82. Orr, A.W., et al., *Mechanisms of mechanotransduction*. Dev Cell, 2006. **10**(1): p. 11-20.
83. LaMack, J.A., et al., *Endothelial Gene Expression in Regions of Defined Shear Exposure in the Porcine Iliac Arteries*. Annals of Biomedical Engineering, Submitted.
84. Zhang, J., K.A. Burrige, and M.H. Friedman, *In vivo differences between endothelial transcriptional profiles of coronary and iliac arteries revealed by microarray analysis*. Am J Physiol Heart Circ Physiol, 2008. **295**(4): p. H1556-61.
85. Augustin, H.G., *Methods in endothelial cell biology*. Springer lab manuals. 2004, Berlin ; New York: Springer. xx, 383 p.
86. Cancel, L.M., A. Fitting, and J.M. Tarbell, *In vitro study of LDL transport under pressurized (convective) conditions*. Am J Physiol Heart Circ Physiol, 2007. **293**(1): p. H126-32.
87. Bacabac, R.G., et al., *Dynamic shear stress in parallel-plate flow chambers*. J Biomech, 2005. **38**(1): p. 159-67.
88. Novak, L., et al., *An integrated fluorescence detection system for lab-on-a-chip applications*. Lab Chip, 2007. **7**(1): p. 27-9.
89. DeMaio, L., et al., *A transmural pressure gradient induces mechanical and biological adaptive responses in endothelial cells*. Am J Physiol Heart Circ Physiol, 2004. **286**(2): p. H731-41.
90. Yang, B., F. Tan, and Y. Guan, *A collinear light-emitting diode-induced fluorescence detector for capillary electrophoresis*. Talanta, 2005. **65**(5): p. 1303-6.
91. Rasooly, A. and K.E. Herold, *Biosensors and biodetection : methods and protocols*. 2009, New York: Humana Press.
92. *Lock-In Amplifier Start-Up Kit*. 2002, National Instrument.

93. Lamack, J.A., H.A. Himburg, and M.H. Friedman, *Distinct profiles of endothelial gene expression in hyperpermeable regions of the porcine aortic arch and thoracic aorta*. *Atherosclerosis*, 2007.
94. Murase, T., et al., *Gallates inhibit cytokine-induced nuclear translocation of NF-kappaB and expression of leukocyte adhesion molecules in vascular endothelial cells*. *Arteriosclerosis, thrombosis, and vascular biology*, 1999. **19**(6): p. 1412-20.
95. Cullere, X., et al., *Regulation of vascular endothelial barrier function by Epac, a cAMP-activated exchange factor for Rap GTPase*. *Blood*, 2005. **105**(5): p. 1950-5.
96. Wei, Q. and R.S. Adelstein, *Conditional expression of a truncated fragment of nonmuscle myosin II-A alters cell shape but not cytokinesis in HeLa cells*. *Molecular biology of the cell*, 2000. **11**(10): p. 3617-27.
97. Gallagher, P.J., et al., *Alterations in expression of myosin and myosin light chain kinases in response to vascular injury*. *American journal of physiology Cell physiology*, 2000. **279**(4): p. C1078-87.
98. Huang, Y., et al., *The angiogenic function of nucleolin is mediated by vascular endothelial growth factor and nonmuscle myosin*. *Blood*, 2006. **107**(9): p. 3564-71.
99. Yagi, T. and M. Takeichi, *Cadherin superfamily genes: functions, genomic organization, and neurologic diversity*. *Genes & development*, 2000. **14**(10): p. 1169-80.
100. *Genome-wide association study of 14,000 cases of seven common diseases and 3,000 shared controls*. *Nature*, 2007. **447**(7145): p. 661-78.
101. Bell, A.W., et al., *Proteomics characterization of abundant Golgi membrane proteins*. *The Journal of biological chemistry*, 2001. **276**(7): p. 5152-65.
102. Andersson, M., et al., *Differential global gene expression response patterns of human endothelium exposed to shear stress and intraluminal pressure*. *J Vasc Res*, 2005. **42**(5): p. 441-52.
103. Fernandez-Chacon, R., et al., *Analysis of SCAMP1 function in secretory vesicle exocytosis by means of gene targeting in mice*. *The Journal of biological chemistry*, 1999. **274**(46): p. 32551-4.

104. Fernandez-Chacon, R. and T.C. Sudhof, *Genetics of synaptic vesicle function: toward the complete functional anatomy of an organelle*. Annual review of physiology, 1999. **61**: p. 753-76.
105. Fernandez-Chacon, R., et al., *SCAMP1 function in endocytosis*. The Journal of biological chemistry, 2000. **275**(17): p. 12752-6.
106. Benezra, R., *Role of Id proteins in embryonic and tumor angiogenesis*. Trends in cardiovascular medicine, 2001. **11**(6): p. 237-41.
107. Hamik, A., B. Wang, and M.K. Jain, *Transcriptional regulators of angiogenesis*. Arteriosclerosis, thrombosis, and vascular biology, 2006. **26**(9): p. 1936-47.
108. Lyden, D., et al., *Id1 and Id3 are required for neurogenesis, angiogenesis and vascularization of tumour xenografts*. Nature, 1999. **401**(6754): p. 670-7.
109. Sakurai, D., et al., *Crucial role of inhibitor of DNA binding/differentiation in the vascular endothelial growth factor-induced activation and angiogenic processes of human endothelial cells*. Journal of immunology (Baltimore, Md : 1950), 2004. **173**(9): p. 5801-9.
110. Nishiyama, K., et al., *Protein kinase A-regulated nucleocytoplasmic shuttling of Id1 during angiogenesis*. The Journal of biological chemistry, 2007. **282**(23): p. 17200-9.
111. Ling, M.-T., et al., *Id-1 expression promotes cell survival through activation of NF-kappaB signalling pathway in prostate cancer cells*. Oncogene, 2003. **22**(29): p. 4498-508.
112. Katsuda, S. and T. Kaji, *Atherosclerosis and extracellular matrix*. J Atheroscler Thromb, 2003. **10**(5): p. 267-74.
113. Busse, R., et al., *EDHF: bringing the concepts together*. Trends in pharmacological sciences, 2002. **23**(8): p. 374-80.
114. Eichler, I., et al., *Selective blockade of endothelial Ca²⁺-activated small- and intermediate-conductance K⁺-channels suppresses EDHF-mediated vasodilation*. British journal of pharmacology, 2003. **138**(4): p. 594-601.

115. Brakemeier, S., et al., *Shear stress-induced up-regulation of the intermediate-conductance Ca(2+)-activated K(+) channel in human endothelium*. Cardiovascular research, 2003. **60**(3): p. 488-96.
116. van Bavel, E., *Shear stress and intermediate-conductance calcium-activated potassium channels*. Cardiovascular research, 2003. **60**(3): p. 457-9.
117. Abraham, S.M. and A.R. Clark, *Dual-specificity phosphatase 1: a critical regulator of innate immune responses*. Biochem Soc Trans, 2006. **34**(Pt 6): p. 1018-23.
118. Miura, H., et al., *Flow-induced dilation of human coronary arterioles: important role of Ca(2+)-activated K(+) channels*. Circulation, 2001. **103**(15): p. 1992-8.
119. Dulak, J., A. Loboda, and A. Jozkowicz, *Effect of heme oxygenase-1 on vascular function and disease*. Current opinion in lipidology, 2008. **19**(5): p. 505-12.
120. Peterson, S.J., W.H. Frishman, and N.G. Abraham, *Targeting heme oxygenase: therapeutic implications for diseases of the cardiovascular system*. Cardiology in review, 2009. **17**(3): p. 99-111.
121. Soares, M.P., et al., *Heme oxygenase-1 modulates the expression of adhesion molecules associated with endothelial cell activation*. Journal of immunology (Baltimore, Md : 1950), 2004. **172**(6): p. 3553-63.
122. Kawamura, K., et al., *Bilirubin from heme oxygenase-1 attenuates vascular endothelial activation and dysfunction*. Arteriosclerosis, thrombosis, and vascular biology, 2005. **25**(1): p. 155-60.
123. Melchionna, R., et al., *Laminar shear stress inhibits CXCR4 expression on endothelial cells: functional consequences for atherogenesis*. The FASEB journal : official publication of the Federation of American Societies for Experimental Biology, 2005. **19**(6): p. 629-31.
124. Sun, X., et al., *RGS2 is a mediator of nitric oxide action on blood pressure and vasoconstrictor signaling*. Molecular pharmacology, 2005. **67**(3): p. 631-9.
125. Osei-Owusu, P., et al., *Regulation of RGS2 and second messenger signaling in vascular smooth muscle cells by cGMP-dependent protein kinase*. The Journal of biological chemistry, 2007. **282**(43): p. 31656-65.

126. Heximer, S.P., et al., *Hypertension and prolonged vasoconstrictor signaling in RGS2-deficient mice*. The Journal of clinical investigation, 2003. **111**(4): p. 445-52.
127. Anger, T., et al., *Role of endogenous RGS proteins on endothelial ERK 1/2 activation*. Experimental and molecular pathology, 2008. **85**(3): p. 165-73.
128. Chachisvilis, M., Y.-L. Zhang, and J.A. Frangos, *G protein-coupled receptors sense fluid shear stress in endothelial cells*. Proceedings of the National Academy of Sciences of the United States of America, 2006. **103**(42): p. 15463-8.
129. Raychaudhuri, S., J.M. Stuart, and R.B. Altman, *Principal components analysis to summarize microarray experiments: application to sporulation time series*. Pacific Symposium on Biocomputing Pacific Symposium on Biocomputing, 2000: p. 455-66.
130. Tousson, A., et al., *Characterization of CFTR expression and chloride channel activity in human endothelia*. The American journal of physiology, 1998. **275**(6 Pt 1): p. C1555-64.
131. Burnstock, G., *Release of vasoactive substances from endothelial cells by shear stress and purinergic mechanosensory transduction*. Journal of anatomy, 1999. **194 (Pt 3)**: p. 335-42.
132. Yamamoto, K., et al., *Involvement of cell surface ATP synthase in flow-induced ATP release by vascular endothelial cells*. American journal of physiology Heart and circulatory physiology, 2007. **293**(3): p. H1646-53.
133. Raemaekers, T., et al., *NuSAP, a novel microtubule-associated protein involved in mitotic spindle organization*. The Journal of cell biology, 2003. **162**(6): p. 1017-29.
134. Ribbeck, K., et al., *NuSAP, a mitotic RanGTP target that stabilizes and cross-links microtubules*. Molecular biology of the cell, 2006. **17**(6): p. 2646-60.
135. Fujiwara, T., et al., *Expression analyses and transcriptional regulation of mouse nucleolar spindle-associated protein gene in erythroid cells: essential role of NF- κ B*. British journal of haematology, 2006. **135**(4): p. 583-90.
136. Oviedo, P.J., et al., *Raloxifene increases proliferation of human endothelial cells in association with increased gene expression of cyclins A and B1*. Fertility and sterility, 2007. **88**(2): p. 326-32.

137. Xie, L., et al., *Endothelial cells isolated from caveolin-2 knockout mice display higher proliferation rate and cell cycle progression relative to their wild-type counterparts*. American journal of physiology Cell physiology. **298**(3): p. C693-701.
138. Oestergaard, V.H., et al., *Deubiquitination of FANCD2 is required for DNA crosslink repair*. Molecular cell, 2007. **28**(5): p. 798-809.
139. Quarmby, L.M. and M.R. Mahjoub, *Caught Nek-ing: cilia and centrioles*. Journal of cell science, 2005. **118**(Pt 22): p. 5161-9.
140. M Valdivia, M., et al., *CENPA a Genomic Marker for Centromere Activity and Human Diseases*. Current genomics, 2009. **10**(5): p. 326-35.
141. Crawford, D.F. and H. Piwnica-Worms, *The G(2) DNA damage checkpoint delays expression of genes encoding mitotic regulators*. The Journal of biological chemistry, 2001. **276**(40): p. 37166-77.
142. Coma, S., et al., *Id2 promotes tumor cell migration and invasion through transcriptional repression of semaphorin 3F*. Cancer research. **70**(9): p. 3823-32.
143. Matsumura, M.E., D.R. Lobe, and C.A. McNamara, *Contribution of the helix-loop-helix factor Id2 to regulation of vascular smooth muscle cell proliferation*. The Journal of biological chemistry, 2002. **277**(9): p. 7293-7.
144. Gray, M.J., et al., *Therapeutic targeting of Id2 reduces growth of human colorectal carcinoma in the murine liver*. Oncogene, 2008. **27**(57): p. 7192-200.
145. Tsunedomi, R., et al., *Decreased ID2 promotes metastatic potentials of hepatocellular carcinoma by altering secretion of vascular endothelial growth factor*. Clinical cancer research : an official journal of the American Association for Cancer Research, 2008. **14**(4): p. 1025-31.
146. Lasorella, A., et al., *Id2 mediates tumor initiation, proliferation, and angiogenesis in Rb mutant mice*. Molecular and cellular biology, 2005. **25**(9): p. 3563-74.
147. Ling, M.-T., et al., *Overexpression of Id-1 in prostate cancer cells promotes angiogenesis through the activation of vascular endothelial growth factor (VEGF)*. Carcinogenesis, 2005. **26**(10): p. 1668-76.

148. Holm, P.W., et al., *Atherosclerotic plaque development and instability: a dual role for VEGF*. *Annals of medicine*, 2009. **41**(4): p. 257-64.
149. Tammela, T., et al., *The biology of vascular endothelial growth factors*. *Cardiovascular research*, 2005. **65**(3): p. 550-63.
150. Testa, U., G. Pannitteri, and G.L. Condorelli, *Vascular endothelial growth factors in cardiovascular medicine*. *Journal of cardiovascular medicine (Hagerstown, Md)*, 2008. **9**(12): p. 1190-221.
151. Yla-Herttuala, S., et al., *Vascular endothelial growth factors: biology and current status of clinical applications in cardiovascular medicine*. *Journal of the American College of Cardiology*, 2007. **49**(10): p. 1015-26.
152. Friesel, R.E. and T. Maciag, *Molecular mechanisms of angiogenesis: fibroblast growth factor signal transduction*. *The FASEB journal : official publication of the Federation of American Societies for Experimental Biology*, 1995. **9**(10): p. 919-25.
153. Bikfalvi, A., et al., *Biological roles of fibroblast growth factor-2*. *Endocrine reviews*, 1997. **18**(1): p. 26-45.
154. Nakamura, T., et al., *Signals via FGF receptor 2 regulate migration of endothelial cells*. *Biochemical and biophysical research communications*, 2001. **289**(4): p. 801-6.
155. Hughes, S.E., *Localisation and differential expression of the fibroblast growth factor receptor (FGFR) multigene family in normal and atherosclerotic human arteries*. *Cardiovascular research*, 1996. **32**(3): p. 557-69.
156. Schmitz, G. and W.E. Kaminski, *ATP-binding cassette (ABC) transporters in atherosclerosis*. *Current atherosclerosis reports*, 2002. **4**(3): p. 243-51.
157. Batetta, B., et al., *Opposite pattern of MDR1 and caveolin-1 gene expression in human atherosclerotic lesions and proliferating human smooth muscle cells*. *Cellular and molecular life sciences : CMLS*, 2001. **58**(8): p. 1113-20.
158. Mueller, C.F.H., et al., *Multidrug resistance protein-1 affects oxidative stress, endothelial dysfunction, and atherogenesis via leukotriene C4 export*. *Circulation*, 2008. **117**(22): p. 2912-8.

159. Mueller, C.F.H., et al., *The role of the multidrug resistance protein-1 in modulation of endothelial cell oxidative stress*. *Circulation research*, 2005. **97**(7): p. 637-44.
160. Roberts, R.L., et al., *Dynamics of rab5 activation in endocytosis and phagocytosis*. *Journal of leukocyte biology*, 2000. **68**(5): p. 627-32.
161. Jopling, H.M., et al., *Rab GTPase regulation of VEGFR2 trafficking and signaling in endothelial cells*. *Arteriosclerosis, thrombosis, and vascular biology*, 2009. **29**(7): p. 1119-24.
162. Bruns, A.F., et al., *VEGF-A-stimulated signalling in endothelial cells via a dual receptor tyrosine kinase system is dependent on co-ordinated trafficking and proteolysis*. *Biochemical Society transactions*, 2009. **37**(Pt 6): p. 1193-7.
163. Michel, C.C. and F.E. Curry, *Microvascular permeability*. *Physiol Rev*, 1999. **79**(3): p. 703-61.
164. Tedgui, A., *Endothelial permeability under physiological and pathological conditions*. *Prostaglandins Leukot Essent Fatty Acids*, 1996. **54**(1): p. 27-9.
165. Kennedy, J.H. and A. Tedgui, *Normal and pathological aspects of mass transport across the vascular wall*. *Cardiovasc Surg*, 1995. **3**(6): p. 611-5.
166. Chen, Y.L., et al., *Ultrastructural studies on macromolecular permeability in relation to endothelial cell turnover*. *Atherosclerosis*, 1995. **118**(1): p. 89-104.
167. Rippe, B., et al., *Transendothelial transport: the vesicle controversy*. *J Vasc Res*, 2002. **39**(5): p. 375-90.
168. Blackman, B.R., G. Garcia-Cardena, and M.A. Gimbrone, Jr., *A new in vitro model to evaluate differential responses of endothelial cells to simulated arterial shear stress waveforms*. *J Biomech Eng*, 2002. **124**(4): p. 397-407.